NASA Technical Memorandum 78786

Effect of an Alternate Winglet on the Pressure and Spanwise Load Distributions of a First-Generation Jet Transport Wing

Lawrence C. Montoya, Stuart G. Flechner,
and Peter F. Jacobs

DECEMBER 1978

NASA

NASA Technical Memorandum 78786

Effect of an Alternate Winglet on the Pressure and Spanwise Load Distributions of a First-Generation Jet Transport Wing

Lawrence C. Montoya
Dryden Flight Research Center
Edwards, California

Stuart G. Flechner and Peter F. Jacobs
Langley Research Center
Hampton, Virginia

National Aeronautics
and Space Administration

**Scientific and Technical
Information Office**

1978

SUMMARY

Pressure and spanwise load distributions on a first-generation jet transport semispan model at subsonic speeds are presented. The data were measured for the wing with and without an alternate winglet. The investigation was conducted in the Langley 8-foot transonic pressure tunnel. Selected data at several test conditions are discussed to show trends. The winglet mainly affected the pressure distributions of the outboard region of the wing and increased the spanwise loading near the tip.

INTRODUCTION

Winglets are intended to provide a substantially greater reduction in induced drag at cruise conditions than that obtained with a simple wing-tip extension designed to impose the same bending-moment increments on the wing structure as the winglets. The National Aeronautics and Space Administration has been conducting extensive experimental investigations of winglets on jet transport wings at subsonic Mach numbers. (See refs. 1 to 6.)

During the wind-tunnel winglet investigations on a first-generation jet transport wing (refs. 2 to 4), two upper-winglet configurations were evaluated. The two upper-winglet configurations (basic and alternate) differed in planform, airfoil section, twist distribution, and radius at the wing-winglet juncture which resulted in a slightly longer wing span for the alternate upper-winglet configuration. The basic upper winglet is a NASA design, and data for this configuration are presented in references 2 to 6. The alternate upper winglet was designed by an aircraft company under contract to the USAF Flight Dynamics Laboratory. Presented herein are pressure and spanwise load distributions on the wing and alternate upper winglet. To achieve the highest possible Reynolds number, a semispan model was used. The tests were conducted in the Langley 8-foot transonic pressure tunnel.

Data are presented at wind-tunnel free-stream Mach numbers of 0.30, 0.70, 0.75, 0.78, and 0.80 for dynamic pressures of 12 kPa (251 psf) at Mach 0.30 and 41 kPa (850 psf) at the higher subsonic Mach numbers. At Mach 0.30, the Reynolds number was 11.68×10^6 per meter (3.56×10^6 per foot) and the angle of attack ranged from about 4° to 12°. The data presented at Mach 0.30 are with trailing-edge flaps deflected approximately 20°. For the higher subsonic Mach numbers, the Reynolds number varied slightly from about 18.67×10^7 per meter (5.69×10^6 per foot) at Mach 0.70 to 16.90×10^6 per meter (5.15×10^6 per foot) at Mach 0.80. The angle of attack ranged from about -1° to 7°.

SYMBOLS

Force and moment data have been reduced to coefficient form based on the exposed trapezoidal area of the basic wing. All dimensional values are given

in both SI Units (ref. 7) and U.S. Customary Units. All measurements and calculations were made in U.S. Customary Units.

Coefficients and symbols used herein are defined as follows:

b' exposed semispan of wing with basic tip, 125.88 cm (49.56 in.)

c local chord, cm (in.)

$\bar{c}$ mean geometric chord of exposed basic wing, 39.75 cm (15.65 in.)

c_{av} average chord of exposed basic wing, S/b', 37.19 cm (14.64 in.)

C_L lift coefficient, $\frac{\text{Lift}}{q_\infty S}$

C_m pitching-moment coefficient, $\frac{\text{Pitching moment}}{q_\infty S\bar{c}}$

c_n section normal-force coefficient obtained from integration of pressure measurements

C_p pressure coefficient, $\frac{p_l - p_\infty}{q_\infty}$

$C_{p,sonic}$ pressure coefficient corresponding to local speed of sound

c_t tip chord of basic wing, cm (in.)

h span of winglet from chord plane of wing tip (see fig. 4), cm (in.)

M_∞ free-stream Mach number

p_l local static pressure, Pa (psf)

p_∞ free-stream static pressure, Pa (psf)

q_∞ free-stream dynamic pressure, Pa (psf)

S exposed trapezoidal area of basic wing, 0.4680 m^2 (5.0379 ft^2)

x chordwise distance from leading edge, positive aft, cm (in.)

y spanwise distance from wing-fuselage juncture, positive outboard, cm (in.)

z vertical coordinate of wing airfoil, positive upward, cm (in.)

z' distance along winglet span from chord plane of wing, cm (in.)

α angle of attack, deg

η exposed wing semispan station (based on exposed basic-wing panel), y/b'

Abbreviations:

L.S. wing lower surface

U.S. wing upper surface

EXPERIMENTAL APPARATUS AND PROCEDURES

Test Facility

This investigation was conducted in the Langley 8-foot transonic pressure tunnel, a continuous-flow, single-return tunnel with a slotted, rectangular test section. The longitudinal slots in the floor and ceiling of the test section reduce tunnel wall interference and allow relatively large models to be tested through the subsonic speed range. Controls are available to permit independent variation of Mach number, stagnation pressure, temperature, and dew point. A more detailed description of the wind tunnel is given in reference 8.

Model Description

To obtain the highest possible winglet Reynolds number and sufficient winglet size in which to install surface pressure measurement tubes, a semispan model was utilized. The semispan model used in this investigation was a 0.07-scale KC-135A transport aircraft. A drawing of the model is shown in figure 1.

Fuselage.- The fuselage contours closely simulate the full-scale fuselage shape, with the exception of the wheel-well area. An enlargement of this area was necessary to enclose the model mounting apparatus. The fuselage midsection covers the strain-gage balance and has a slot in it through which the wing protrudes. The fuselage is not attached to the balance, but it does rotate with the wing through the angle-of-attack range.

Wing.- The basic wing of the KC-135A model has 7° of dihedral and 2° of incidence at the root chord. The wing has no geometric twist. A typical outboard airfoil section is shown in figure 2 with its coordinates presented in table I. The wing thickness ratio varies nonlinearly from 15 percent at the wing-fuselage juncture to 9 percent at the trailing-edge break station and then remains constant at 9 percent to the wing tip. The trapezoidal planform of the total wing (extended to the fuselage center line) has a sweep at the quarter-chord of 35°, an aspect ratio of 7.11, and a taper ratio of 0.33. For all data analysis, the reference geometry parameters S, b', $\bar{c}$, and c_{av} are based on the exposed trapezoidal planform of the basic wing. To account for the increased wing span resulting from the alternate winglet installation, the "basic" wing for this investigation was lengthened by a corresponding amount (0.013b') so that winglet-off and winglet-on could be compared as in references 1 to 6. The

model wing stiffness was designed so that the relative model bending deflection was approximately the same as that for the actual airplane at cruise conditions.

Nacelles.- Flow-through nacelles were used with an inlet diameter of 5.79 cm (2.28 in.) and exit diameter of 4.14 cm (1.63 in.). The inlet diameter was maintained back to approximately 0.66 of the nacelle length and then tapered linearly to the exit.

Trailing-edge flaps.- Fixed-position trailing-edge flaps were attached to the model to simulate second-segment-climb characteristics at Mach 0.30. The flaps tested were designed merely to be representative and were not modeled after the actual KC-135A flaps. The flaps were deflected 20°. Details of the trailing-edge flaps are shown in figure 3.

Winglet.- A drawing of the winglet used in this investigation is presented in figure 4. The winglet employed an advanced technology pressure distribution airfoil. A typical winglet airfoil section is shown in figure 5, with the twist distribution presented in figure 6. Positive twist is leading edge inboard.

The winglet has a span equal to 95 percent of the wing-tip chord, a root chord equal to 61 percent of the wing-tip chord, a leading-edge sweep of 37°, a taper ratio of 0.344, and an aspect ratio of 2.32. The planform area of the winglet is equal to 3.5 percent of the exposed trapezoidal planform area of the basic wing. The winglet is canted outboard 6° from vertical (84° dihedral).

Boundary-Layer Transition Strips

Boundary-layer transition strips were placed on both surfaces of the wing and winglet. These strips were comprised of a 0.159-cm (0.06-in.) wide band of carborundum grains sized on the basis of reference 9 and set in a plastic adhesive. The transition patterns for the wing and winglet are shown in figure 7.

The transition strips on the lower (outboard) surface of the winglet were located rearward in an attempt to simulate full-scale Reynolds number boundary-layer conditions. (See ref. 10.) The transition strips on the upper (inboard) surface of the winglet were located forward to insure transition ahead of the shock wave for the various test conditions.

The fluorescent-oil-film flow-visualization technique described in reference 11 was employed to verify the presence of laminar flow ahead of the transition strip and turbulent flow behind the transition strip.

Test Conditions

The data presented herein are for wind-tunnel free-stream Mach numbers of 0.30, 0.70, 0.75, 0.78, and 0.80. The angle of attack ranged from approximately 4° to 12° at Mach 0.30 and from about -1° to 7° at the higher subsonic Mach numbers.

The Reynolds numbers and dynamic pressures at which data were taken are shown in the following table:

M_∞	Reynolds number		Dynamic pressure	
	per meter	per foot	kPa	psf
0.30	11.68×10^6	3.56×10^6	12	251
.70	18.67	5.69	41	850
.75	17.72	5.40	41	850
.78	17.22	5.25	41	850
.80	16.90	5.15	41	850

During the tests, the stagnation temperature was maintained at 322 K (120° F) and the air was dried until the dew point was sufficiently low to prevent condensation effects.

Measurements

Force and moment data were obtained using a five-component electrical strain-gage balance. Side-force measurements were not taken. An accelerometer attached to the wing mounting block inside the fuselage was used to measure angle of attack. Chordwise pressure distributions were measured at the 0.25, 0.76, 0.91, and 0.98 semispan stations of the wing. (See fig. 8(a).) Additionally, they were measured at two stations on the winglet (fig. 8(b)) for the winglet configuration. These stations were located at 0.25 and 0.75 of the winglet span, which correspond to the 1.01 and 1.03 wing semispan stations, respectively. (Note that semispan stations are defined as a fraction of the distance from the wing-fuselage juncture to the tip of the wing panel. As the winglet extends beyond this distance, semispan stations can be greater than 1.0.) The wing and winglet pressures were measured with pressure-scanning valves. The ranges of the pressure sensors in the valves were sized for the expected upper or lower wing or winglet surface pressures and wind-tunnel test conditions.

Wing-tip deflections (vertical displacements) were determined from photographs of a chordwise line on the edge of the wing tip and are shown in figure 9 for Mach numbers of 0.30 and 0.78. The wing-tip deflection data for M_∞ = 0.70, 0.75, and 0.80 are nearly identical to the data at M_∞ = 0.78 (fig. 9(b)) and therefore are not presented.

Corrections

The wind-tunnel slotted test section is designed to reduce wall effects on lift. Data from this investigation show that the wing spanwise load distributions for all configurations at the same conditions are nearly identical over the major portion of the span. Therefore, the wall effects on the wing lift

can be considered systematic, and no correction is made to the data for these effects. The angle of attack of the model was corrected for flow angularity in the wind tunnel. No Mach number correction was made for blockage effects. No corrections were made for nacelle internal mass flow or spillage effects.

PRESENTATION OF RESULTS

The results of the study are presented in the following figures:

Since limited alternate-winglet pressure data were obtained at the high subsonic speeds, upper-winglet configuration data from reference 3 can be used to determine the general trends at off-design conditions.

DISCUSSION OF RESULTS

The discussion presented herein is limited to a few selected cases. The data discussed are considered representative of the trends for the various configurations. The variation of angle of attack with lift coefficient has been included to show the relationship between angle of attack and lift coefficient for the figures presented herein. The near-design cruise conditions of the basic wing are represented by the data at Mach 0.78 and at an angle of attack of 2.5°. The data presented at Mach 0.30 are with trailing-edge flaps deflected.

Throughout the figures of this paper, an effort has been made to retain a particular symbol with each of the two configurations tested (basic and winglet). This practice is intended to facilitate identification of a particular set of data. Also, for the pressure distributions (figs. 11 to 14), the configuration is indicated at the top of each page. Note that in figures 12, 14, and 16, the vertical-scale increments of the insert plots are larger than the main-scale increments.

The chordwise pressure distributions for the basic configuration are representative of first-generation jet transport airfoils and will not be discussed.

In figure 15, comparisons of wing chordwise pressure distributions for the basic and winglet configurations at two Mach numbers are presented. The comparison at Mach 0.70 (fig. 15(a)) shows no differences in the pressure distributions on the inboard wing stations. The wing pressure coefficients at $\eta = 0.91$ for the winglet configuration are slightly more negative on the aft portions of the upper wing surface. At $\eta = 0.98$, the winglet-configuration pressure coefficients become more negative on the aft portion of the wing upper surface. The wing lower-surface pressure coefficients for both configurations are the same. At Mach 0.78 (fig. 15(b)), the trends are similar to those at Mach 0.70 (fig. 15(a)). From these comparisons, it can be seen that the winglet mainly affects the wing pressure coefficients near the tip.

A comparison of the chordwise pressure distributions at Mach 0.30 for the winglet and basic configurations with trailing-edge flaps (fig. 16) shows the effect of the winglet at high lift conditions. As with the data at higher Mach numbers, the winglet had no effect at the inboard stations. However, outboard stations show differences near the wing leading edge. At $\eta = 0.98$, the winglet-configuration pressure coefficients on the forward region of the wing are more negative.

Figures 17 and 18 show the effect of the winglet on the spanwise loads. As expected, the winglet increases the wing loading near the tip for all Mach numbers and angles of attack presented.

SUMMARY OF RESULTS

Wind-tunnel wing and winglet pressure and spanwise load distributions on a first-generation jet transport semispan model, with and without an alternate winglet, have been presented. An analysis of selected data which are considered to be representative of the general trends indicated the following:

1. The winglet mainly affected the pressure distributions of the outboard region of the wing. In general, the pressure coefficients are more negative on the aft region of the wing upper surface for the winglet configuration.

2. At high lift conditions at Mach 0.30 (with trailing-edge flaps), the pressure coefficients with the winglet are much more negative on the upper surface of the forward region of the wing.

3. The winglet increased the spanwise loads near the wing tip.

Langley Research Center
National Aeronautics and Space Administration
Hampton, VA 23665
October 10, 1978

REFERENCES

1. Whitcomb, Richard T.: A Design Approach and Selected Wind-Tunnel Results at High Subsonic Speeds for Wing-Tip Mounted Winglets. NASA TN D-8260, 1976.

2. Jacobs, Peter F.; Flechner, Stuart G.; and Montoya, Lawrence C.: Effect of Winglets on a First-Generation Jet Transport Wing. I - Longitudinal Aerodynamic Characteristics of a Semispan Model at Subsonic Speeds. NASA TN D-8473, 1977.

3. Montoya, Lawrence C.; Flechner, Stuart G.; and Jacobs, Peter F.: Effect of Winglets on a First-Generation Jet Transport Wing. II - Pressure and Spanwise Load Distributions for a Semispan Model at High Subsonic Speeds. NASA TN D-8474, 1977.

4. Montoya, Lawrence C.; Jacobs, Peter F.; and Flechner, Stuart G.: Effect of Winglets on a First-Generation Jet Transport Wing. III - Pressure and Spanwise Load Distributions for a Semispan Model at Mach 0.30. NASA TN D-8478, 1977.

5. Meyer, Robert R., Jr.: Effect of Winglets on a First-Generation Jet Transport Wing. IV - Stability Chracteristics for a Full-Span Model at Mach 0.30. NASA TP-1119, 1978.

6. Jacobs, Peter F.: Effect of Winglets on a First-Generation Jet Transport Wing. V - Stability Characteristics of a Full-Span Wing With a Generalized Fuselage at High Subsonic Speeds. NASA TP-1163, 1978.

7. Mechtly, E. A.: The International System of Units - Physical Constants and Conversion Factors (Second Revision). NASA SP-7012, 1973.

8. Schaefer, William T., Jr.: Characteristics of Major Active Wind Tunnels at the Langley Research Center. NASA TM X-1130, 1965.

9. Braslow, Albert L.; and Knox, Eugene C.: Simplified Method for Determination of Critical Height of Distributed Roughness Particles for Boundary-Layer Transition at Mach Numbers From 0 to 5. NACA TN 4363, 1958.

10. Blackwell, James A., Jr.: Preliminary Study of Effects of Reynolds Number and Boundary-Layer Transition Location on Shock-Induced Separation. NASA TN D-5003, 1969.

11. Loving, Donald L.; and Katzoff, Samuel: The Fluorescent-Oil Film Method and Other Techniques for Boundary-Layer Flow Visualization. NASA MEMO 3-17-59L, 1959.

TABLE I.- COORDINATES OF TYPICAL OUTBOARD WING SECTION

[Wing section at 2° incidence]

Upper surface		Lower surface	
x/c	z/c	x/c	z/c
0	0	0	0
.0011	.0042	.0020	-.0054
.0022	.0056	.0035	-.0063
.0034	.0071	.0061	-.0073
.0058	.0090	.0092	-.0081
.0095	.0116	.0201	-.0097
.0132	.0136	.0391	-.0116
.0180	.0161	.0631	-.0139
.0234	.0186	.0950	-.0168
.0324	.0221	.1016	-.0174
.0415	.0253	.1445	-.0212
.0536	.0291	.1826	-.0245
.0716	.0338	.2235	-.0284
.0897	.0377	.2597	-.0314
.0990	.0394	.2950	-.0341
.1132	.0417	.3326	-.0366
.1408	.0454	.3726	-.0391
.1589	.0471	.4276	-.0418
.1740	.0483	.4690	-.0429
.1861	.0492	.5110	-.0433
.2011	.0501	.5560	-.0430
.2192	.0510	.5967	-.0424
.2342	.0516	.6386	-.0414
.2584	.0522	.6818	-.0406
.3432	.0522	.7243	-.0397
.3729	.0524	.7620	-.0389
.4090	.0513	.7951	-.0381
.4572	.0489	.8308	-.0377
.5054	.0454	.8662	-.0371
.5416	.0420	.9029	-.0363
.5897	.0367	.9392	-.0358
.6379	.0304	.9790	-.0348
.6862	.0226	.9999	-.0350
.7343	.0153		
.7582	.0108		
.7823	.0065		
.8040	.0027		
.8344	-.0023		
.8642	-.0076		
.8874	-.0119		
.9223	-.0180		
.9492	-.0229		
.9718	-.0269		
.9920	-.0308		
1.0001	-.0347		

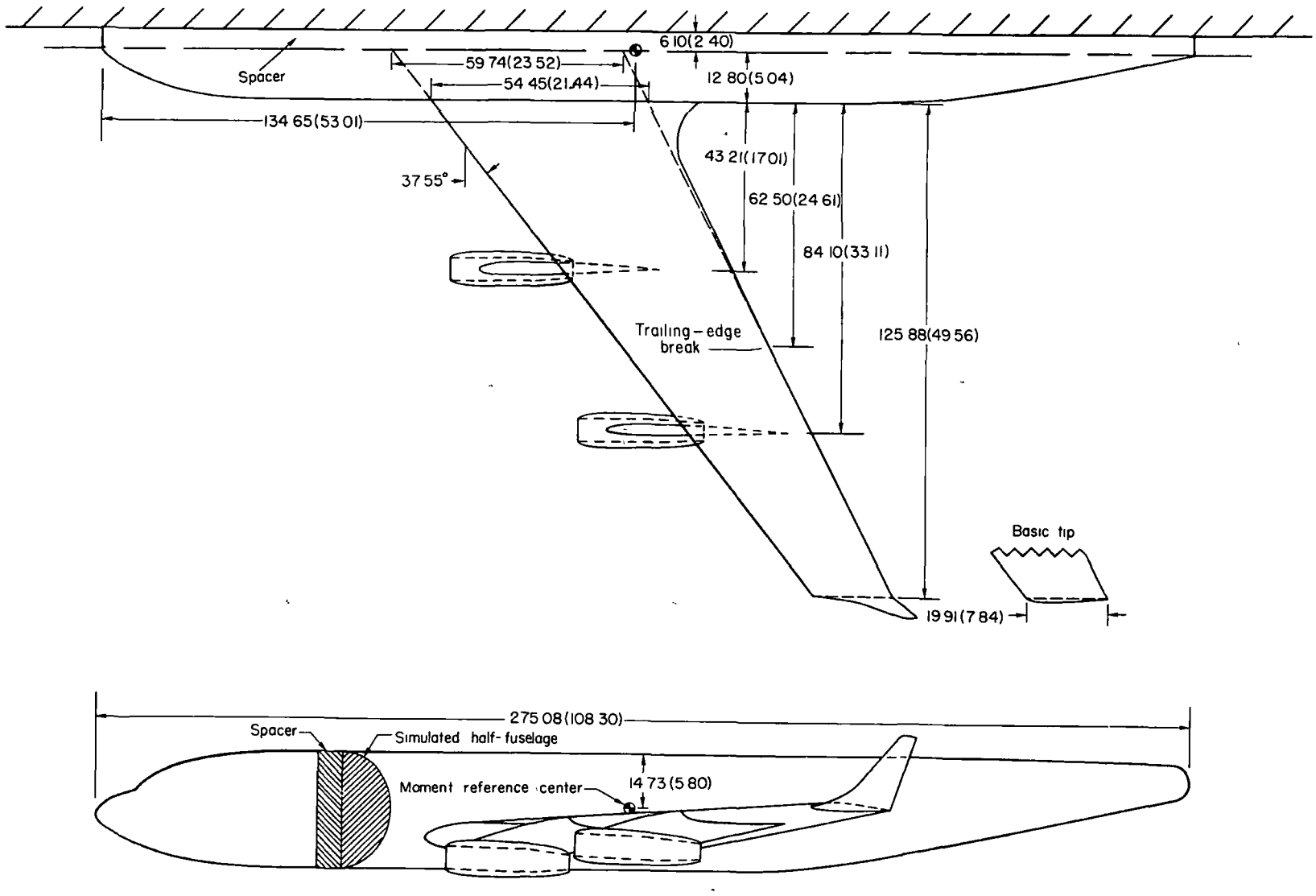

Figure 1.- Drawing of semispan model. Dimensions are in centimeters (inches).

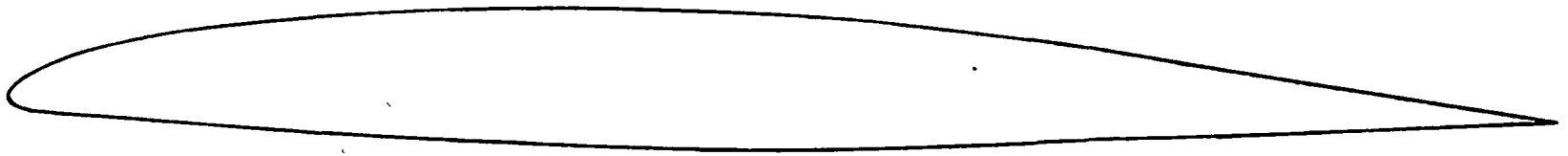

Figure 2.- Typical outboard wing airfoil section.

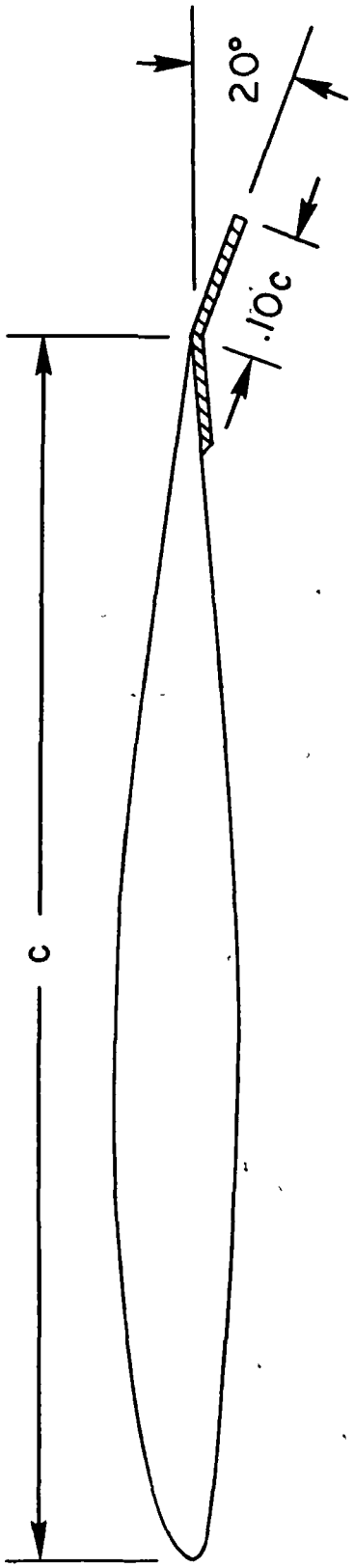

(a) Cross section.

Figure 3.- Drawings of flaps.

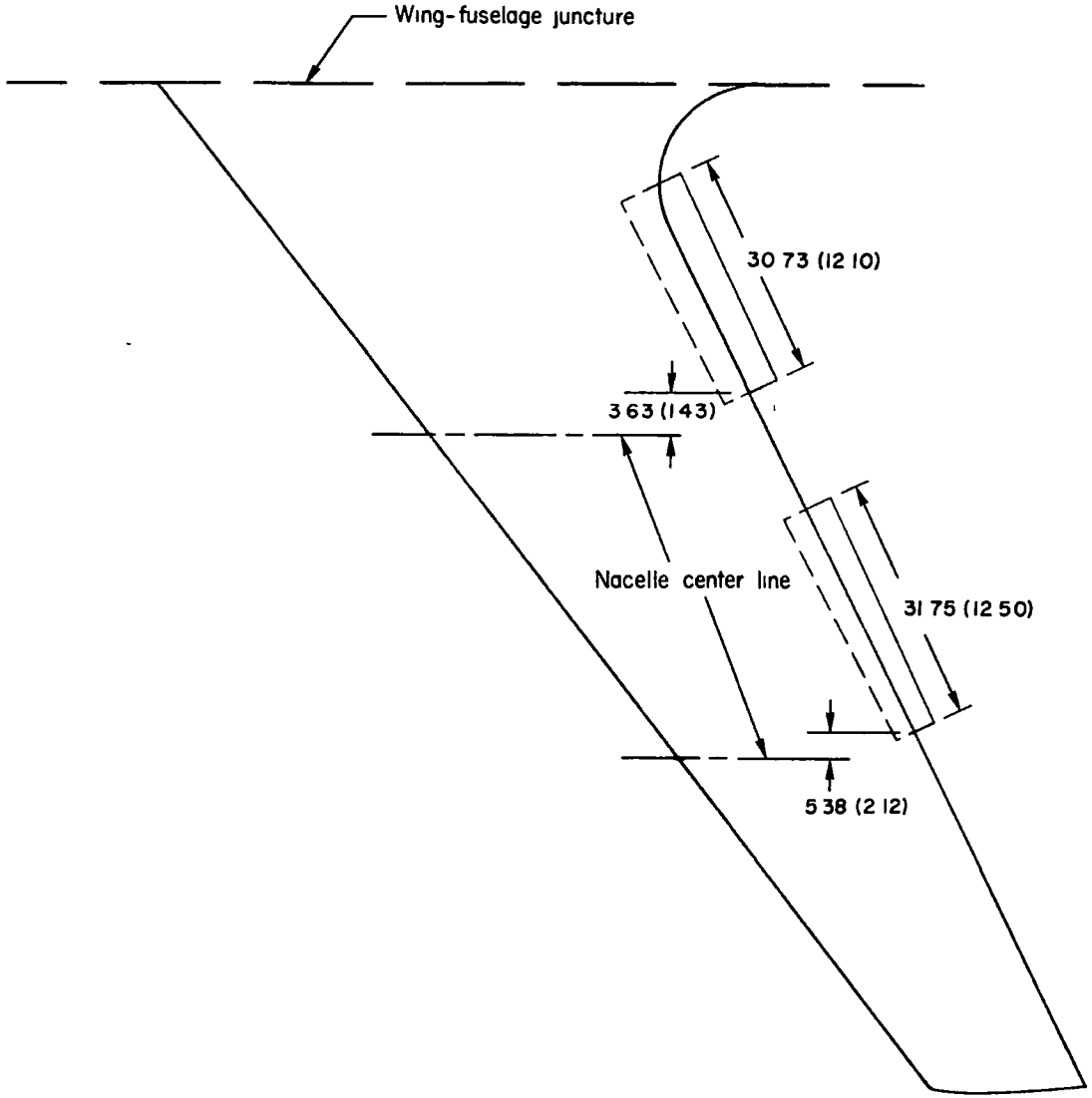

(b) Flap locations. Dimensions are in centimeters (inches).

Figure 3.- Concluded.

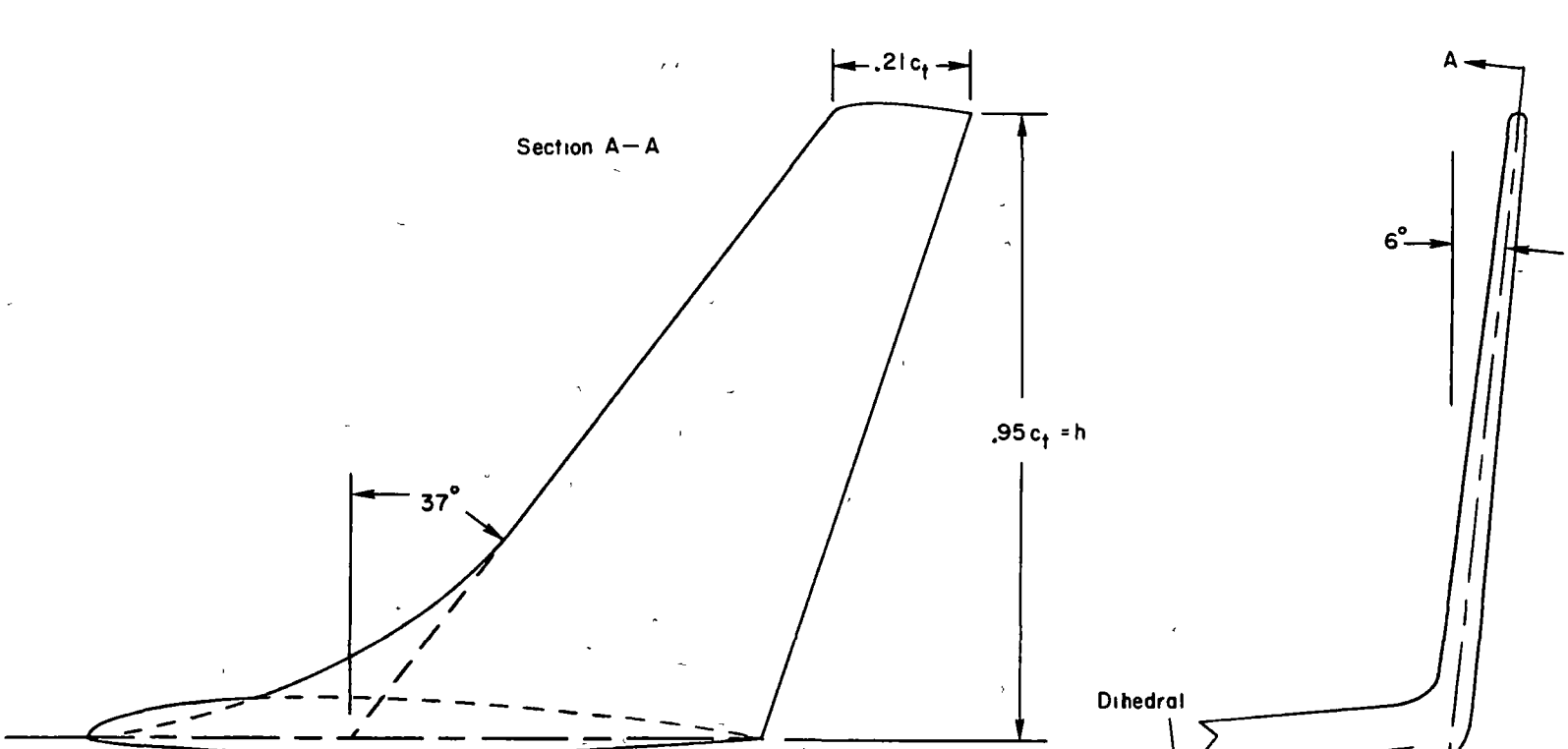

Figure 4.- Drawing of winglet.

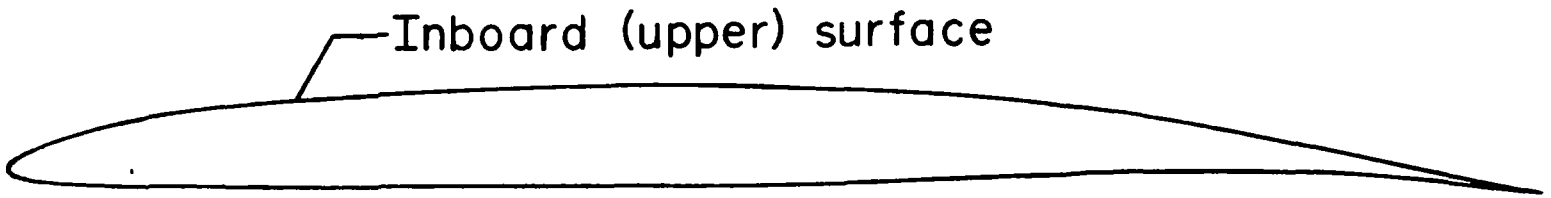

Figure 5.- Typical winglet airfoil section.

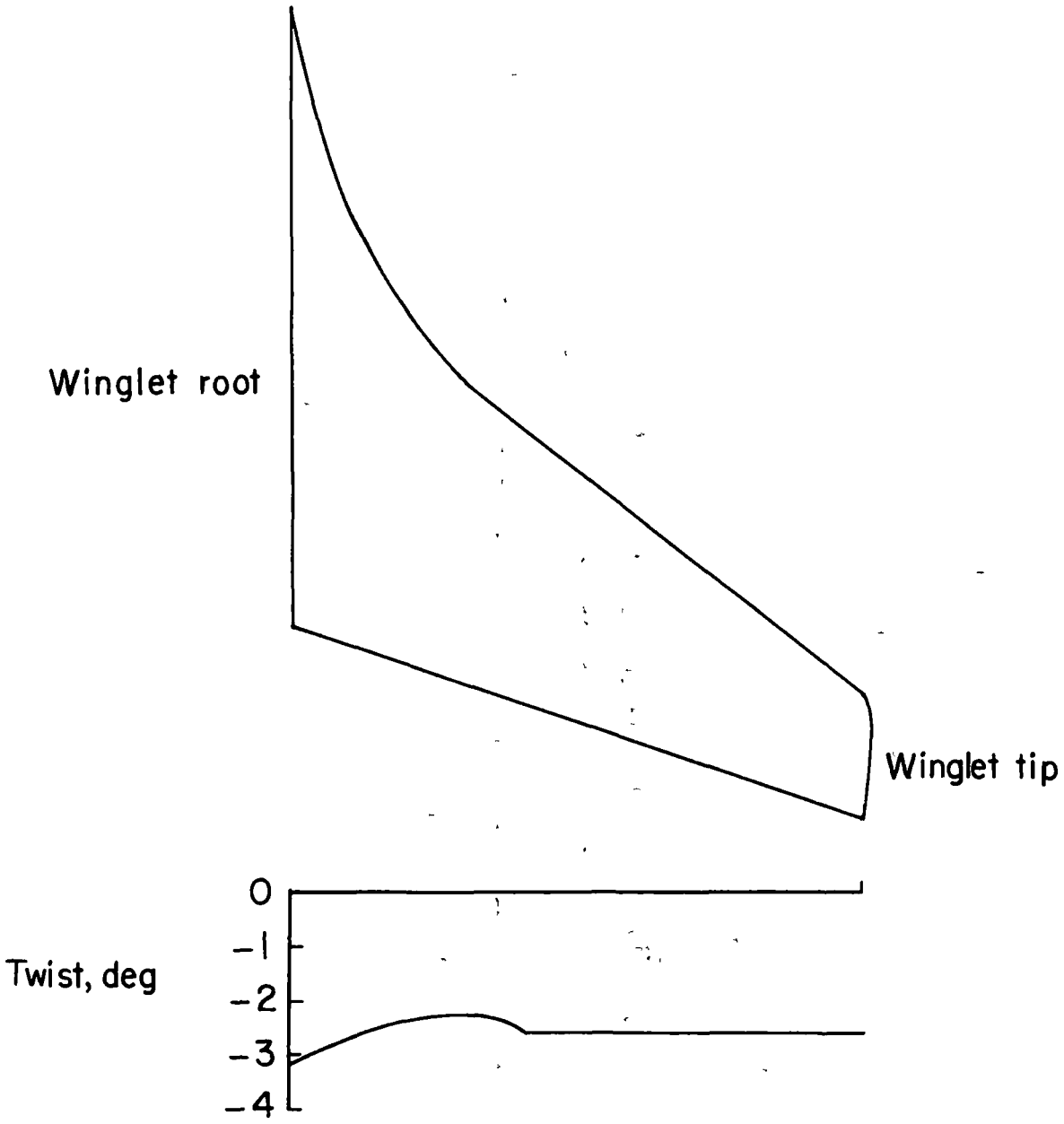

Figure 6.- Winglet spanwise twist distribution. Positive twist is leading edge inboard.

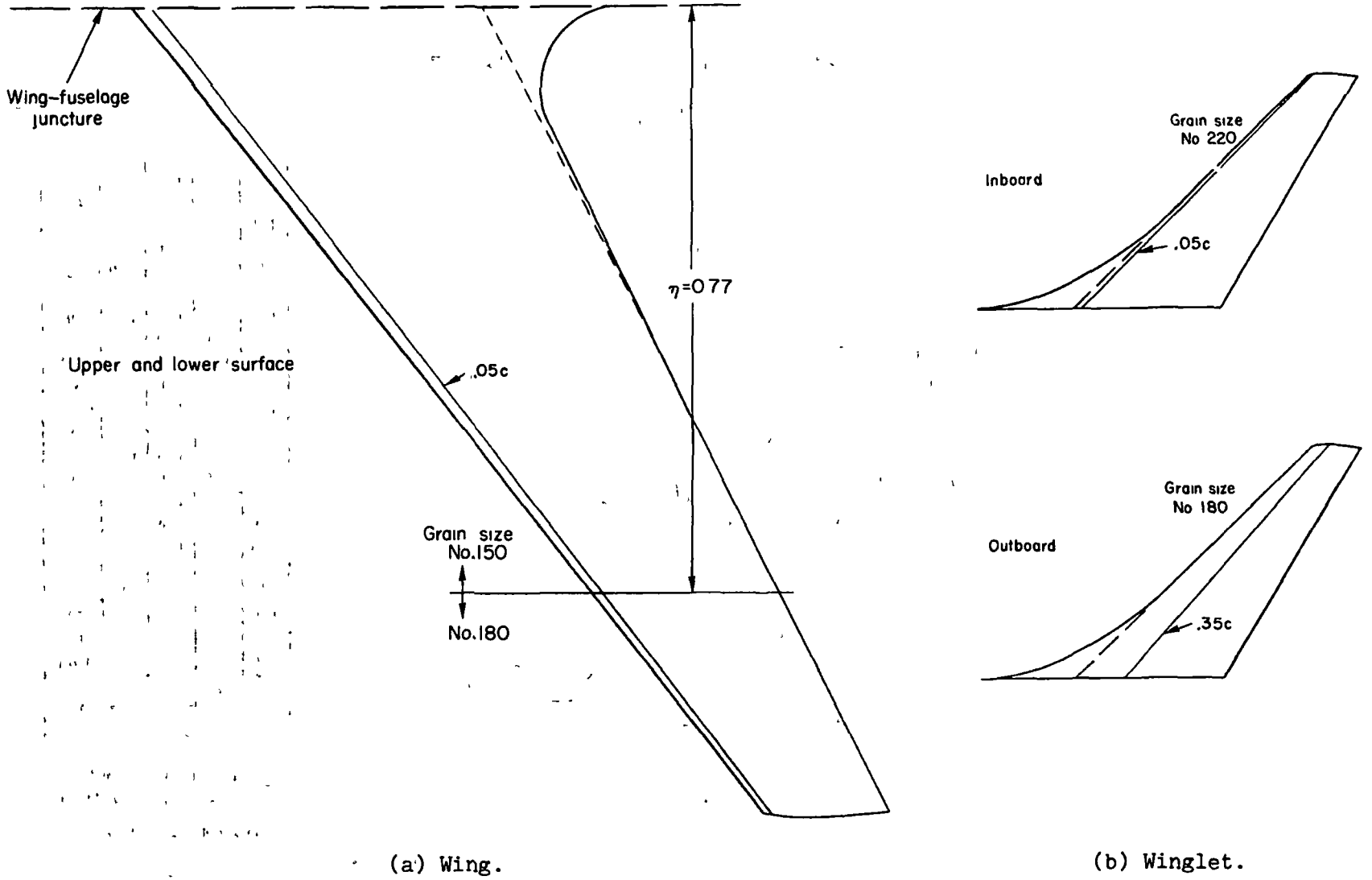

(a) Wing.

(b) Winglet.

Figure 7.- Location of transition strips.

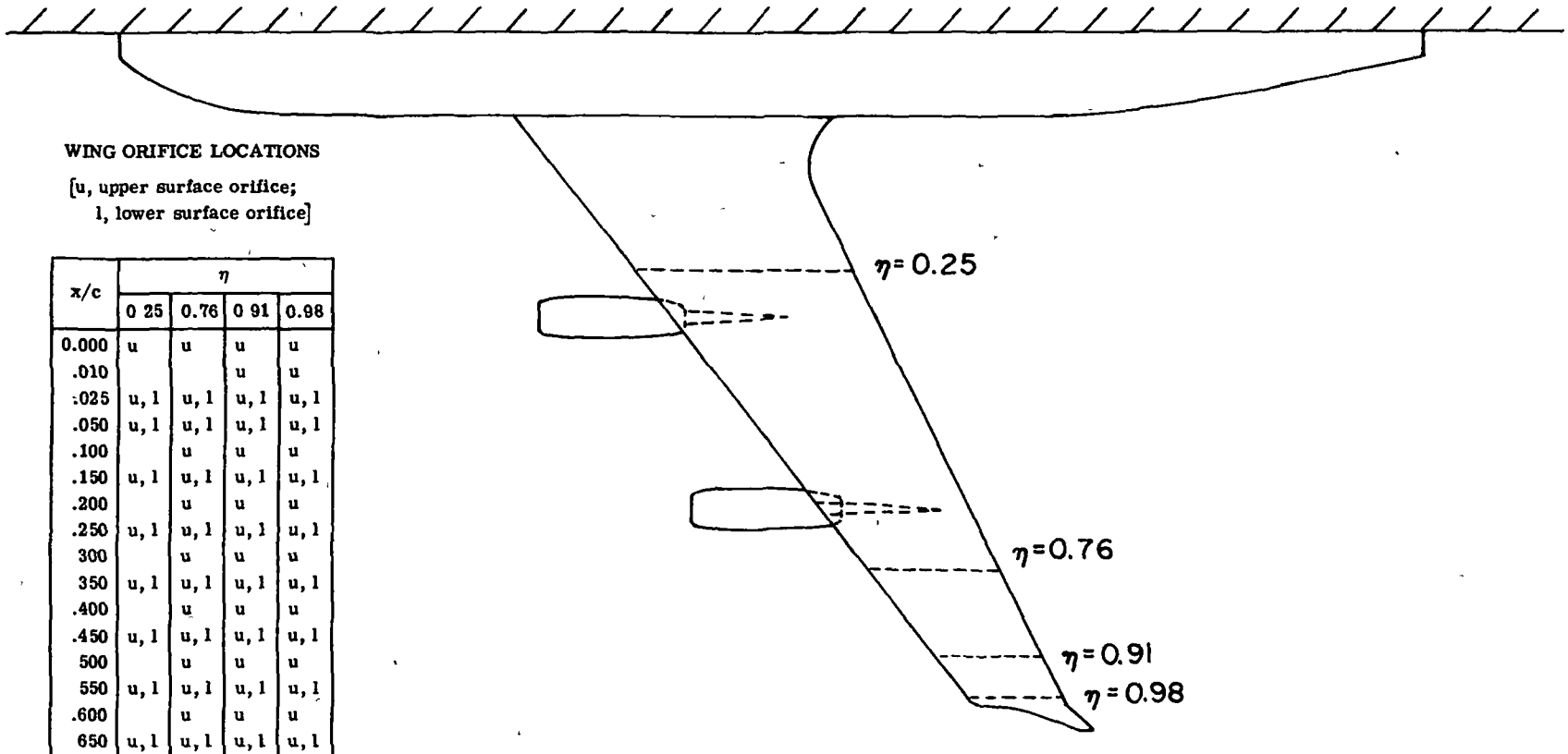

WING ORIFICE LOCATIONS

[u, upper surface orifice;
l, lower surface orifice]

x/c	η			
	0 25	0.76	0 91	0.98
0.000	u	u	u	u
.010			u	u
:025	u, l	u, l	u, l	u, l
.050	u, l	u, l	u, l	u, l
.100		u	u	u
.150	u, l	u, l	u, l	u, l
.200		u	u	u
.250	u, l	u, l	u, l	u, l
300		u	u	u
350	u, l	u, l	u, l	u, l
.400		u	u	u
.450	u, l	u, l	u, l	u, l
500		u	u	u
550	u, l	u, l	u, l	u, l
.600		u	u	u
650	u, l	u, l	u, l	u, l
.700		u	u	u
.750	u, l	u, l	u, l	u, l
.800		u	u	
.850	u	u, l	u, l	u, l
.900		u	u	u
.950	u, l	u, l	u, l	u, l

(a) On wing.

Figure 8.- Wing and winglet orifice locations.

WINGLET ORIFICE LOCATIONS

[u, upper surface orifice;
l, lower surface orifice]

	η	
x/c	1.01	1.03
.005	u	u
.025	u	u
.050	l	l
.080	u	u
.200	u	u
.225	l	l
.350	u	u
.400	l	l
.500	u	u
.600	l	l
.650	u	u
.775	l	l
.800	u	u
.950	u, l	u, l

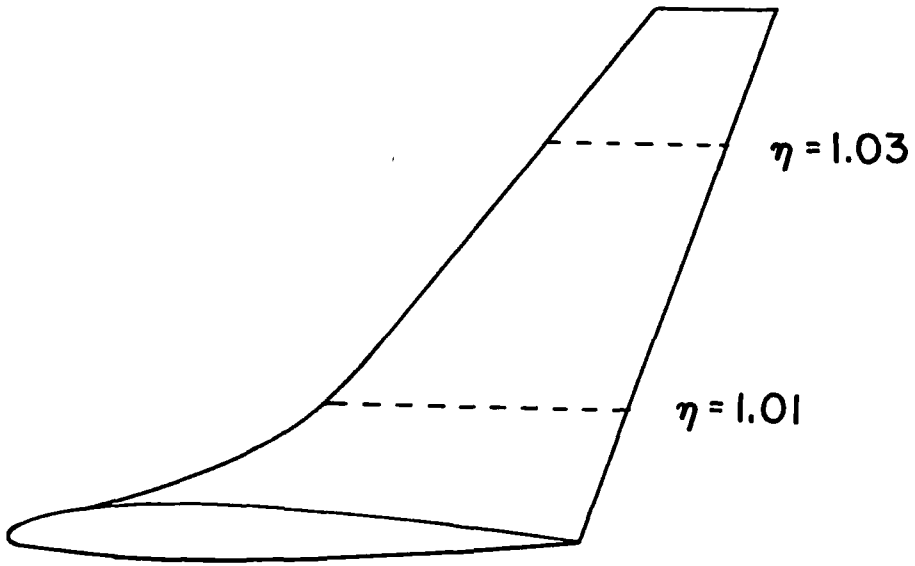

(b) On winglet.

Figure 8.- Concluded.

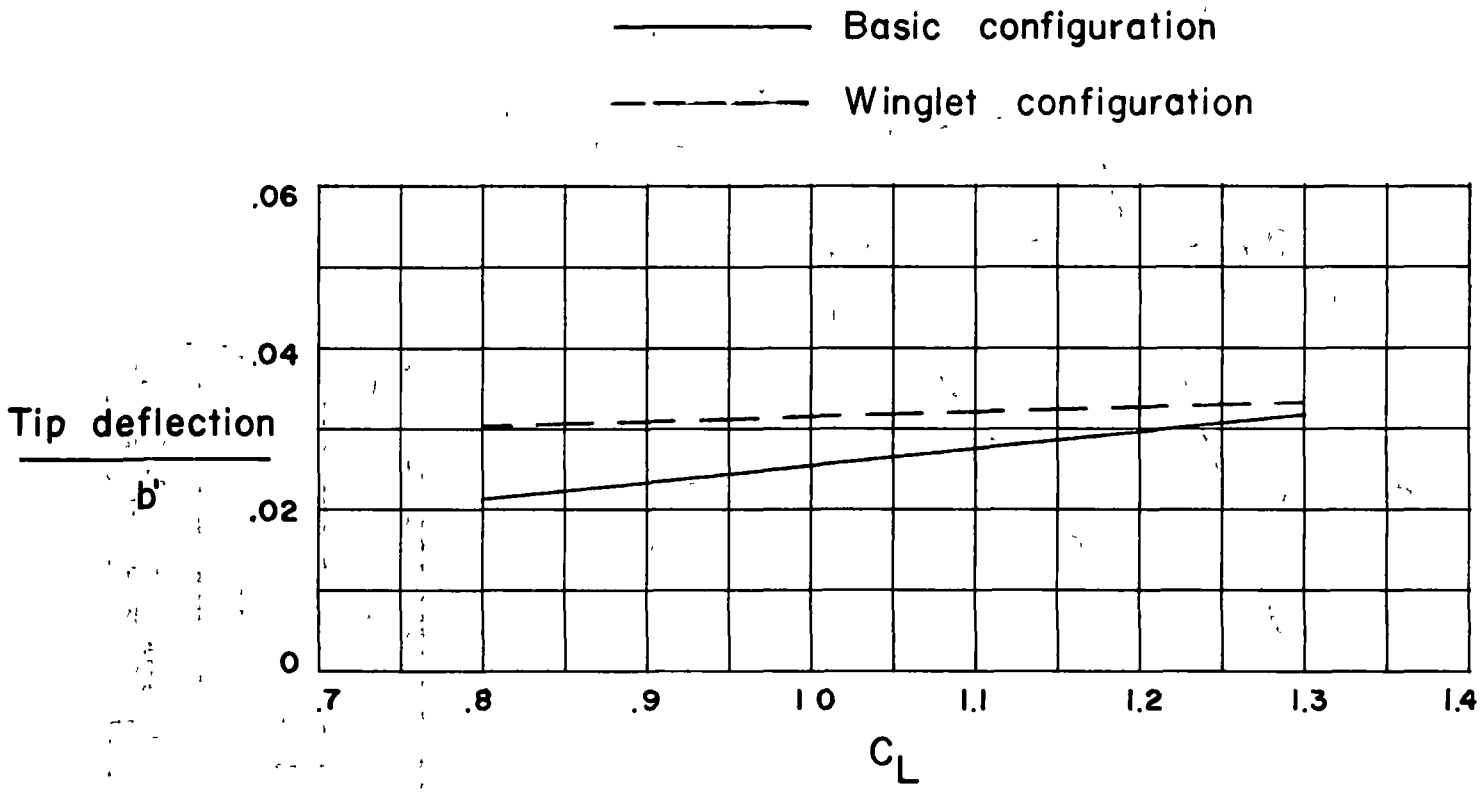

(a) $M_\infty = 0.30$, with trailing-edge flaps.

Figure 9.- Wing-tip deflections.

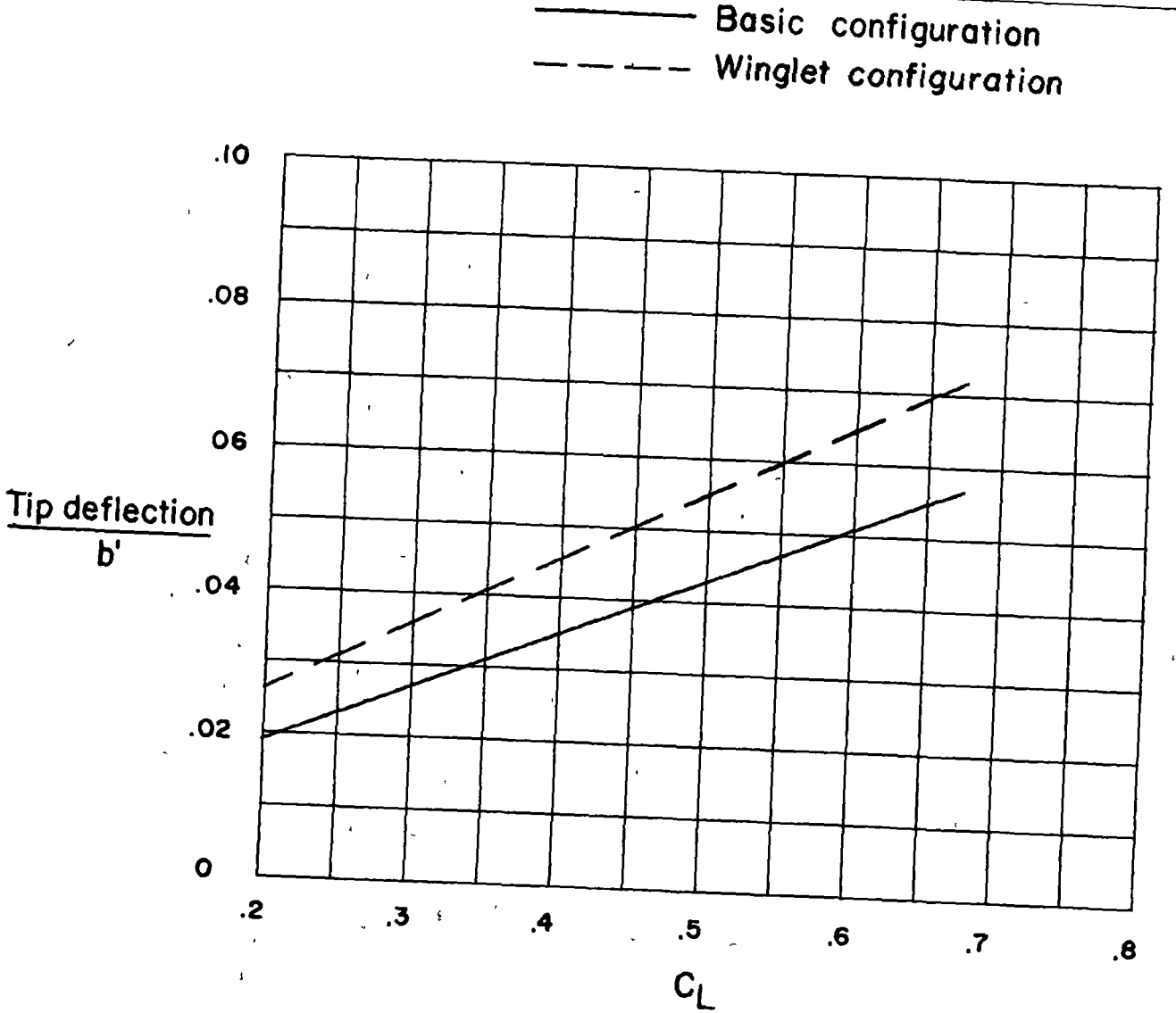

(b) $M_\infty = 0.78$.

Figure 9.- Concluded.

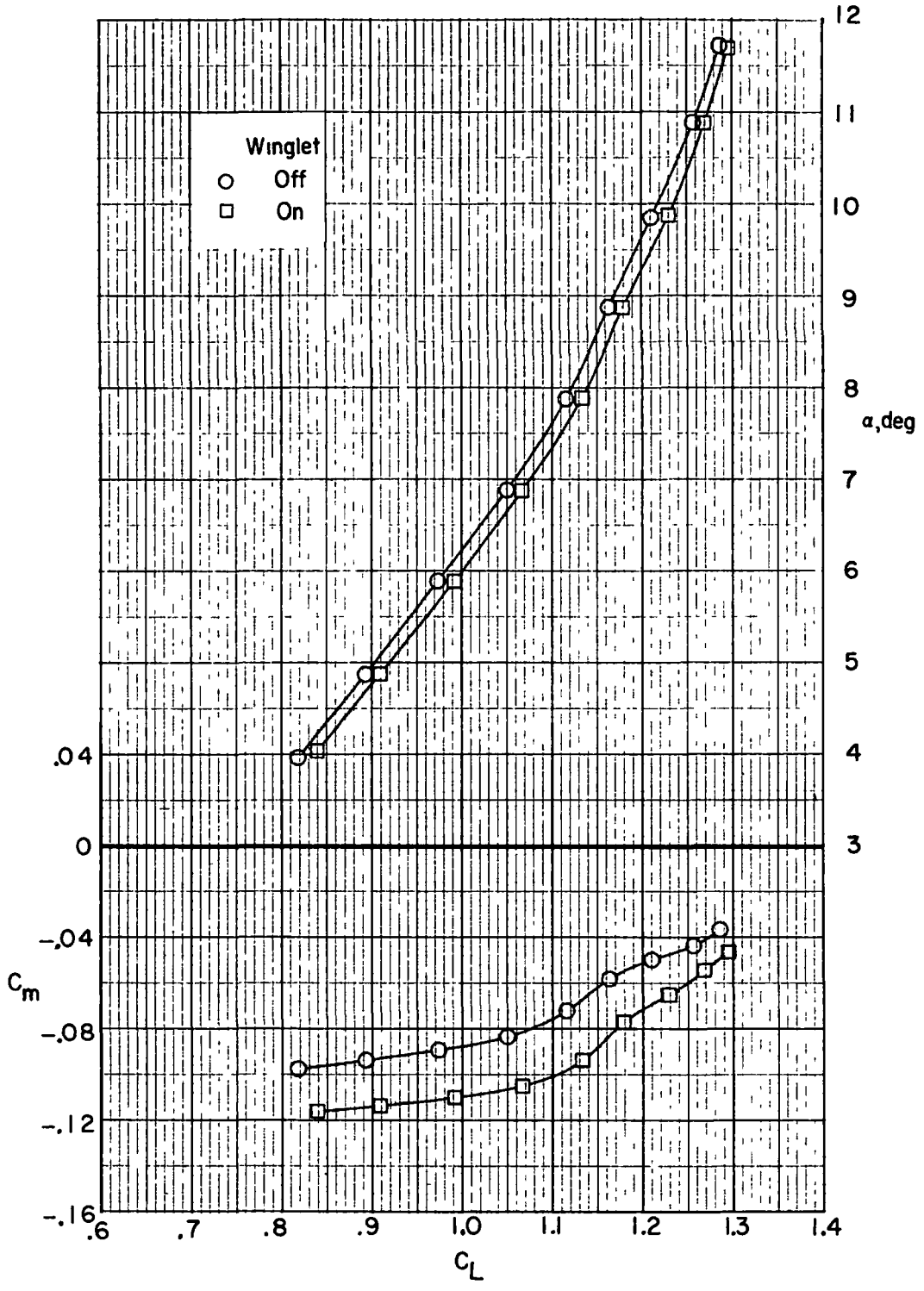

(a) M_∞ = 0.30, with trailing-edge flaps.

Figure 10.- Variation of pitching-moment coefficient and angle of attack with lift coefficient.

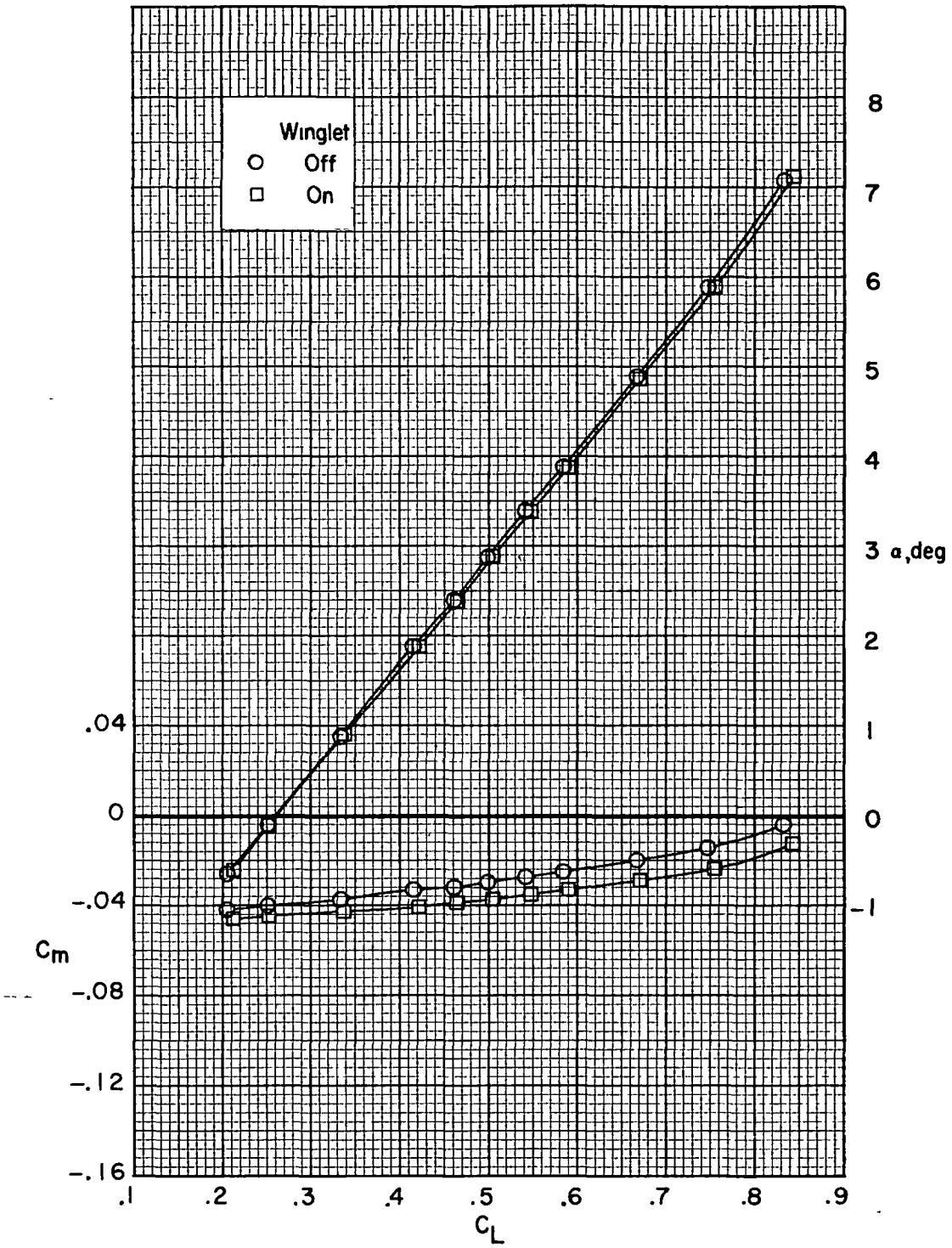

(b) $M_\infty = 0.70$.

Figure 10.- Continued.

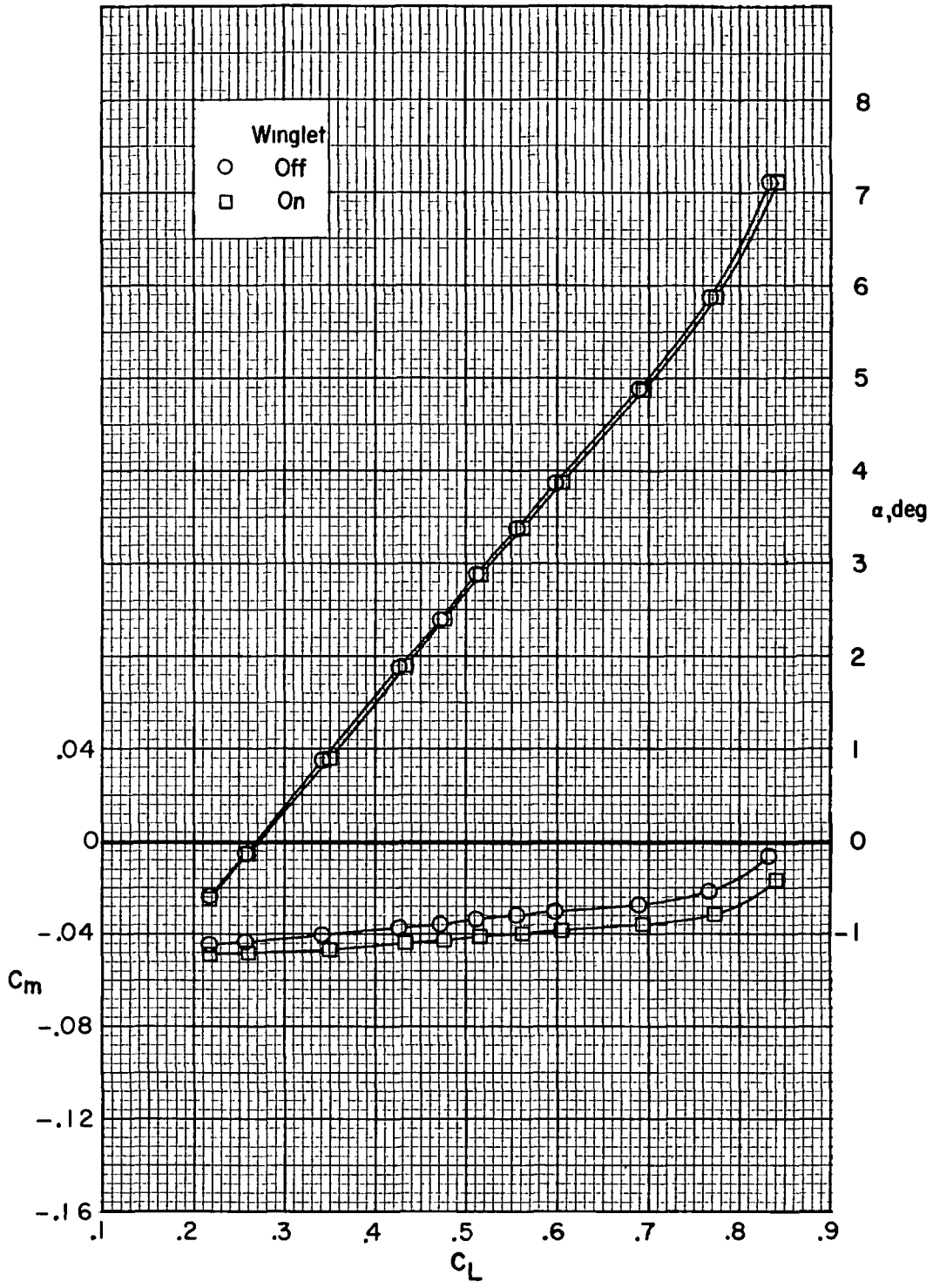

(c) $M_\infty = 0.75$.

Figure 10.- Continued.

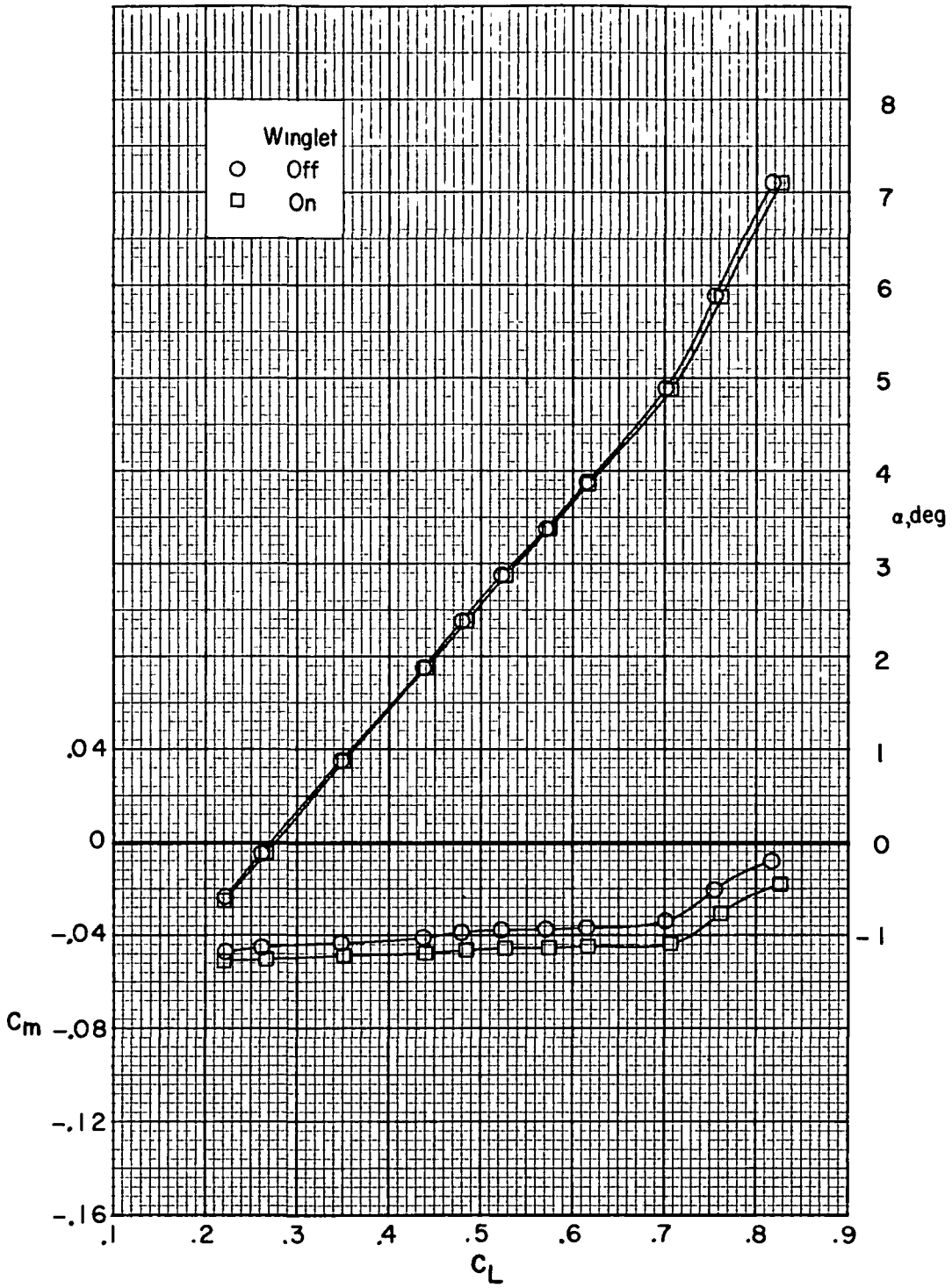

(d) $M_\infty = 0.78$.

Figure 10.- Continued.

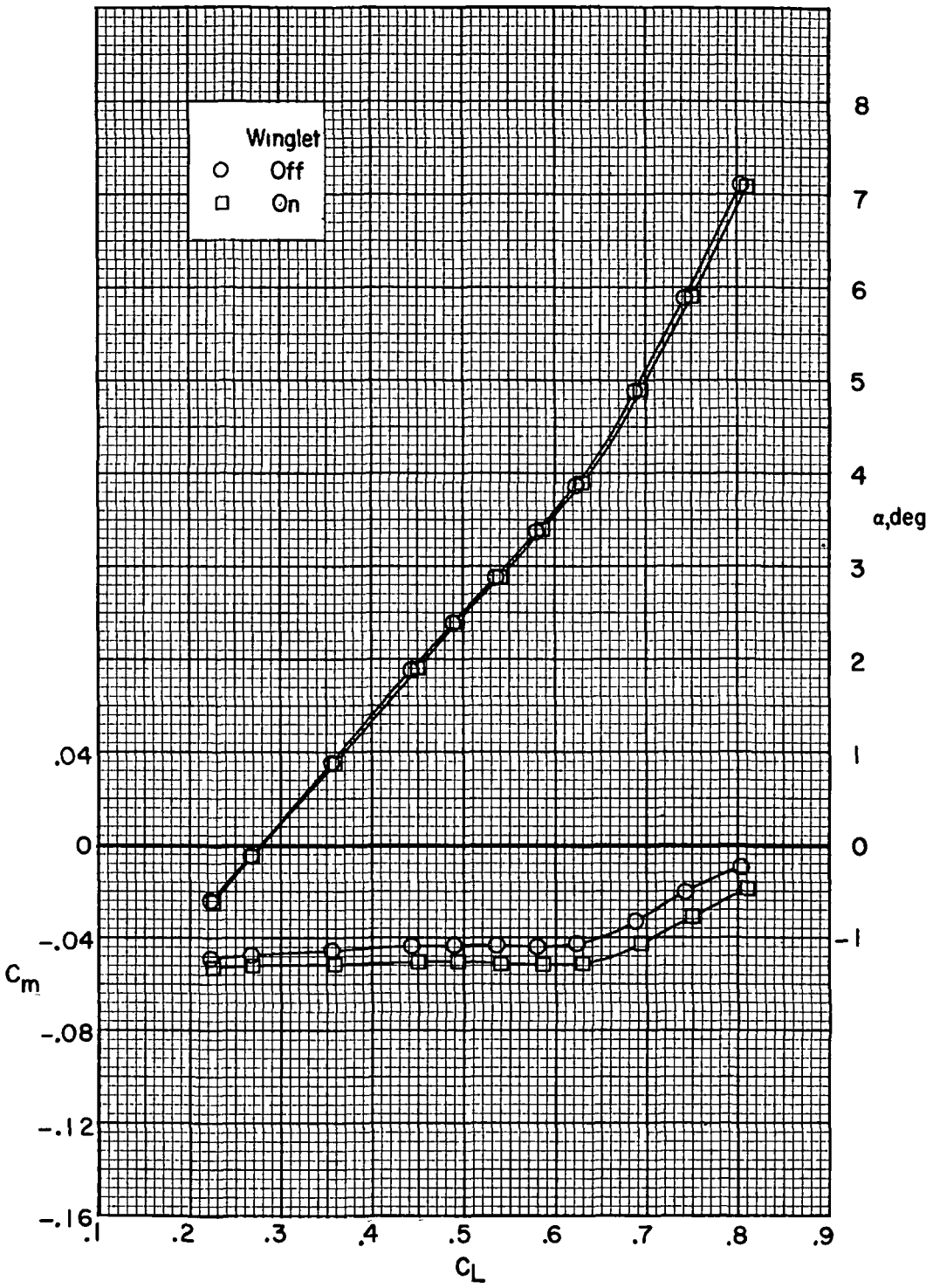

(e) $M_\infty = 0.80$.

Figure 10.- Concluded.

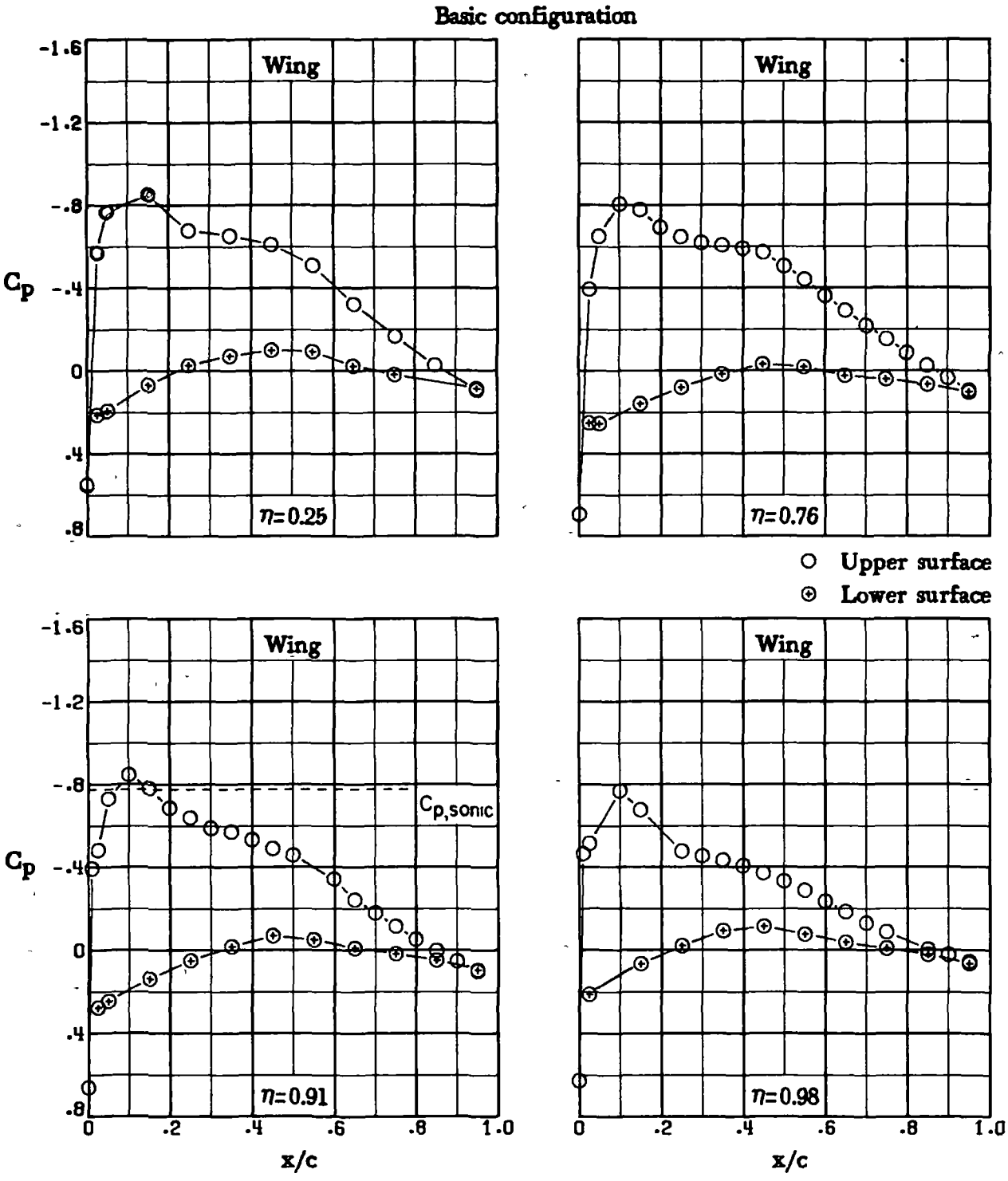

(a) $M_\infty = 0.70$; $\alpha = 2.5^\circ$.

Figure 11.- Chordwise pressure distributions for basic configuration.

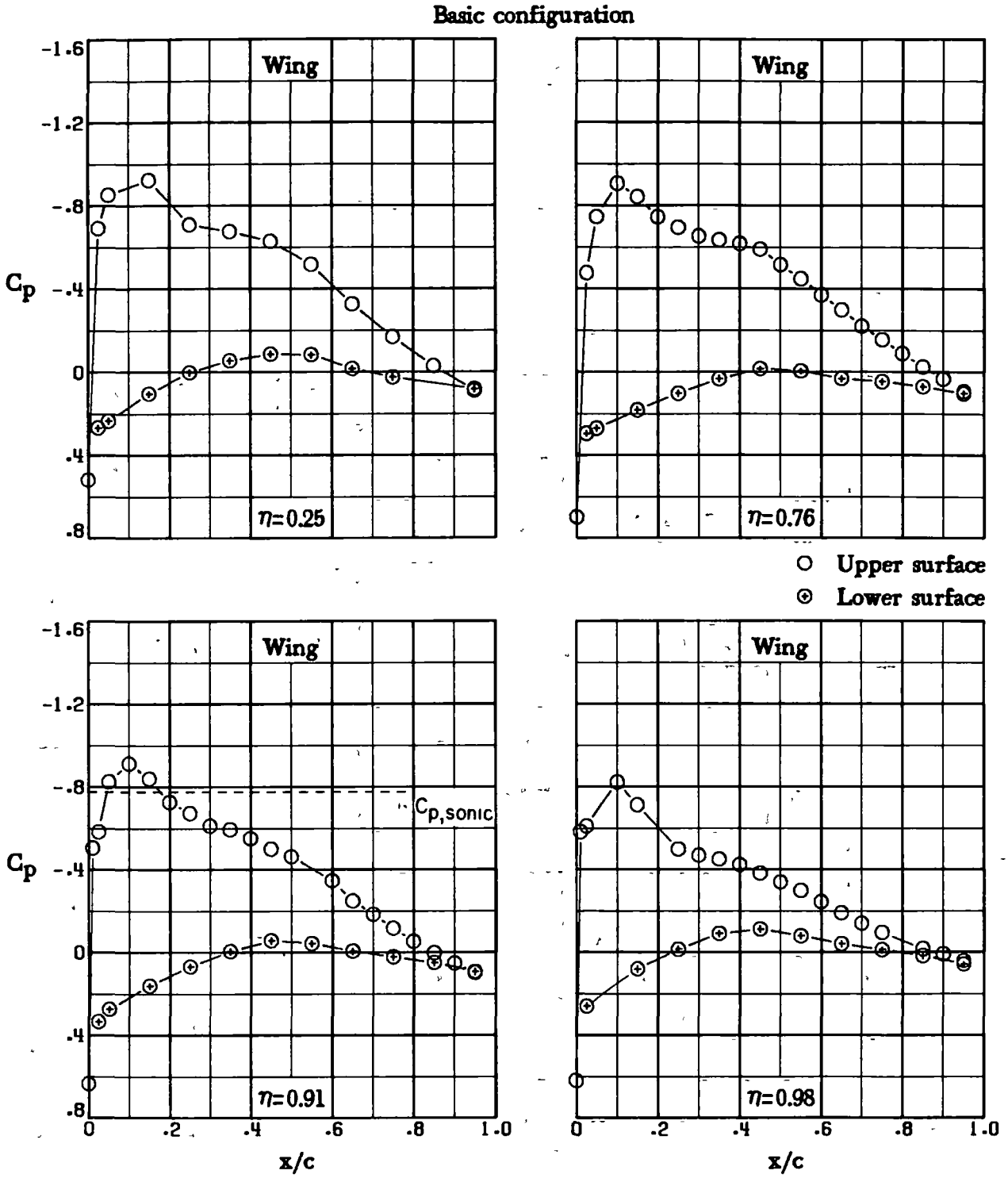

(b) $M_\infty = 0.70$; $\alpha = 3.0^\circ$.

Figure 11.- Continued.

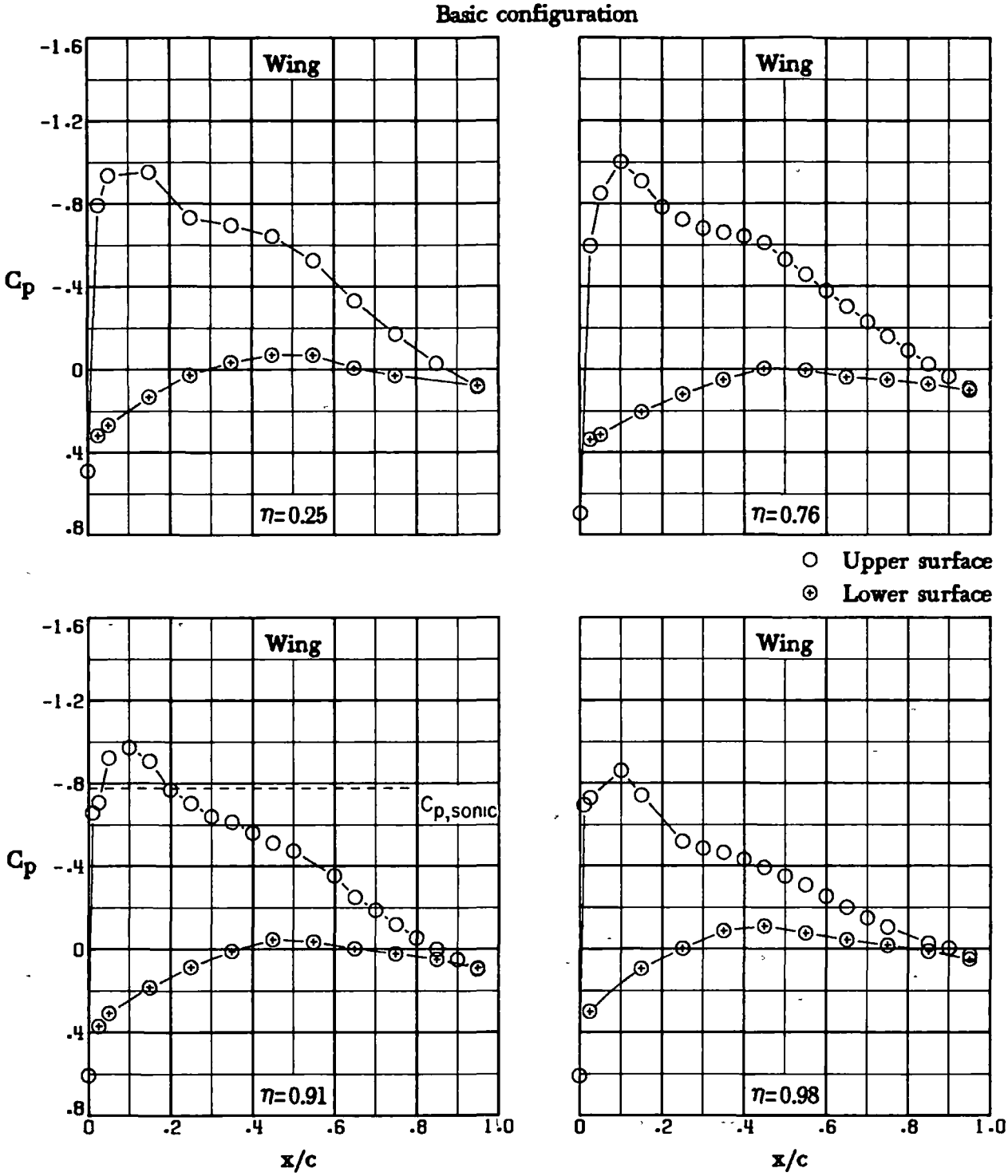

(c) $M_\infty = 0.70$; $\alpha = 3.5^\circ$.

Figure 11.- Continued.

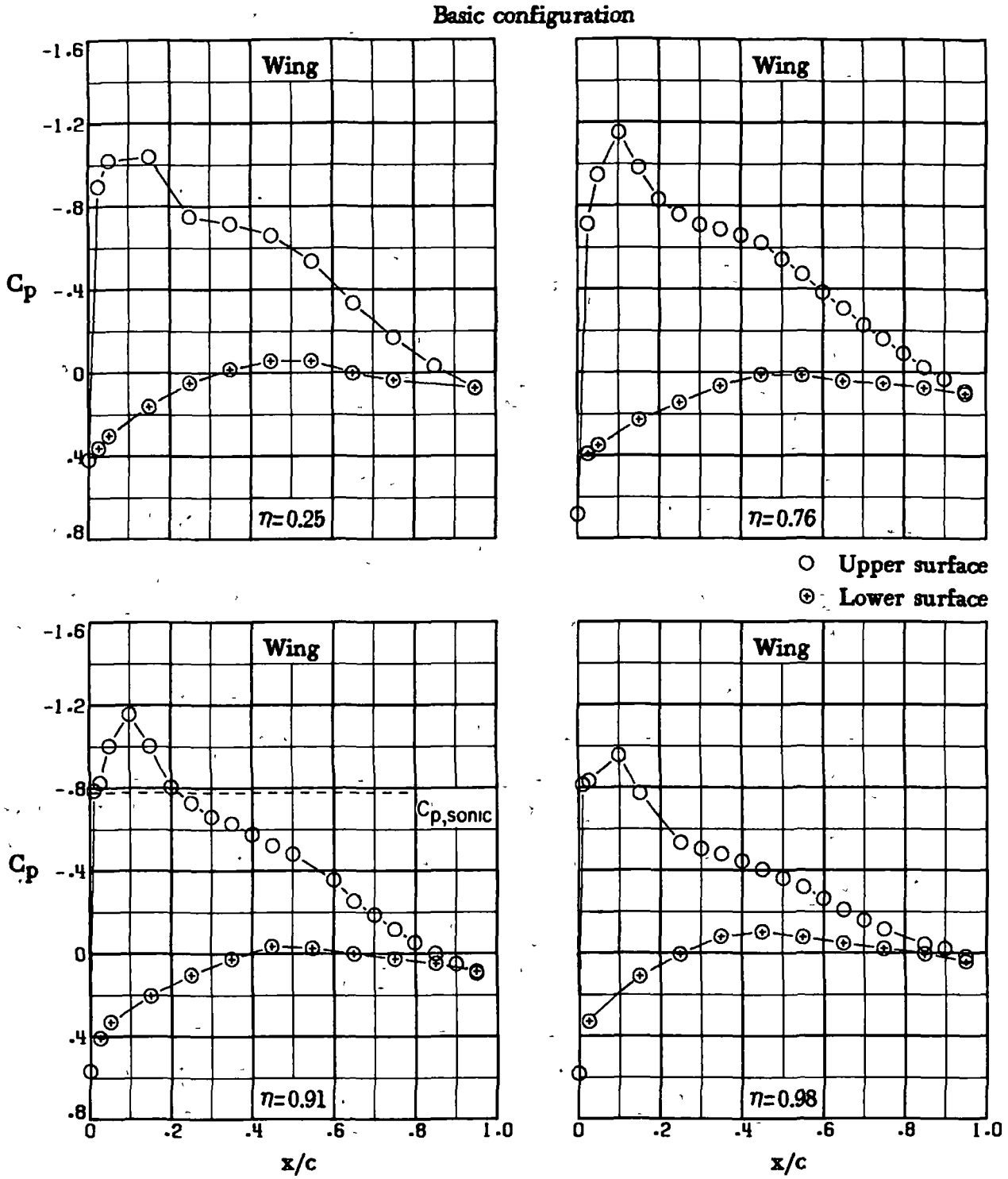

(d) $M_\infty = 0.70$; $\alpha = 4.0^\circ$.

Figure 11.- Continued.

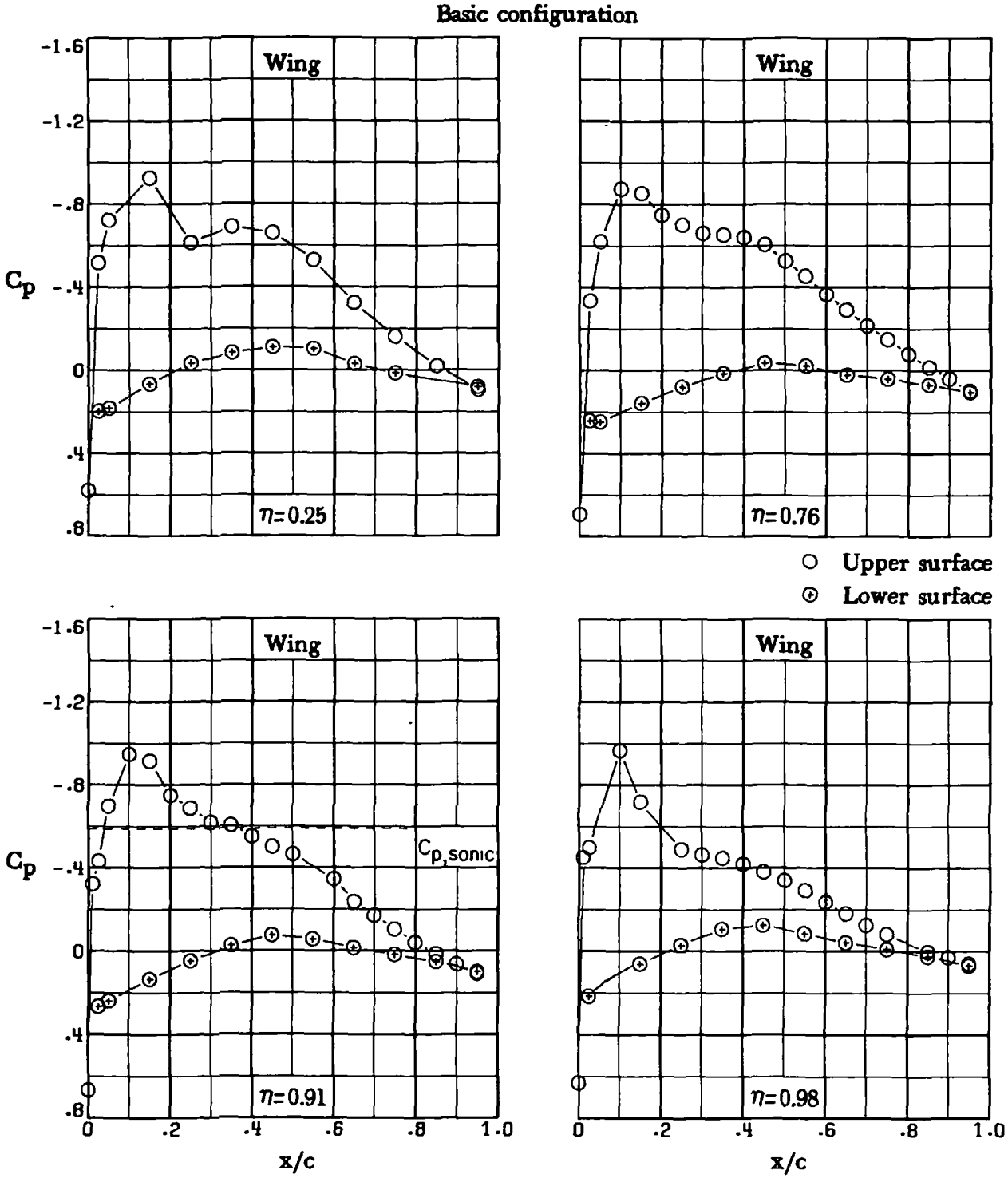

(e) $M_\infty = 0.75$; $\alpha = 2.5^\circ$.

Figure 11.- Continued.

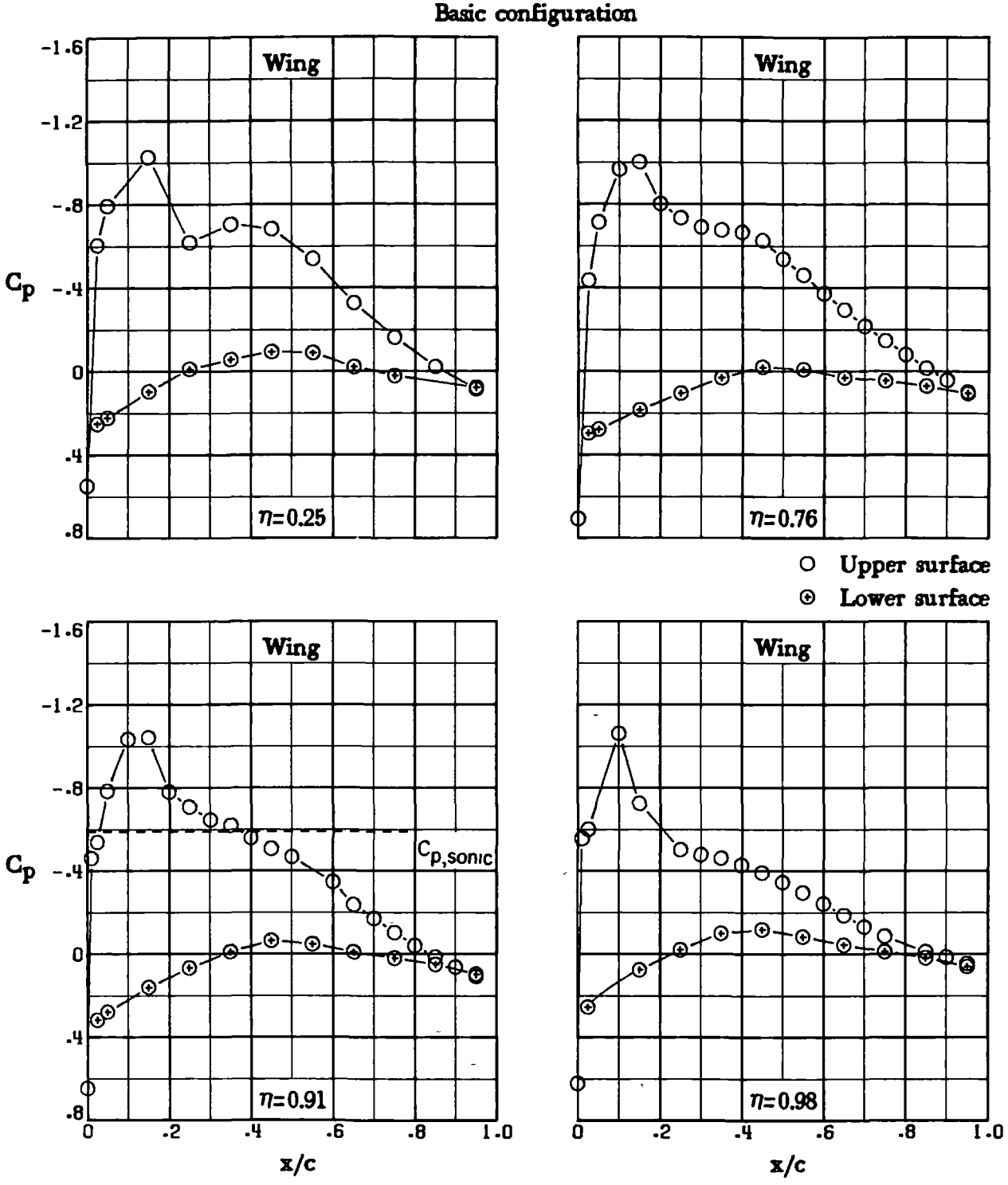

(f) $M_\infty = 0.75$; $\alpha = 3.0^\circ$.

Figure 11.- Continued.

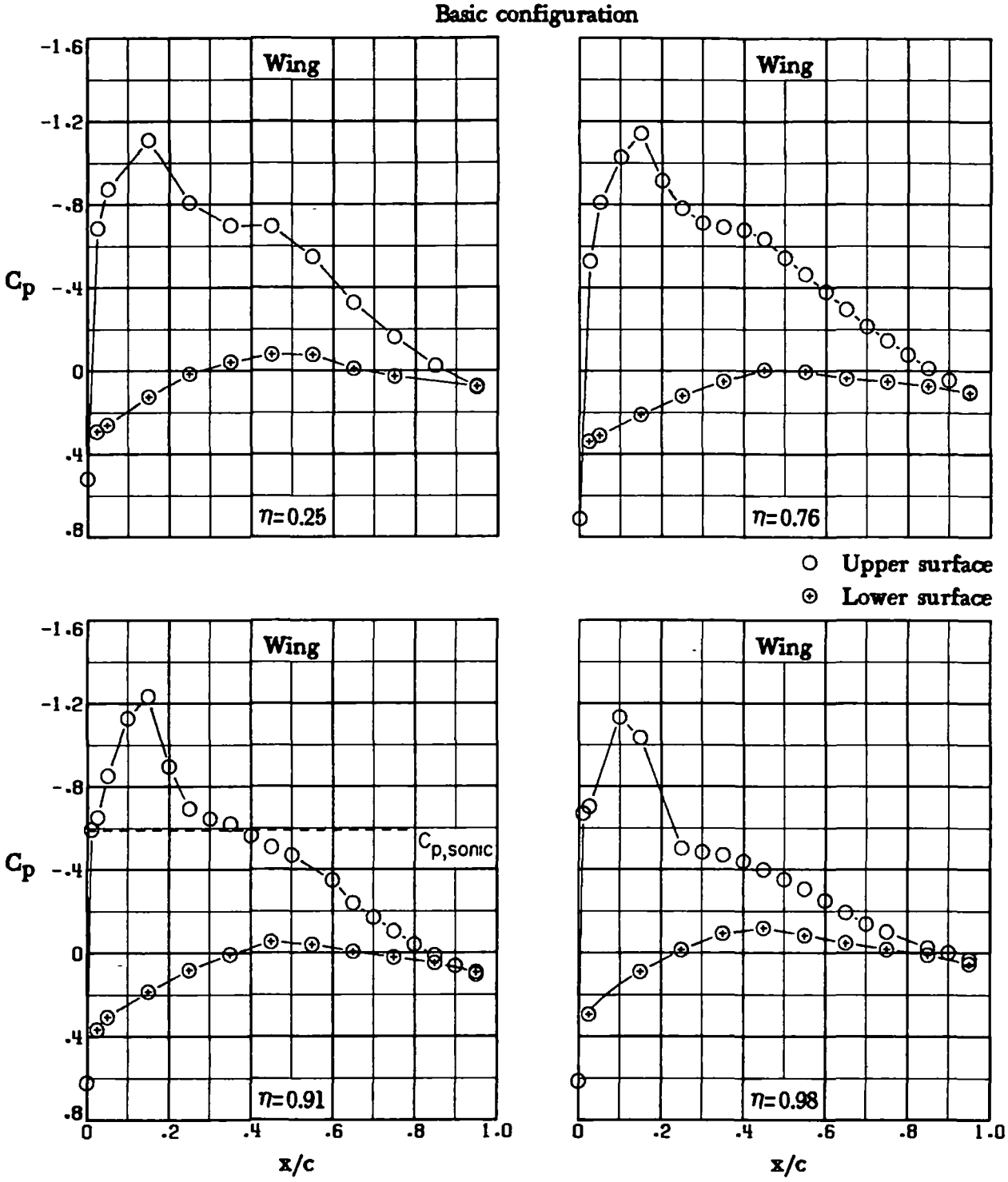

(g) $M_\infty = 0.75$; $\alpha = 3.5^\circ$.

Figure 11.- Continued.

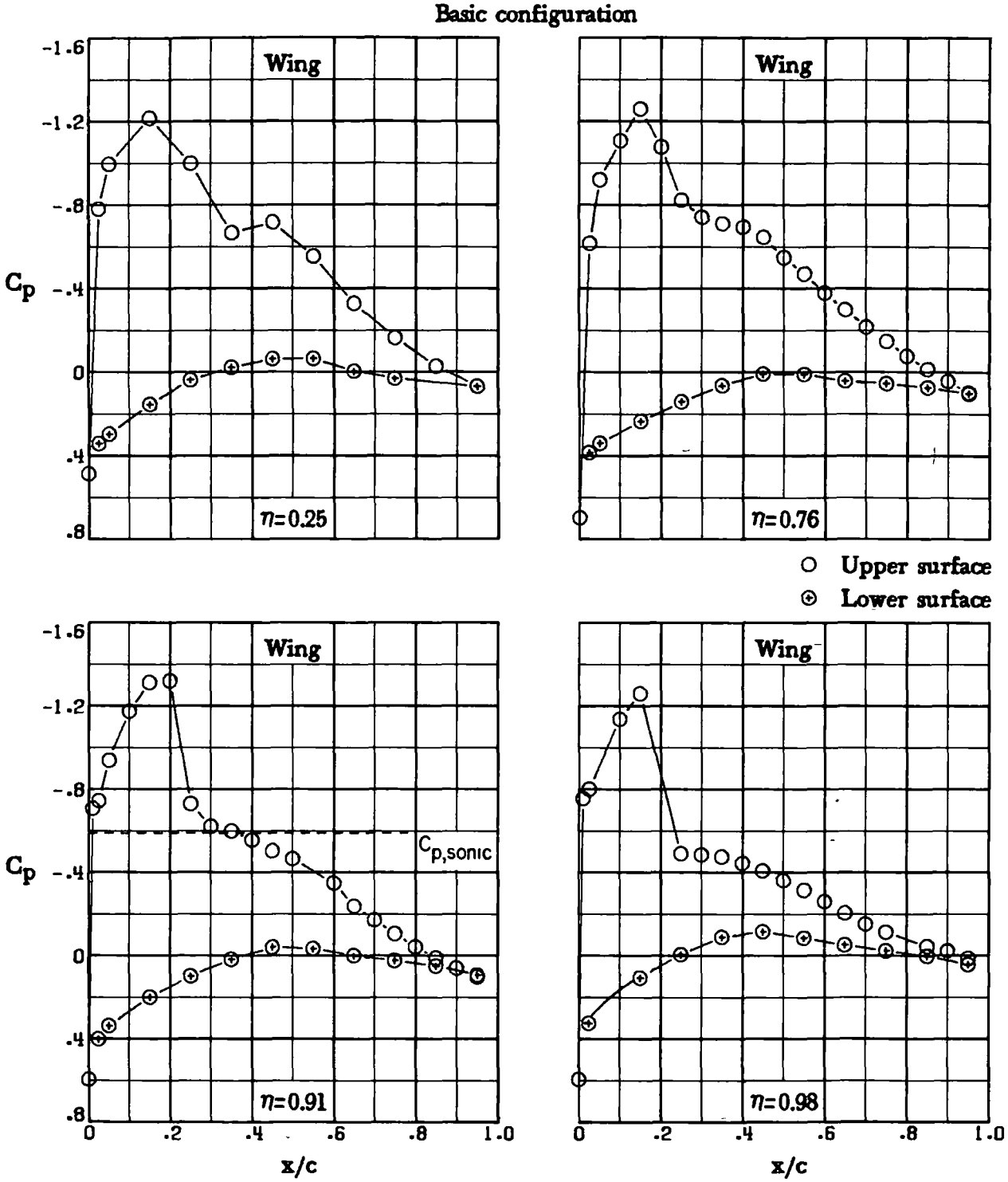

(h) $M_\infty = 0.75$; $\alpha = 4.0^\circ$.

Figure 11.- Continued.

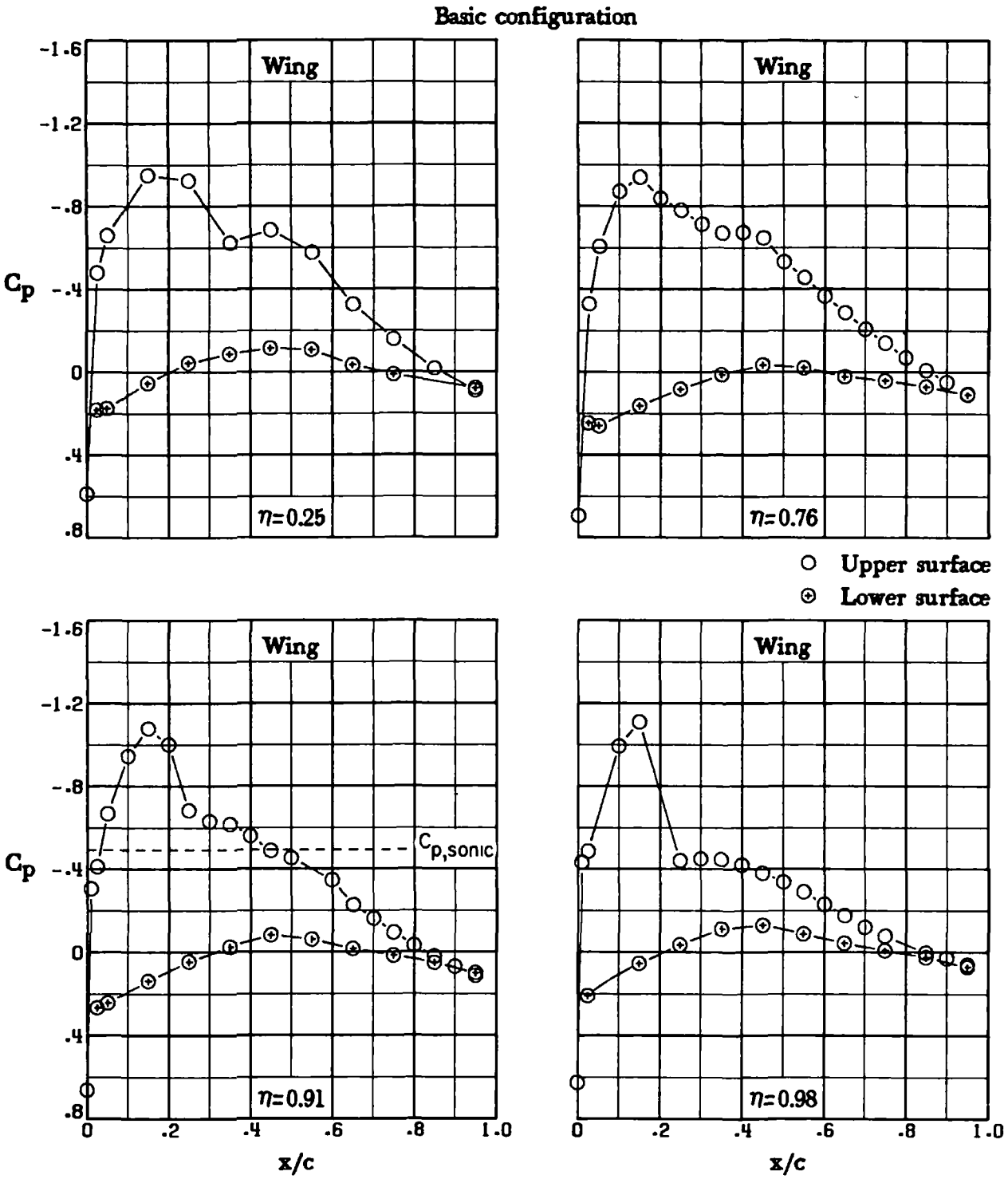

(i) $M_\infty = 0.78$; $\alpha = 2.5^\circ$.

Figure 11.- Continued.

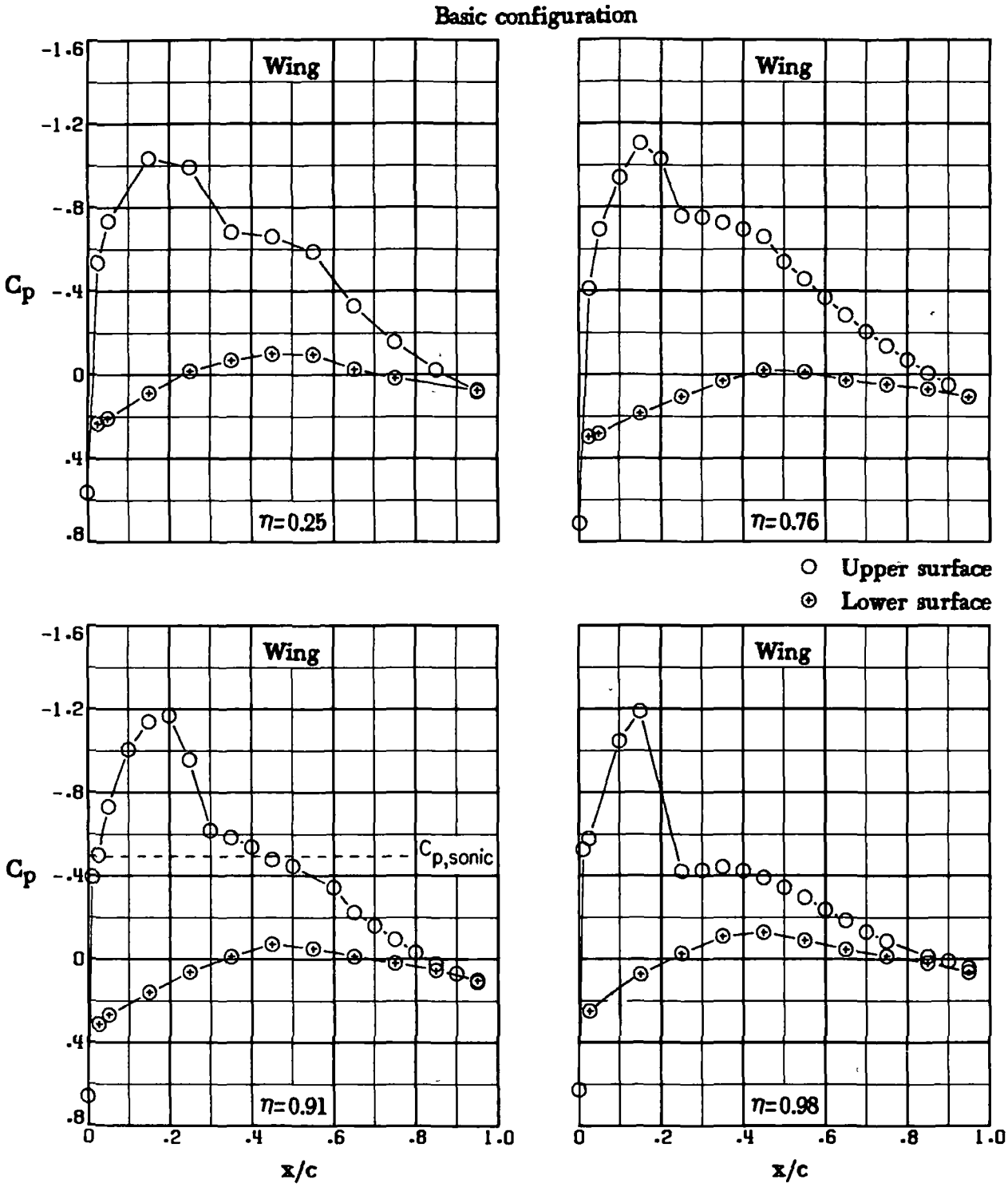

(j) $M_\infty = 0.78$; $\alpha = 3.0^\circ$.

Figure 11.- Continued.

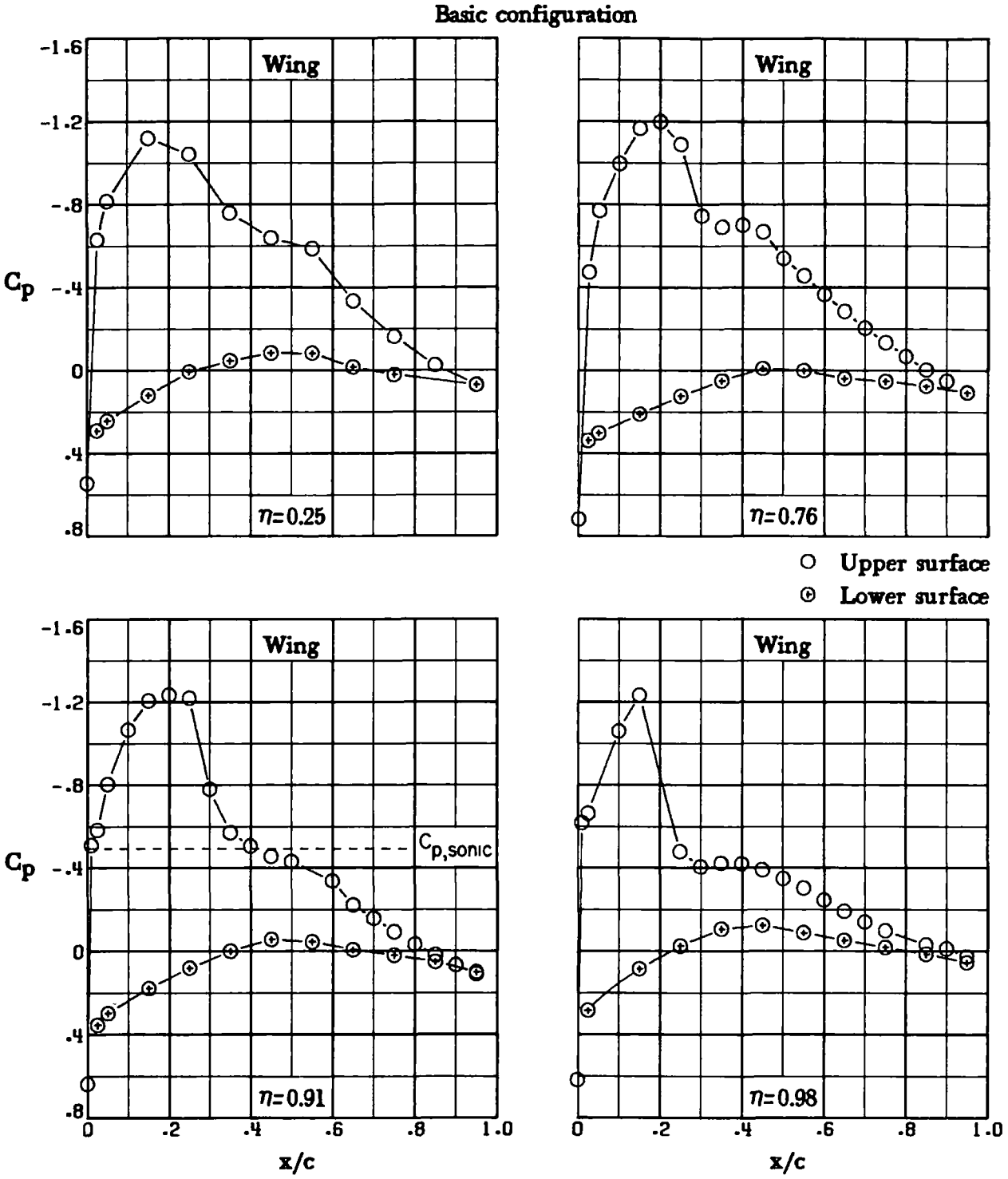

(k) $M_\infty = 0.78$; $\alpha = 3.5^\circ$.

Figure 11.- Continued.

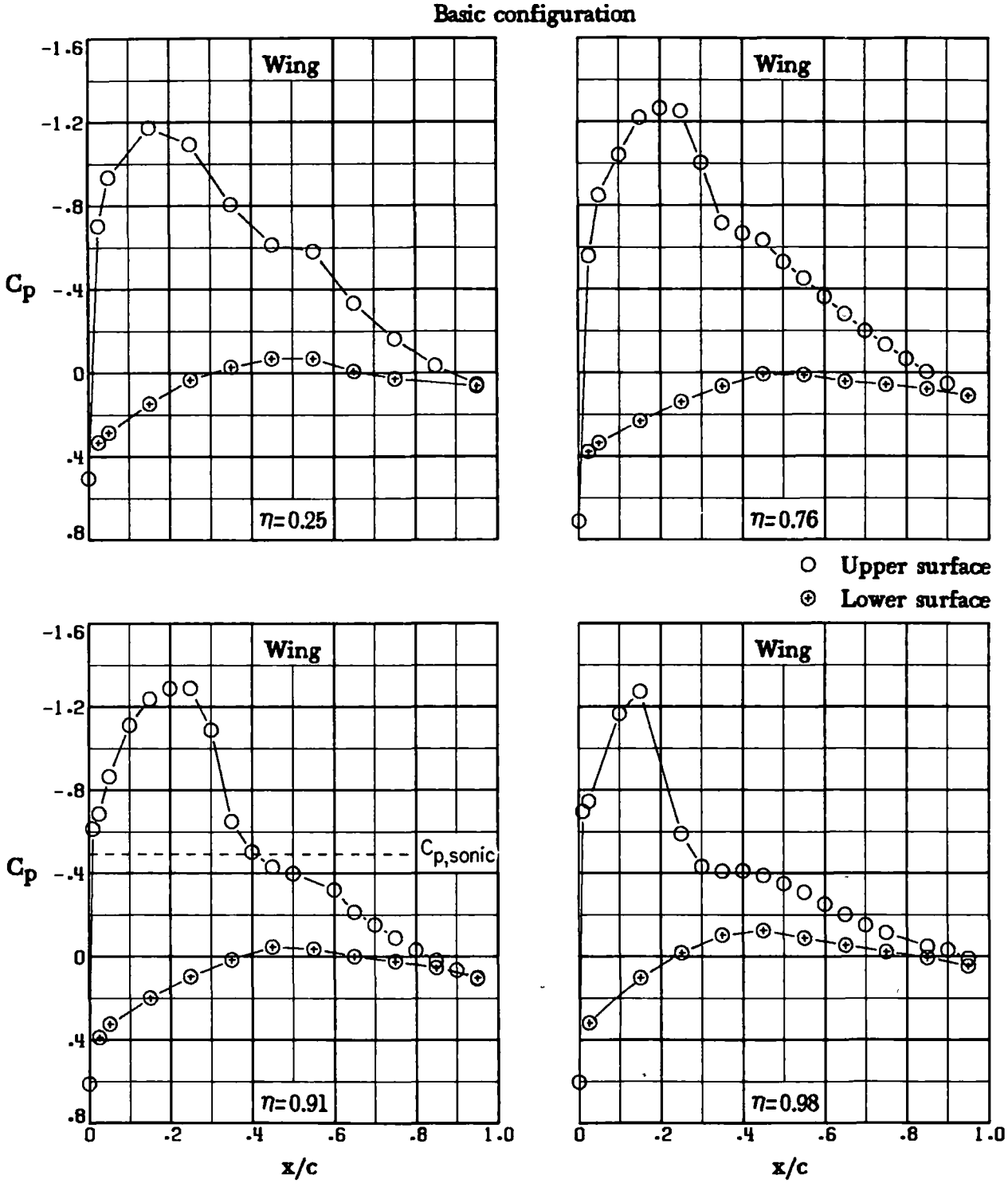

(1) $M_\infty = 0.78$; $\alpha = 4.0^o$.

Figure 11.- Continued.

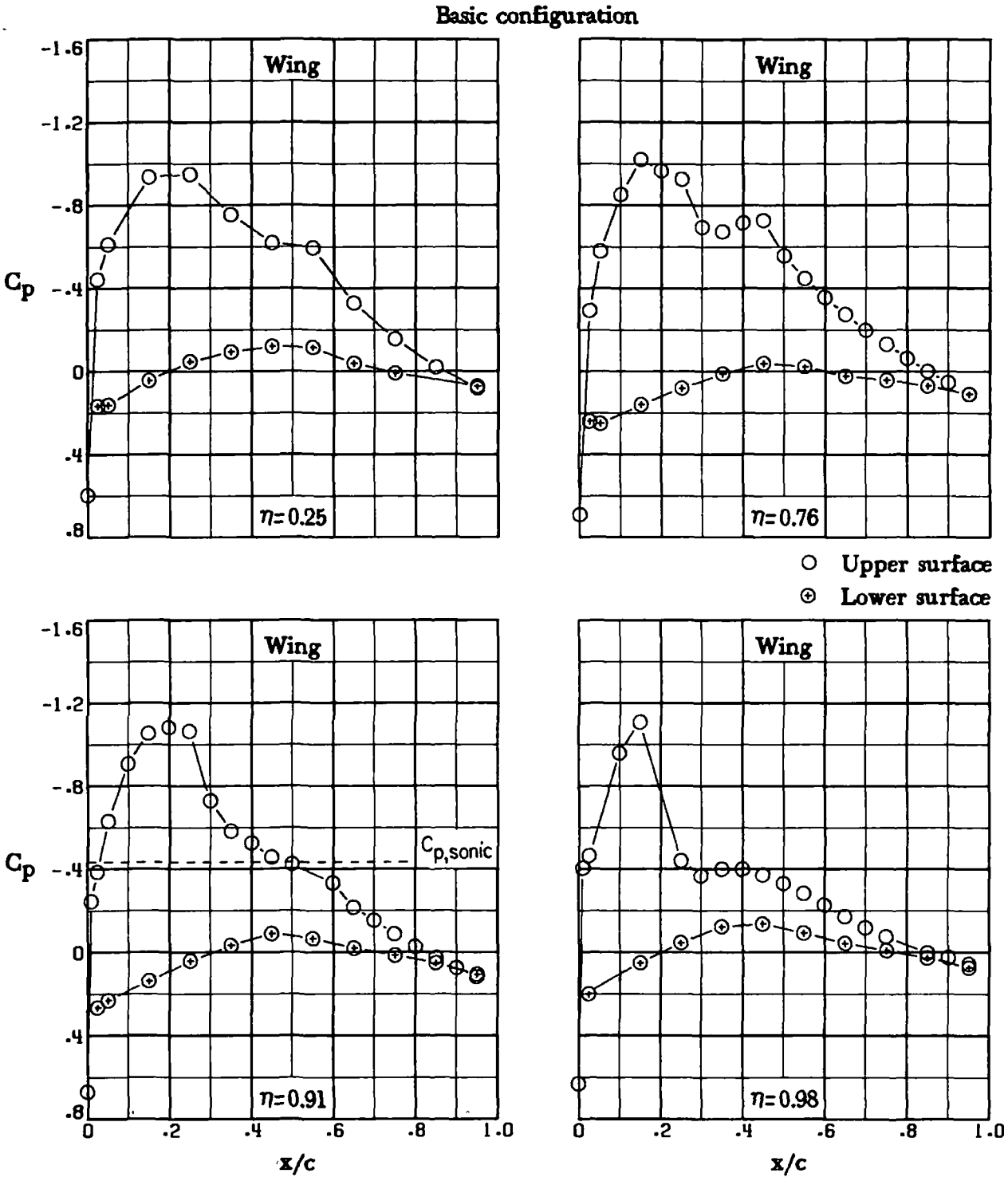

(m) $M_\infty = 0.80$; $\alpha = 2.5^\circ$.

Figure 11.- Continued.

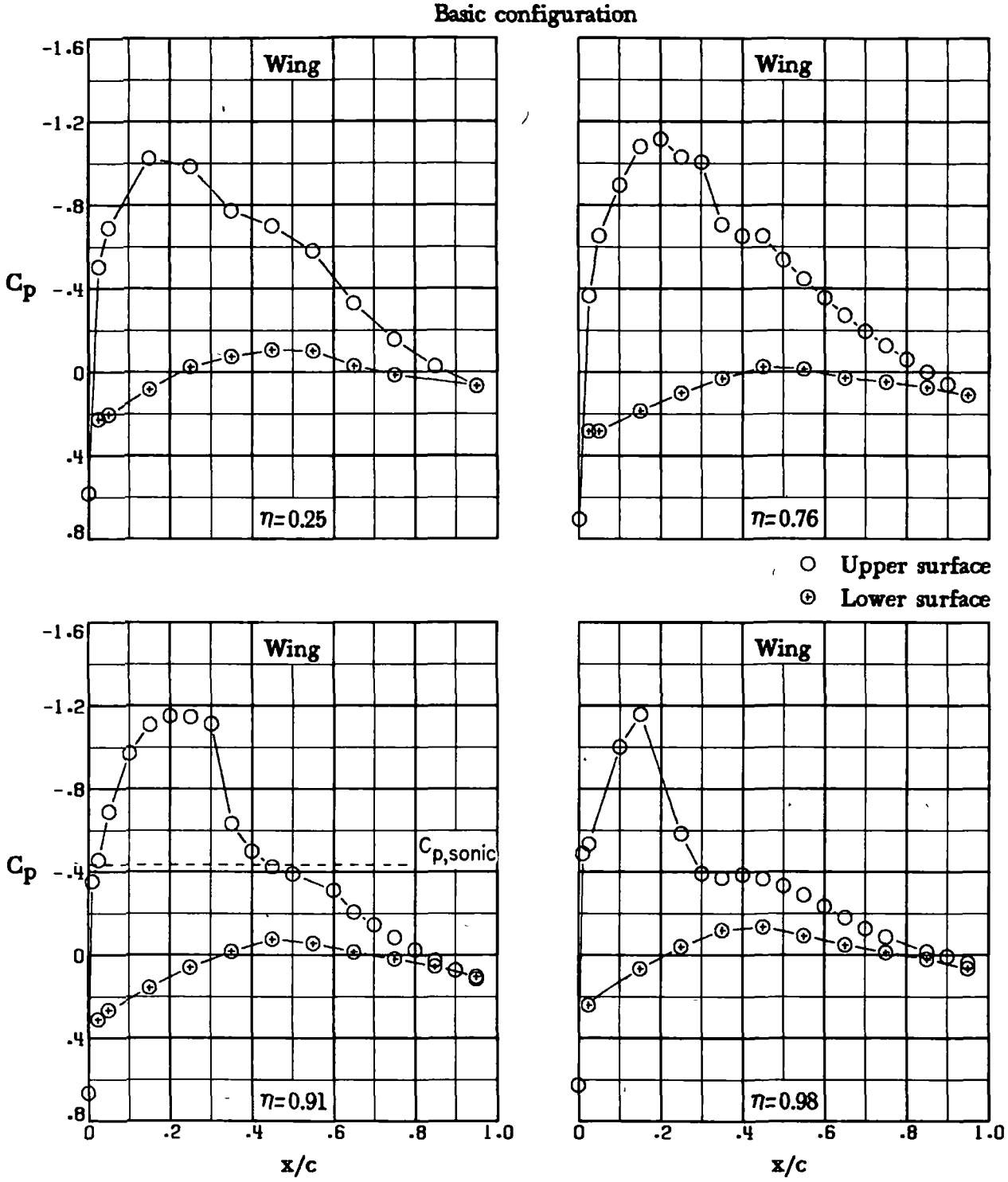

(n) $M_\infty = 0.80$; $\alpha = 3.0^\circ$.

Figure 11.- Continued.

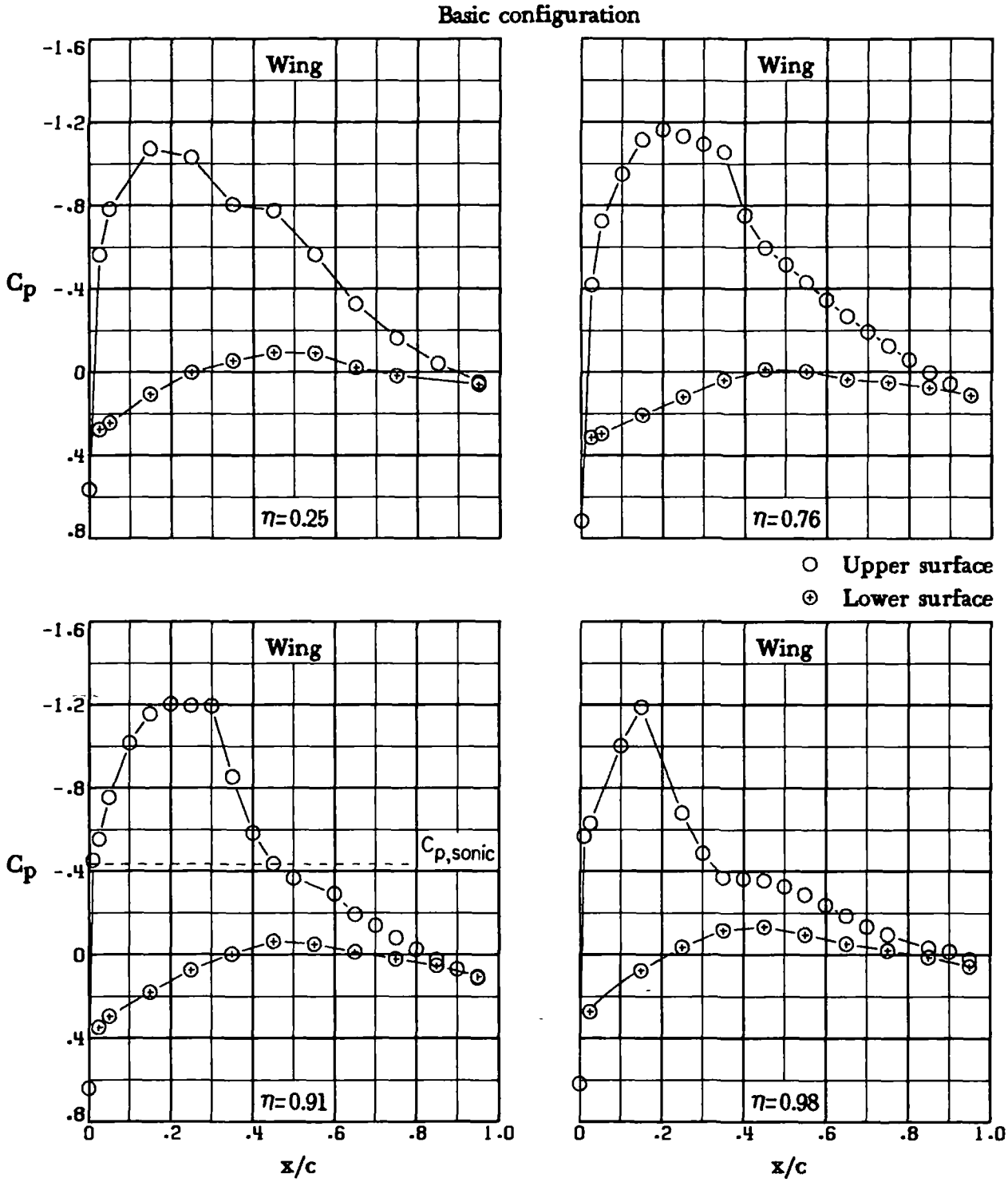

(o) $M_\infty = 0.80$; $\alpha = 3.5^o$.

Figure 11.- Continued.

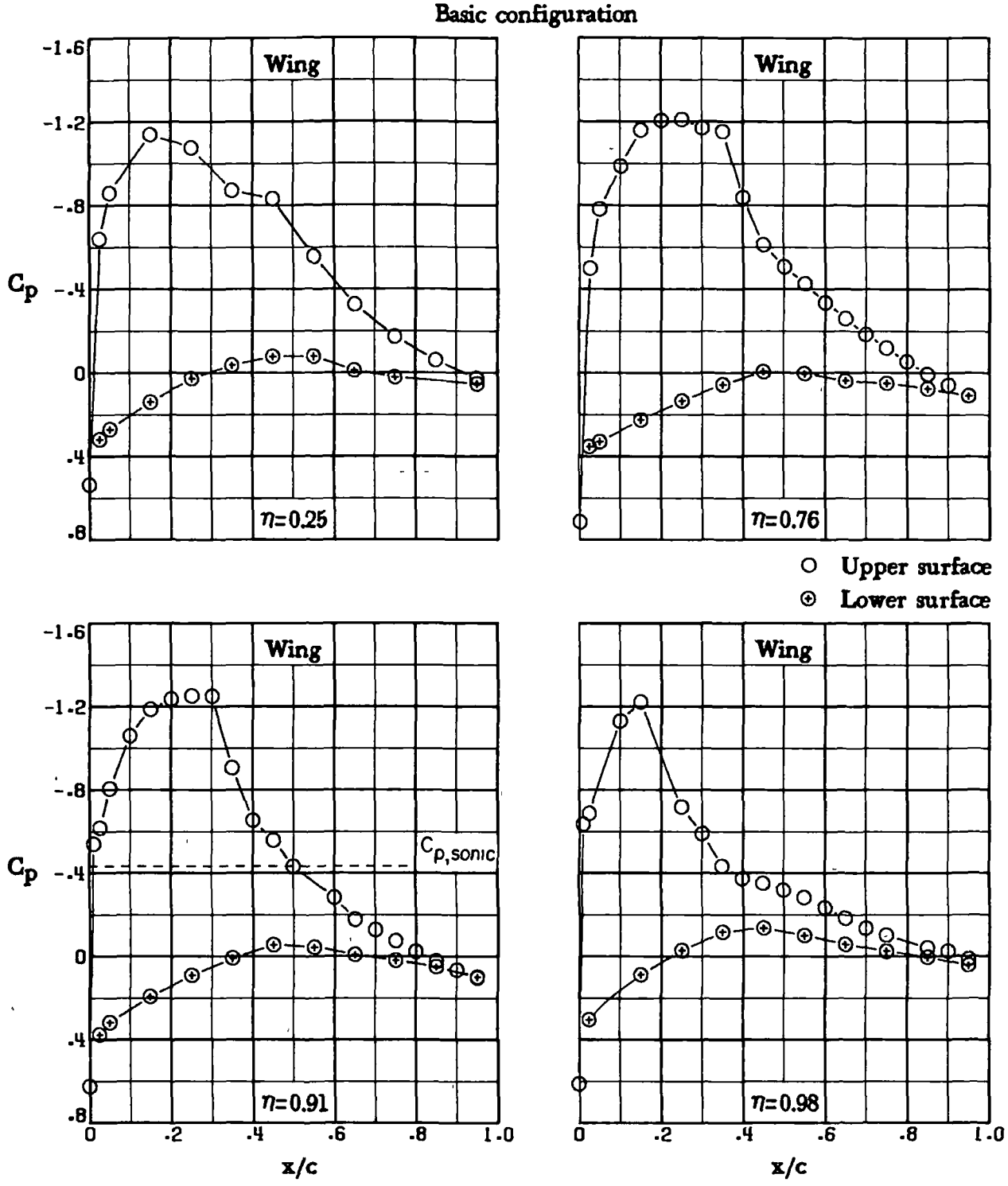

(p) $M_\infty = 0.80$; $\alpha = 4.0^\circ$.

Figure 11.- Concluded.

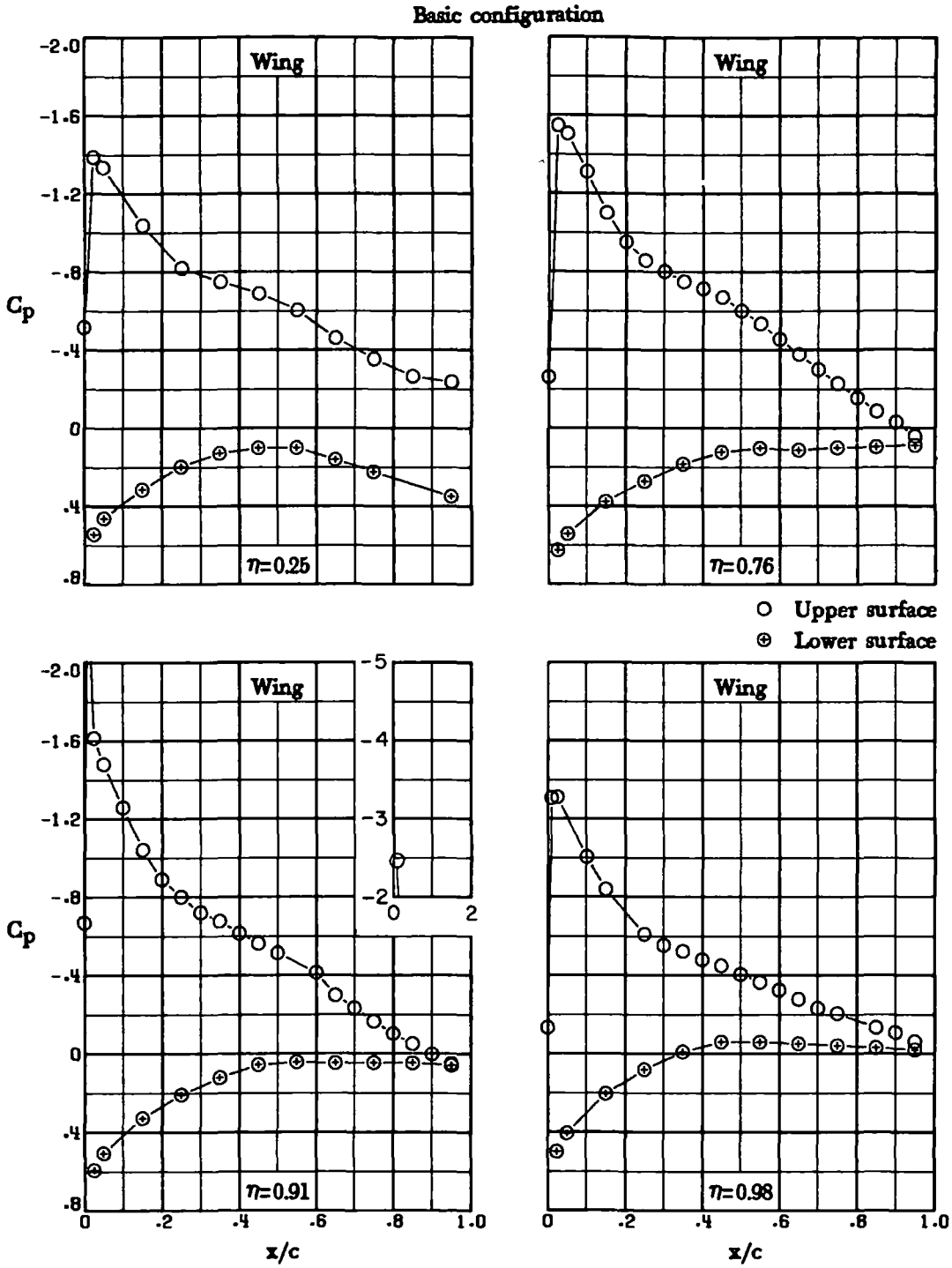

(a) $\alpha = 5^{\circ}$.

Figure 12.- Chordwise pressure distributions for basic configuration with trailing-edge flaps. $M_{\infty} = 0.30$.

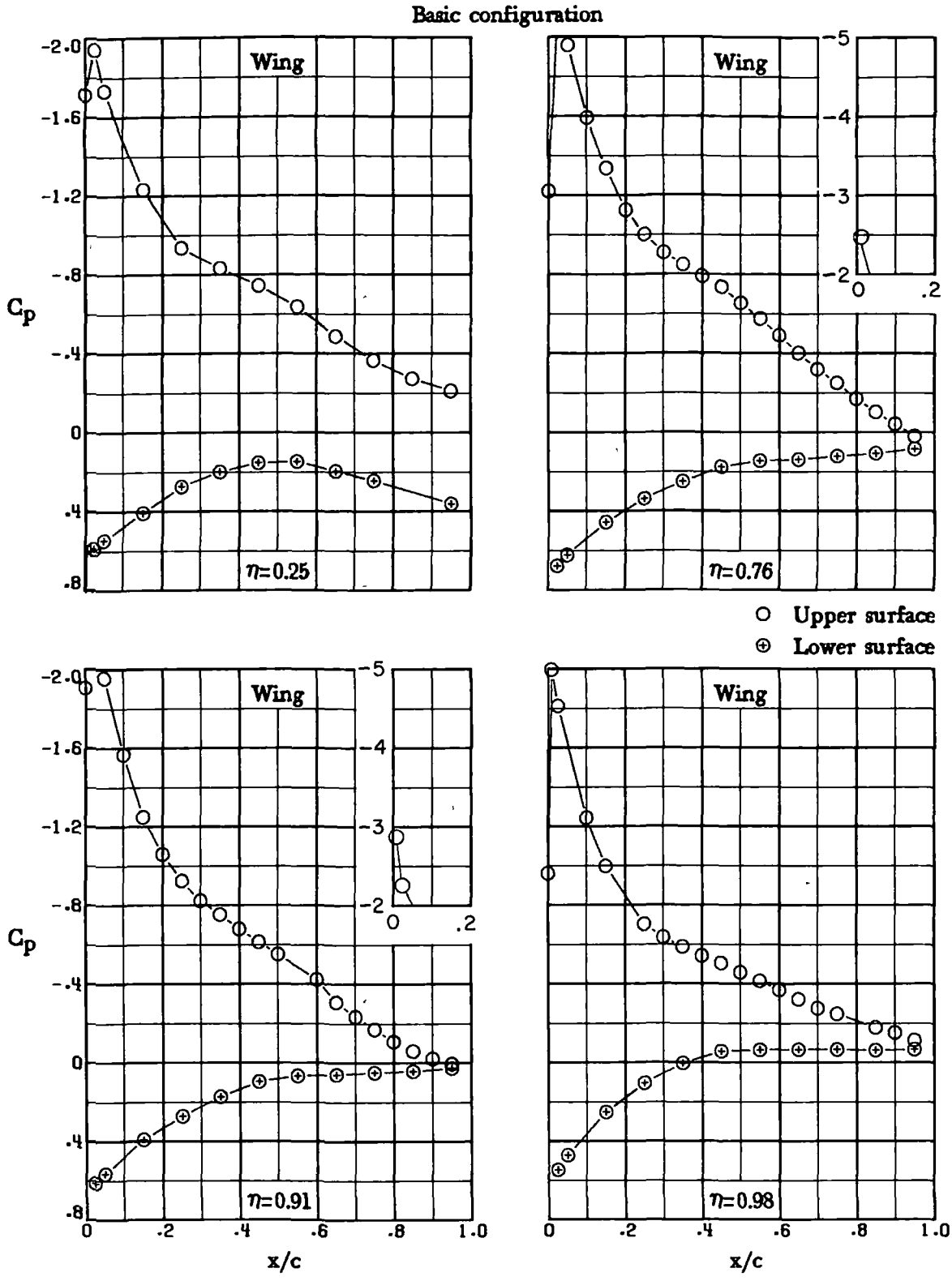

(b) $\alpha = 7^{\circ}$.

Figure 12.- Continued.

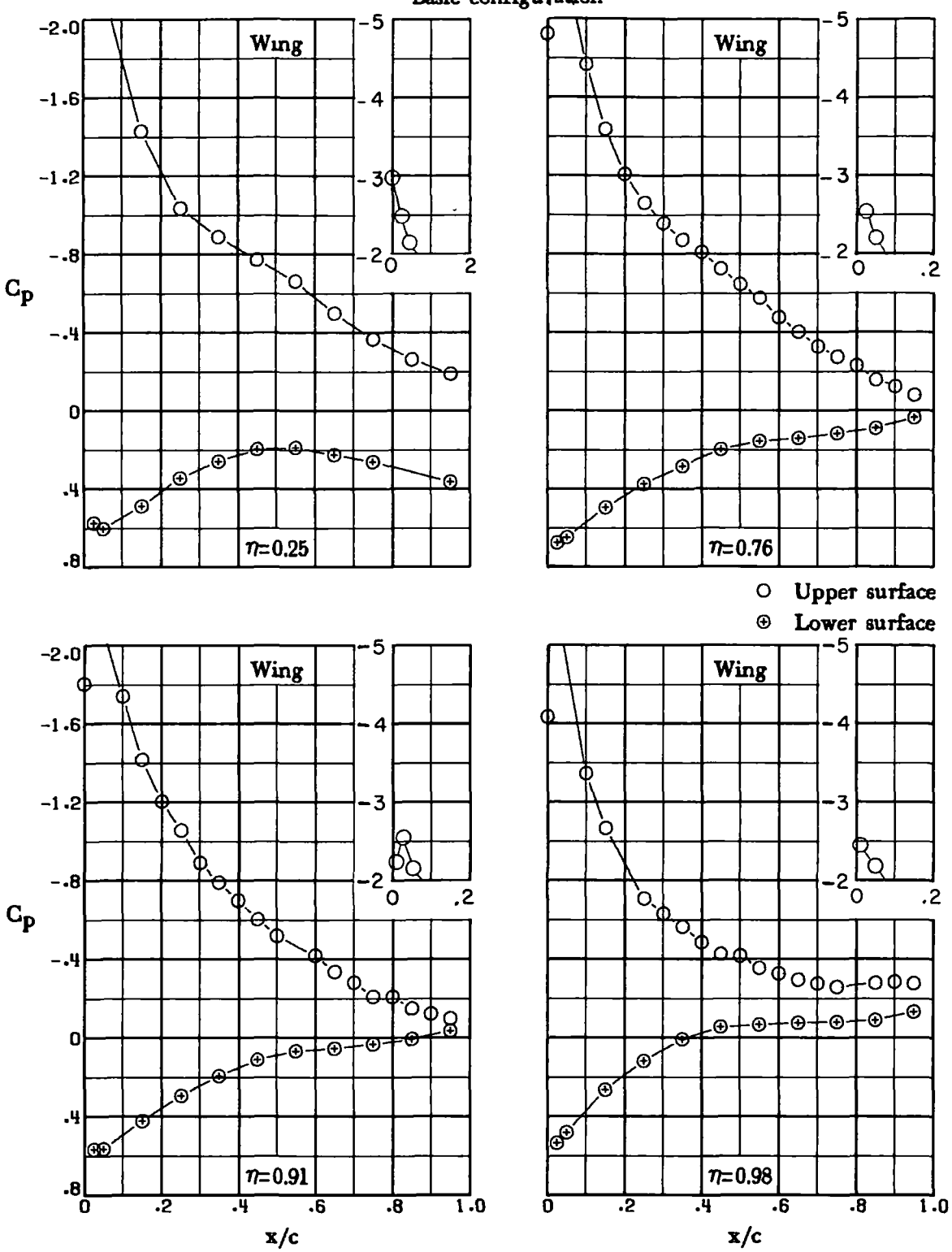

(c) $\alpha = 9^{o}$.

Figure 12.- Continued.

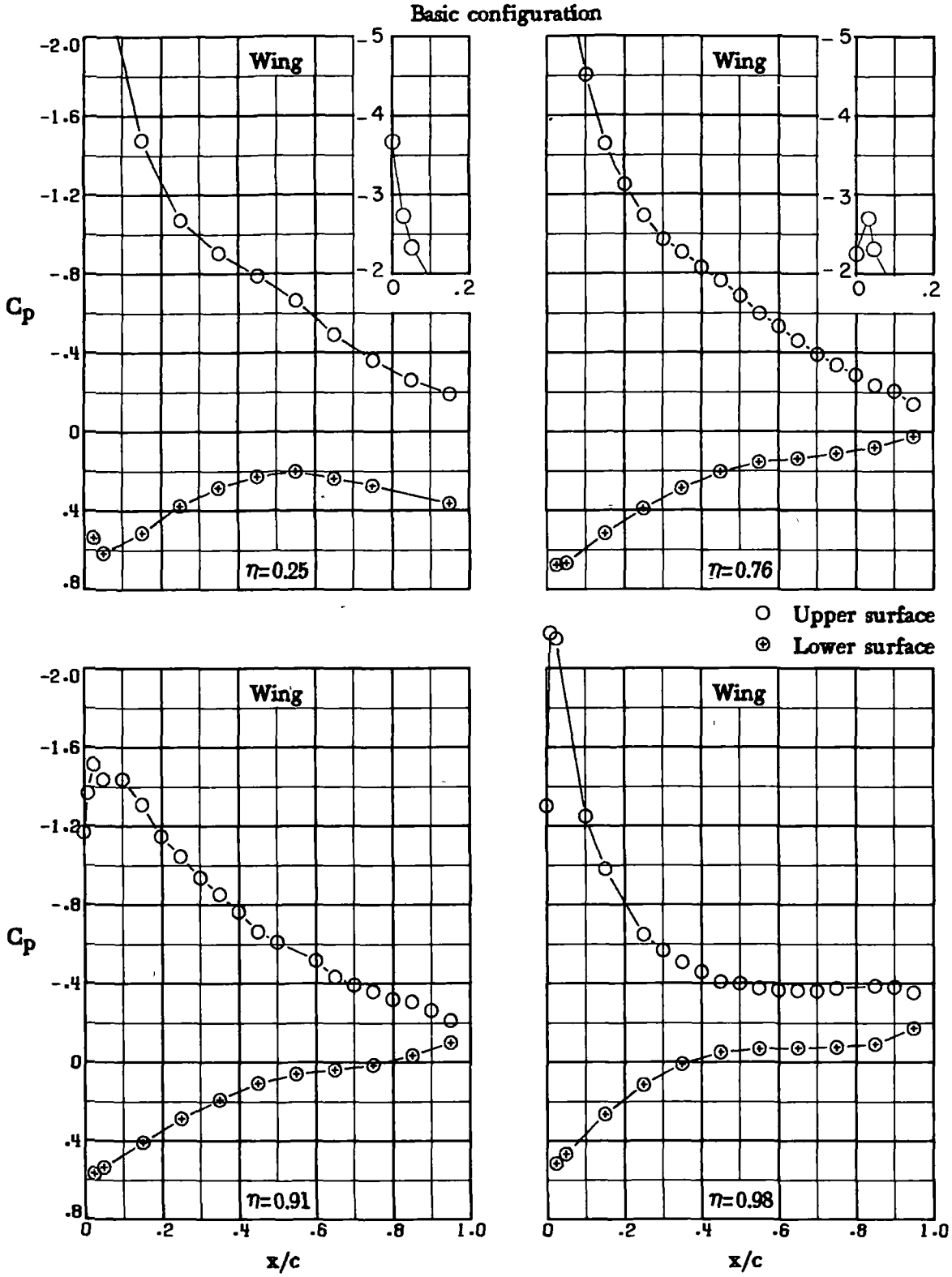

(d) $\alpha = 10^{\circ}$.

Figure 12.- Continued.

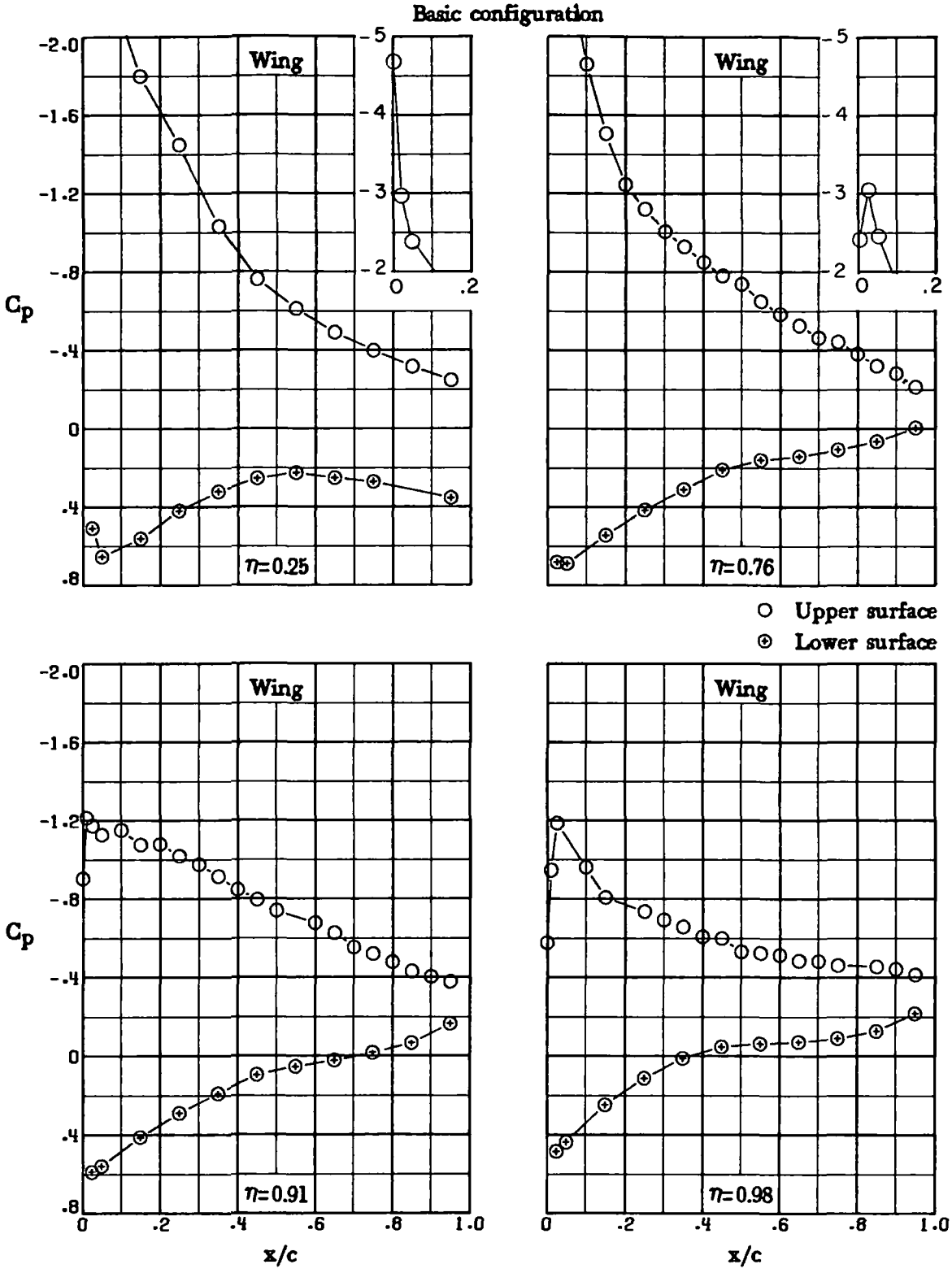

(e) $\alpha = 12^{\circ}$.

Figure 12.- Concluded.

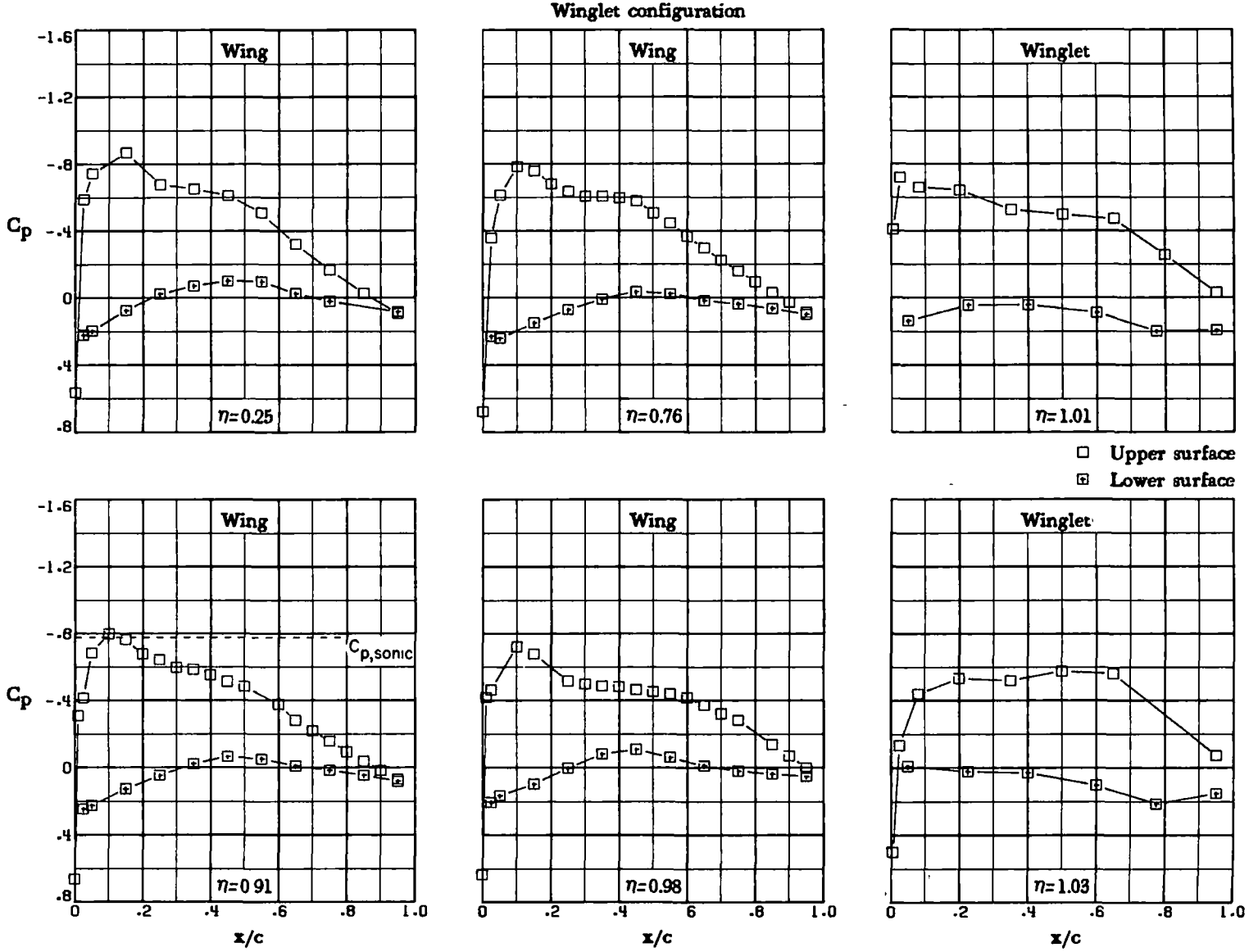

(a) $M_\infty = 0.70$; $\alpha = 2.5^\circ$.

Figure 13.- Chordwise pressure distributions for winglet configuration.

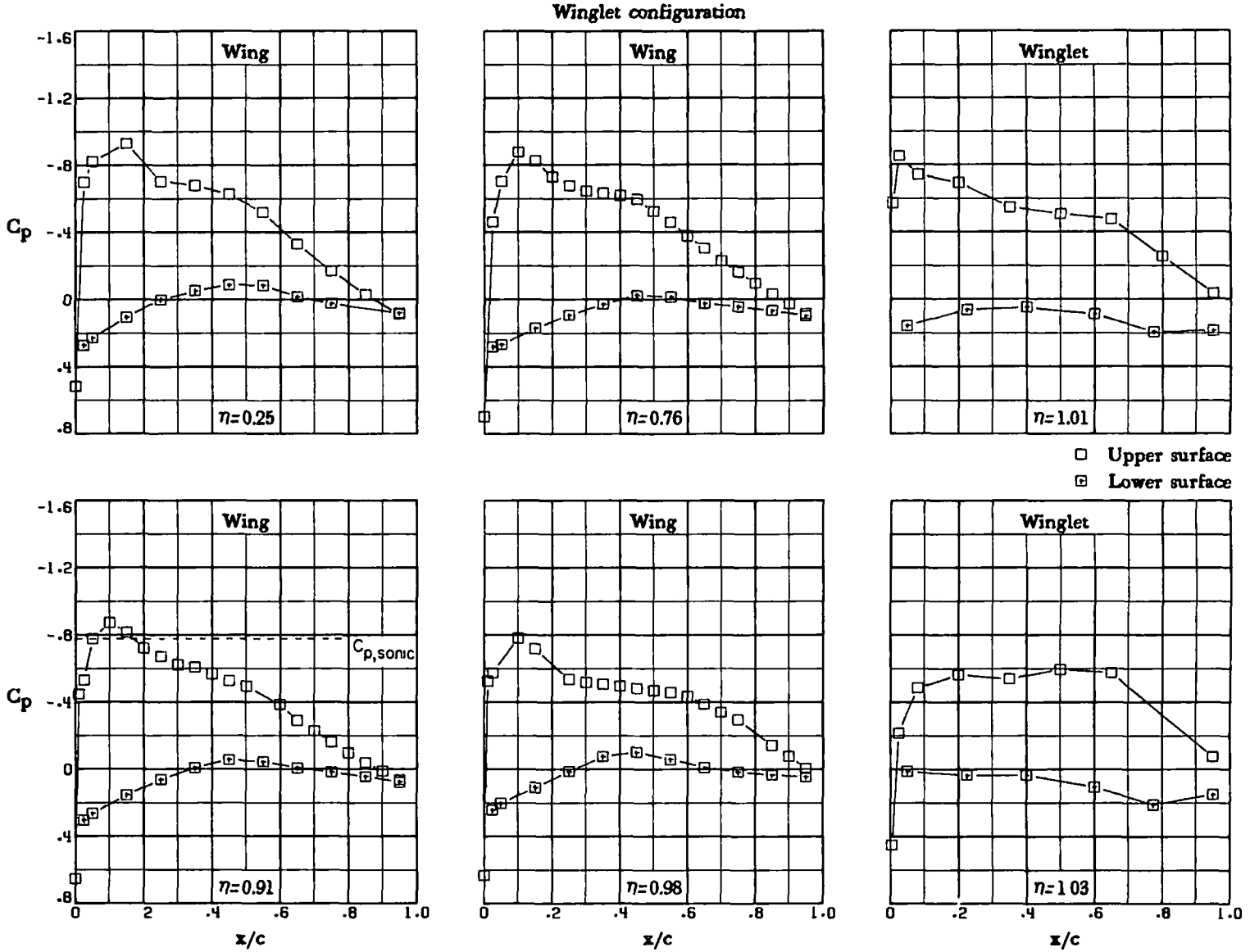

(b) $M_\infty = 0.70$; $\alpha = 3.0^\circ$.

Figure 13.- Continued.

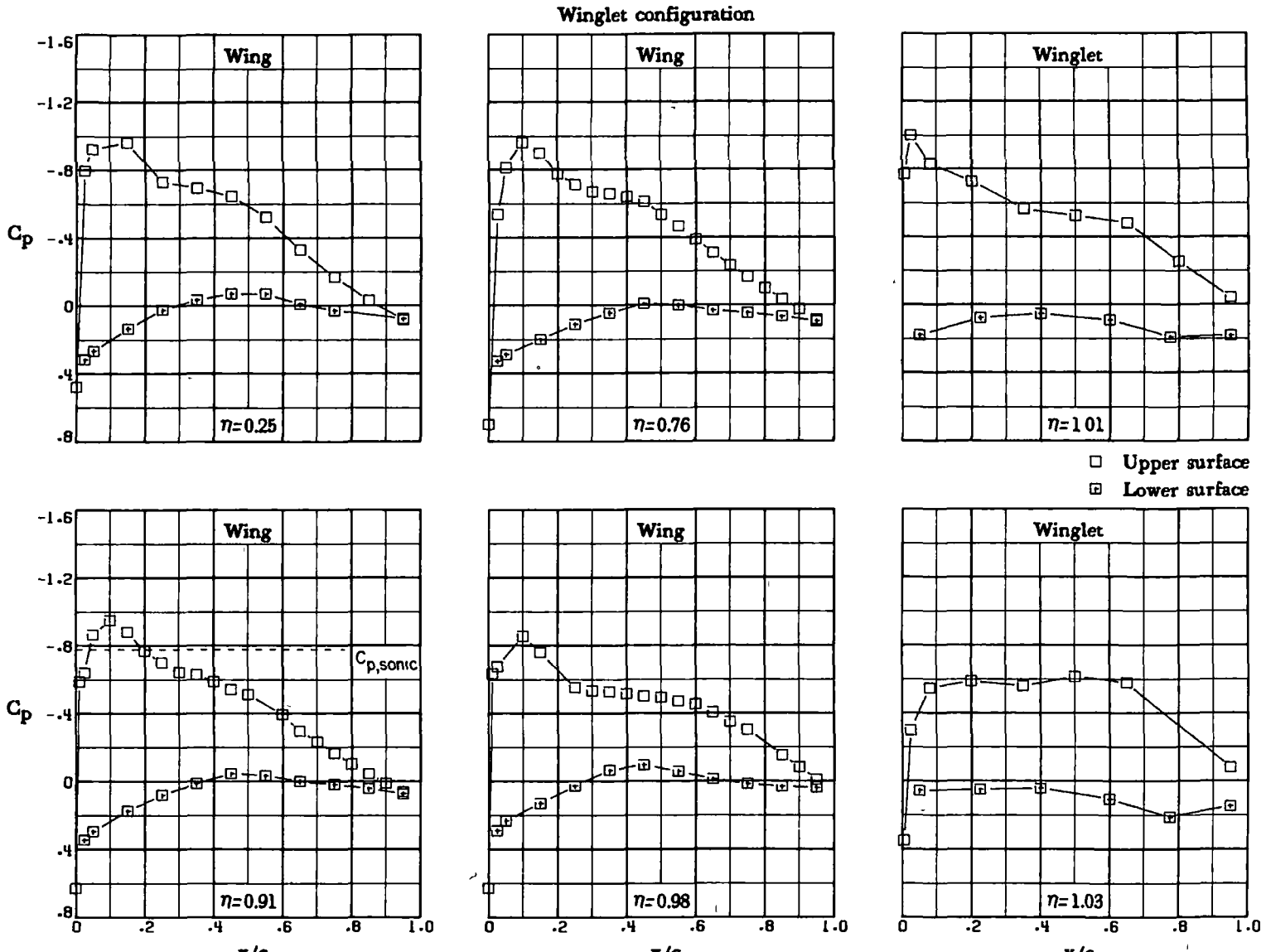

(c) $M_\infty = 0.70$; $\alpha = 3.5^\circ$.

Figure 13.- Continued.

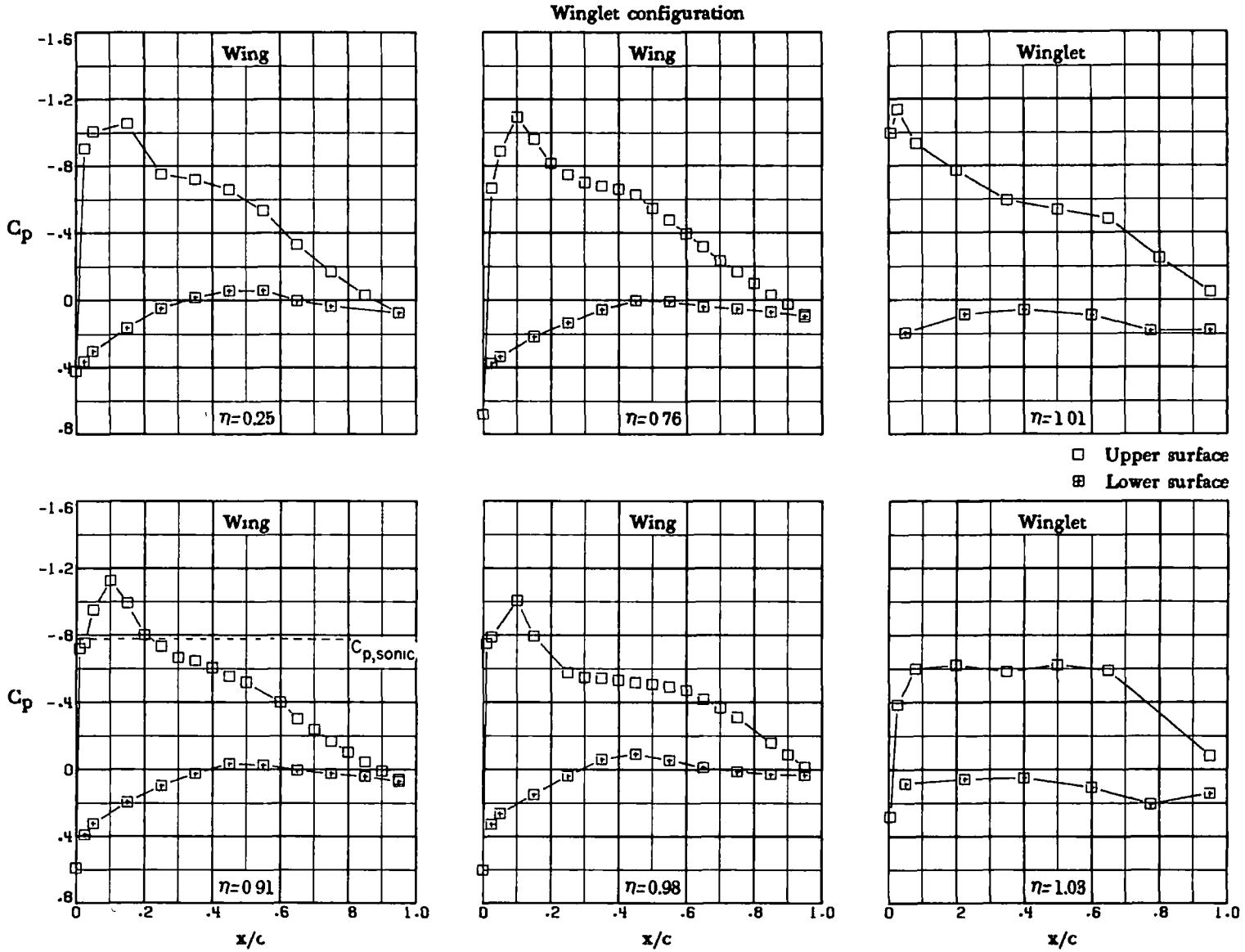

(d) $M_\infty = 0.70$; $\alpha = 4.0^\circ$.

Figure 13.- Continued.

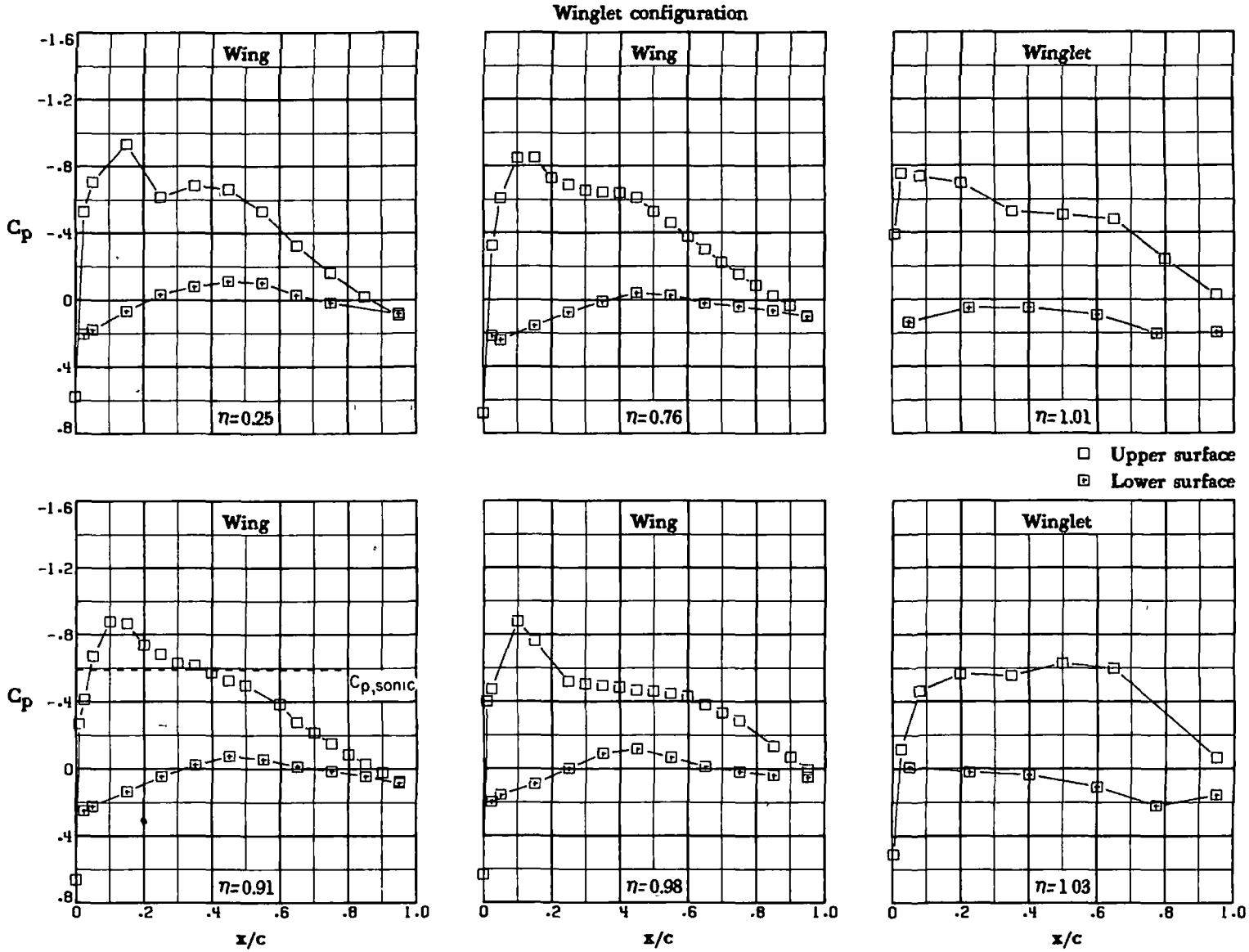

(e) $M_\infty = 0.75$; $\alpha = 2.5^\circ$.

Figure 13.- Continued.

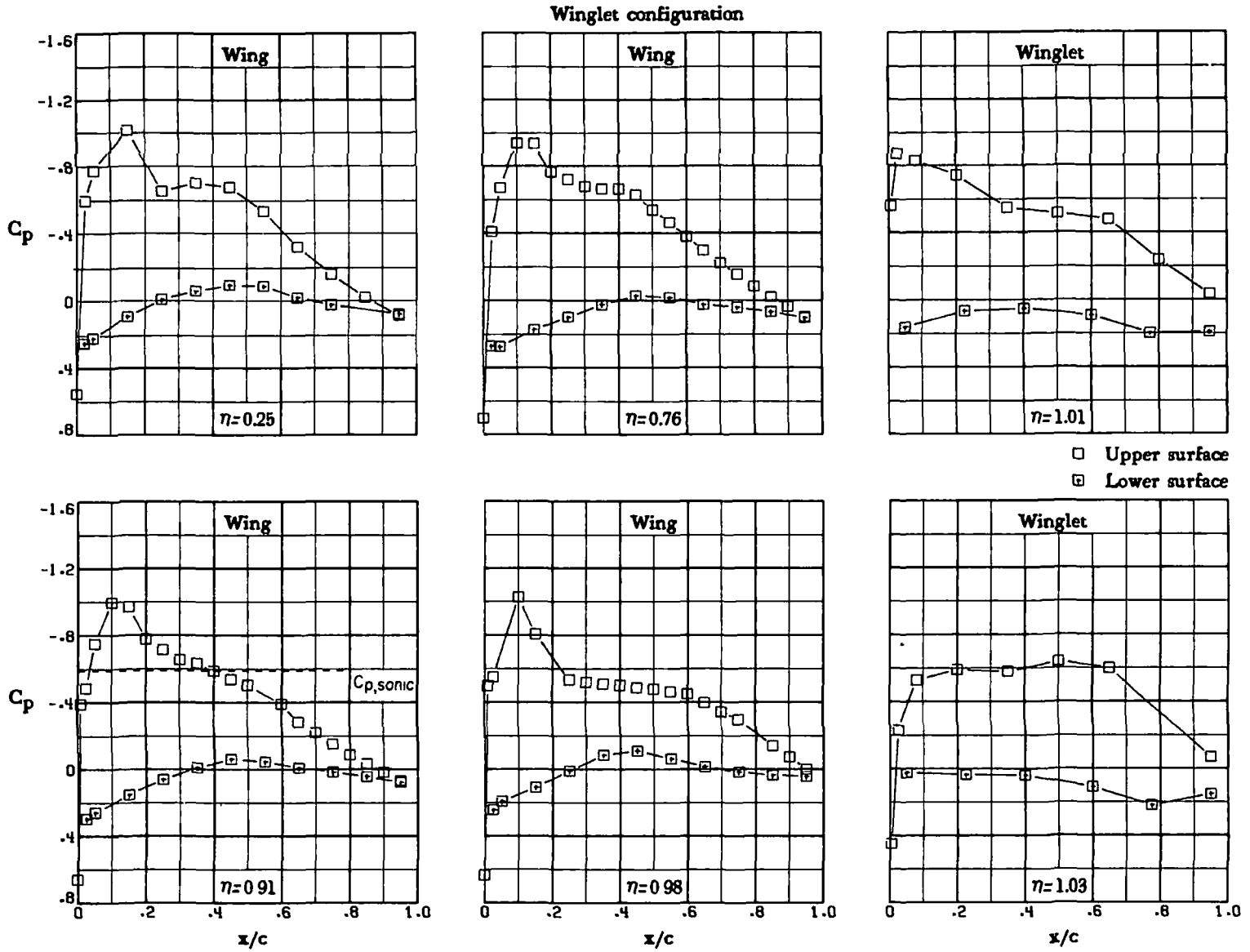

(f) $M_\infty = 0.75$; $\alpha = 3.0^\circ$.

Figure 13.- Continued.

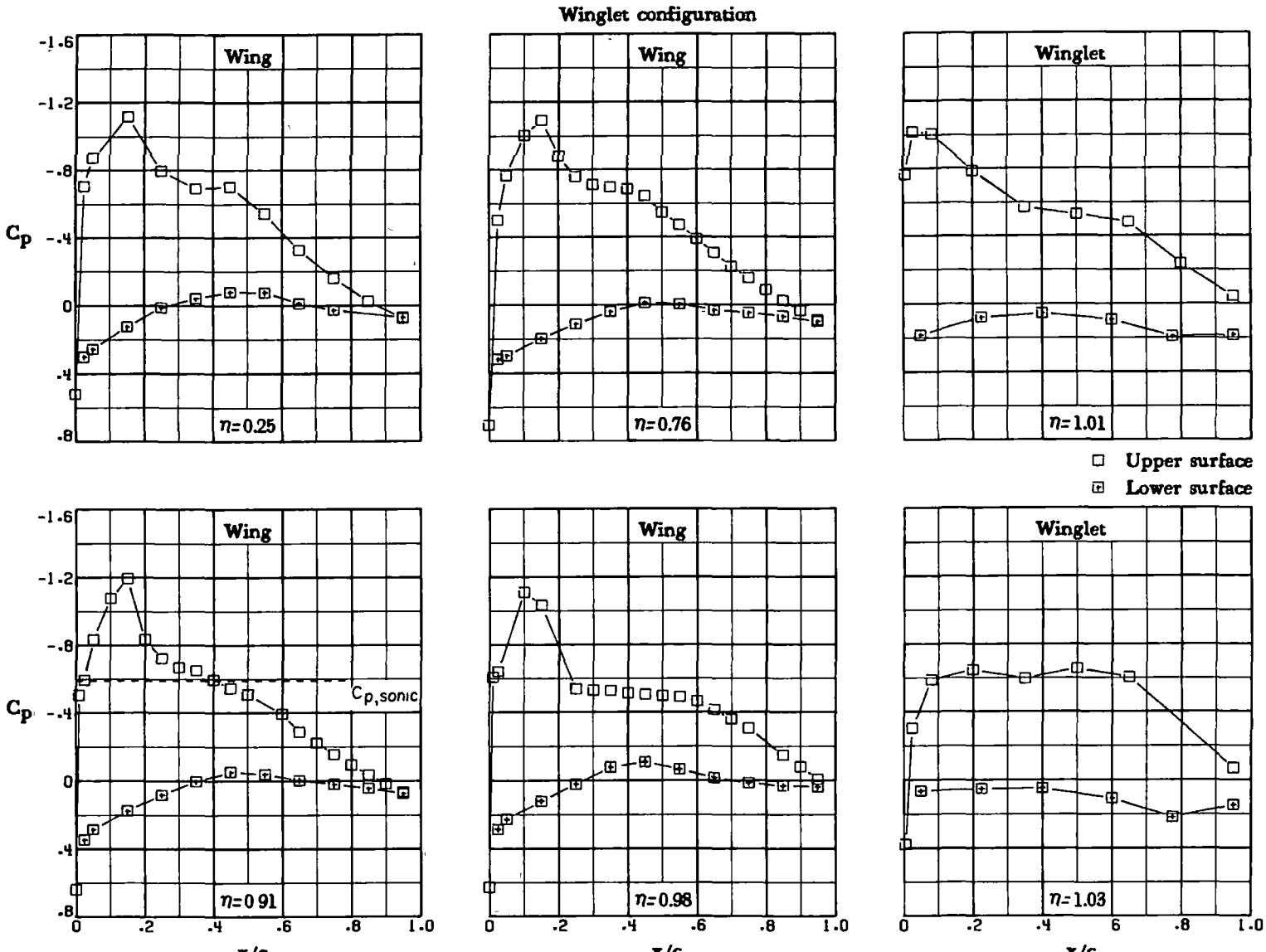

(g) $M_\infty = 0.75$; $\alpha = 3.5^o$.

Figure 13.- Continued.

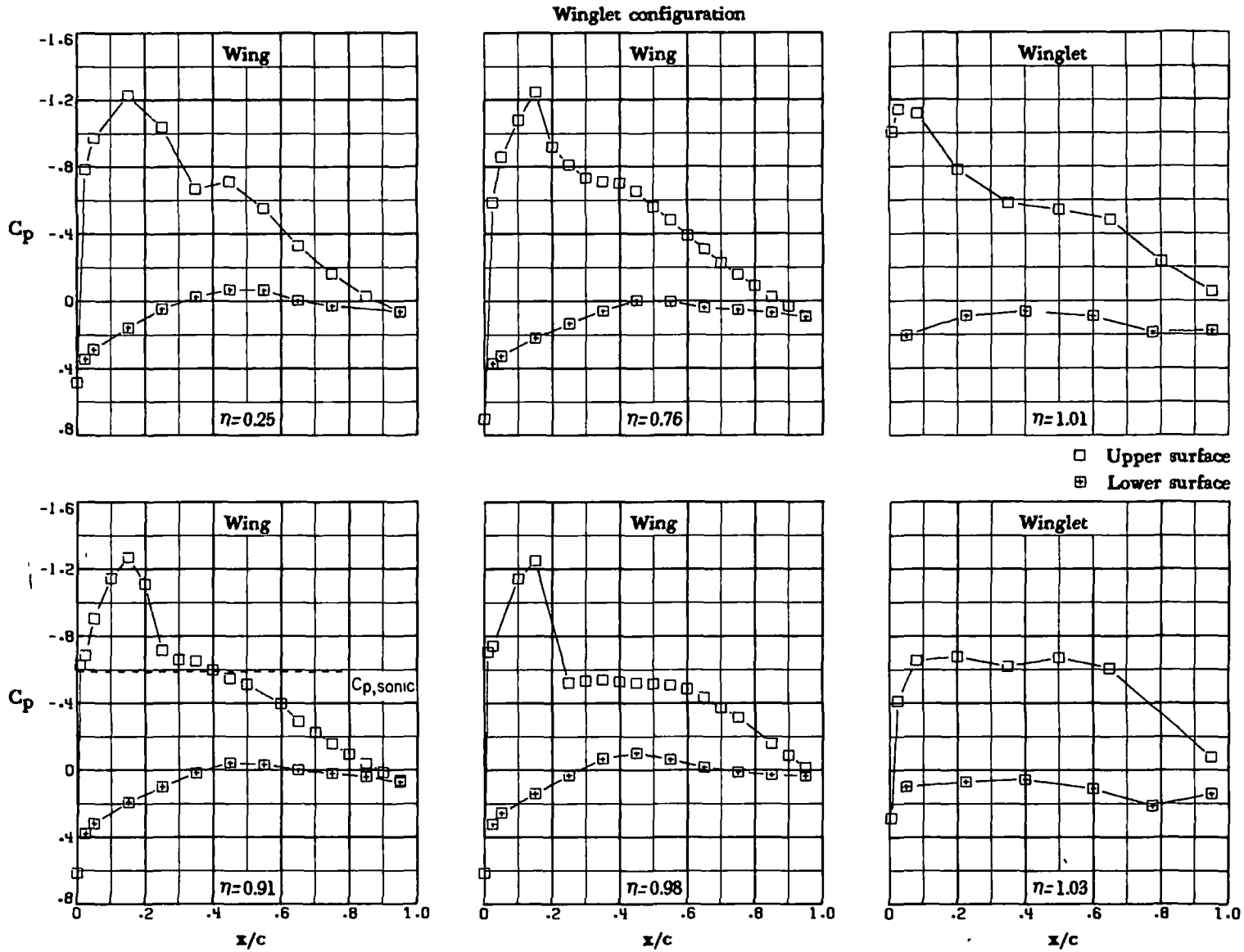

(h) $M_\infty = 0.75$; $\alpha = 4.0^\circ$.

Figure 13.- Continued.

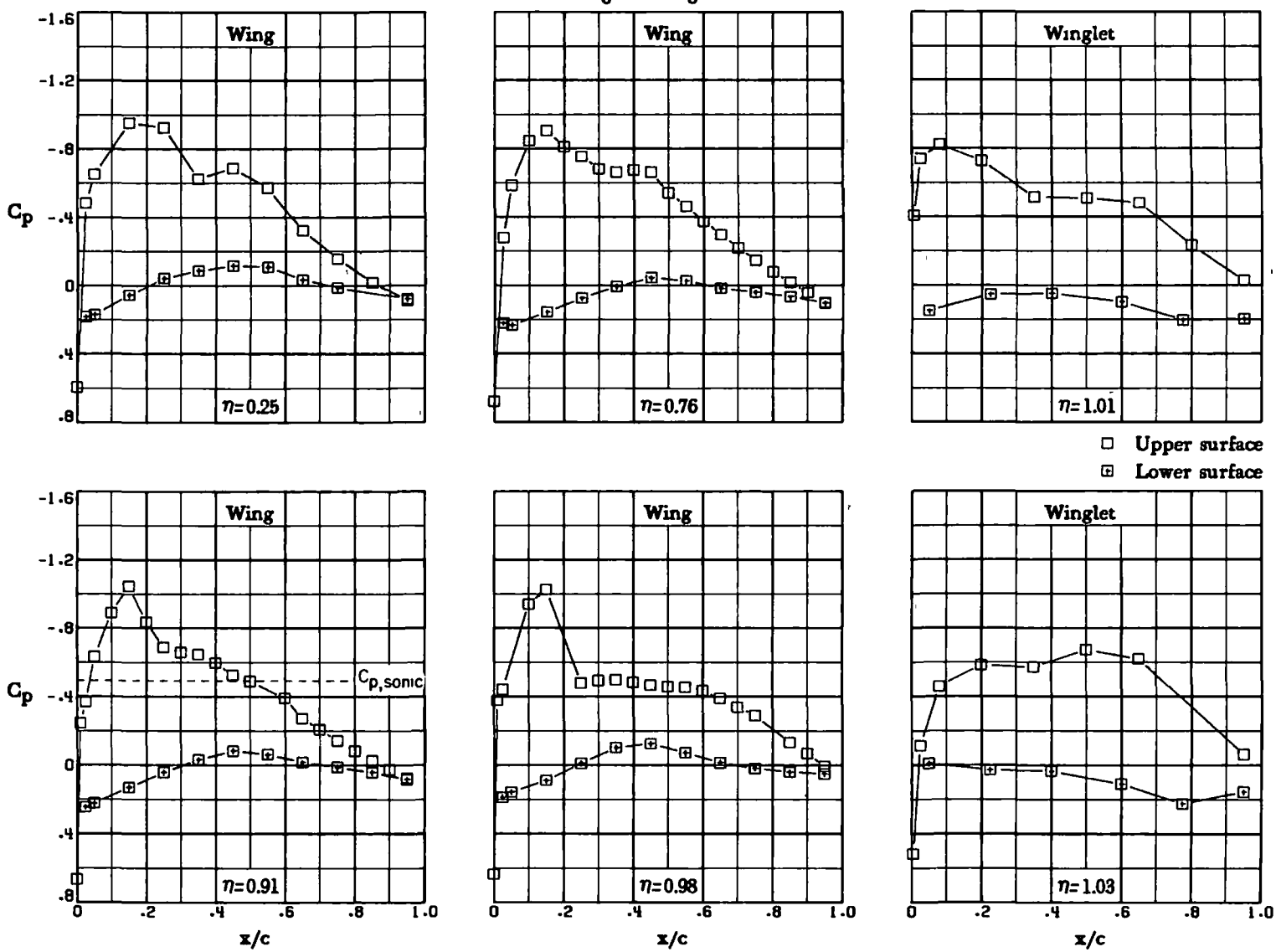

(i) $M_\infty = 0.78$; $\alpha = 2.5^\circ$.

Figure 13.- Continued.

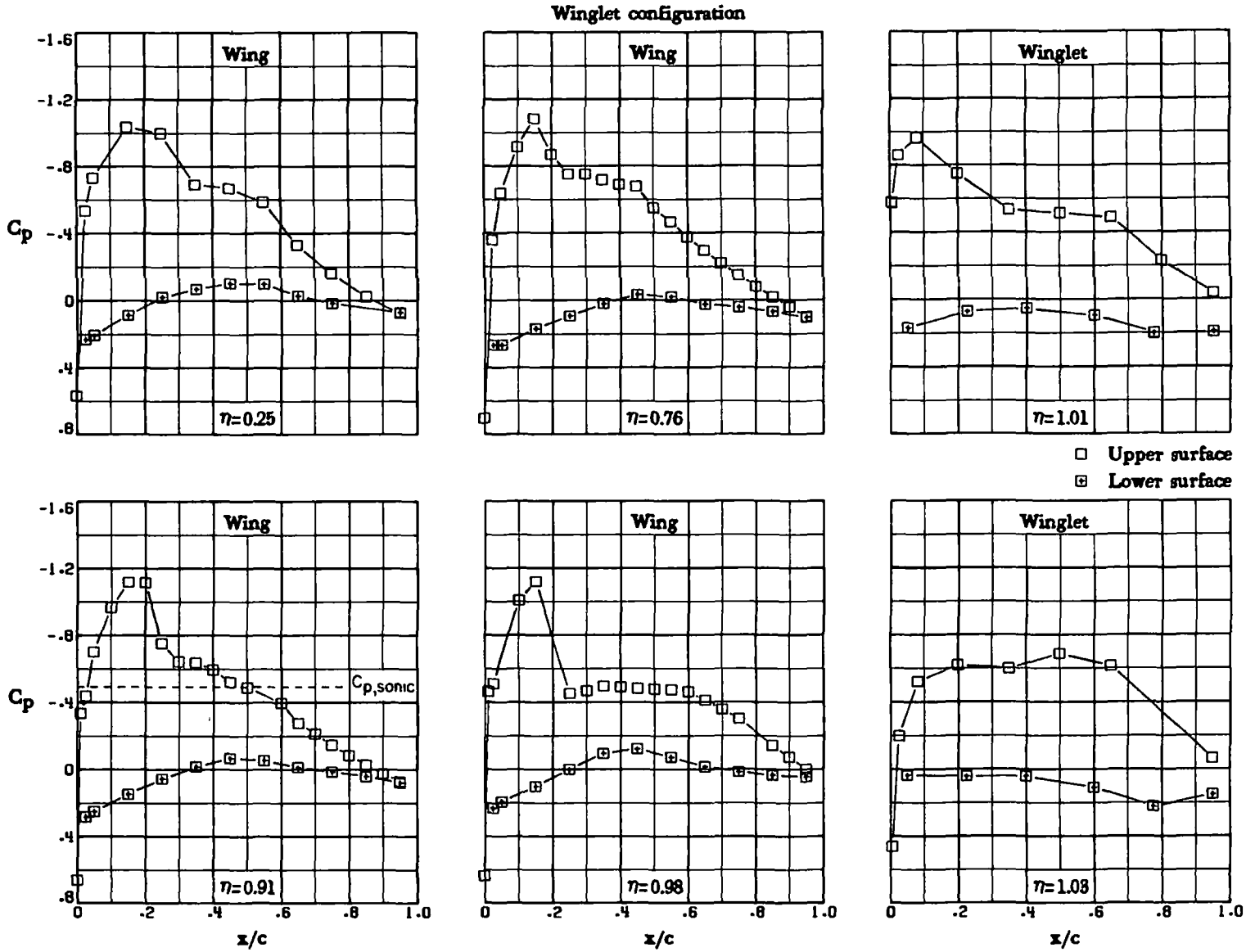

(j) $M_\infty = 0.78$; $\alpha = 3.0^\circ$.

Figure 13.- Continued.

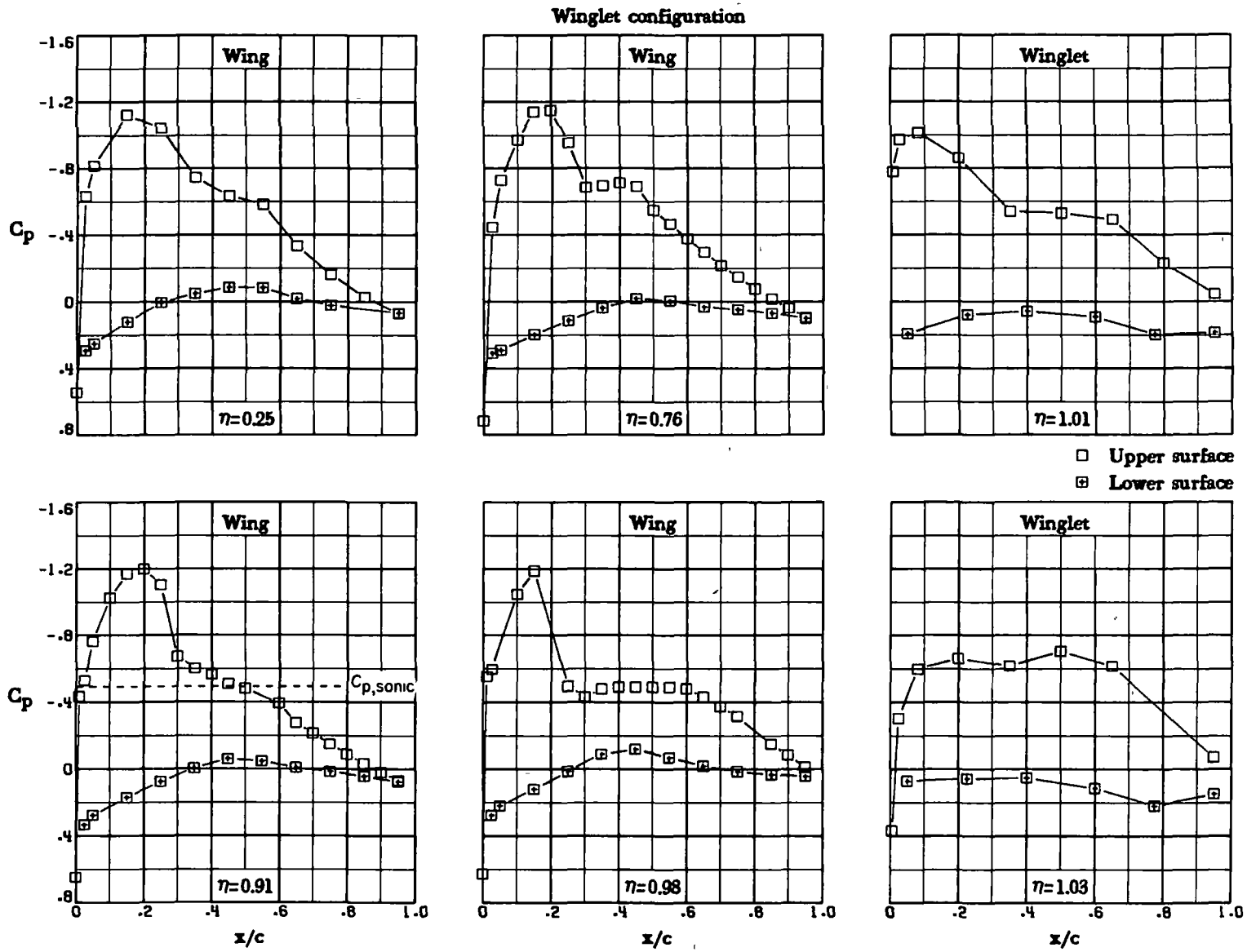

(k) $M_\infty = 0.78$; $\alpha = 3.5^\circ$.

Figure 13.- Continued.

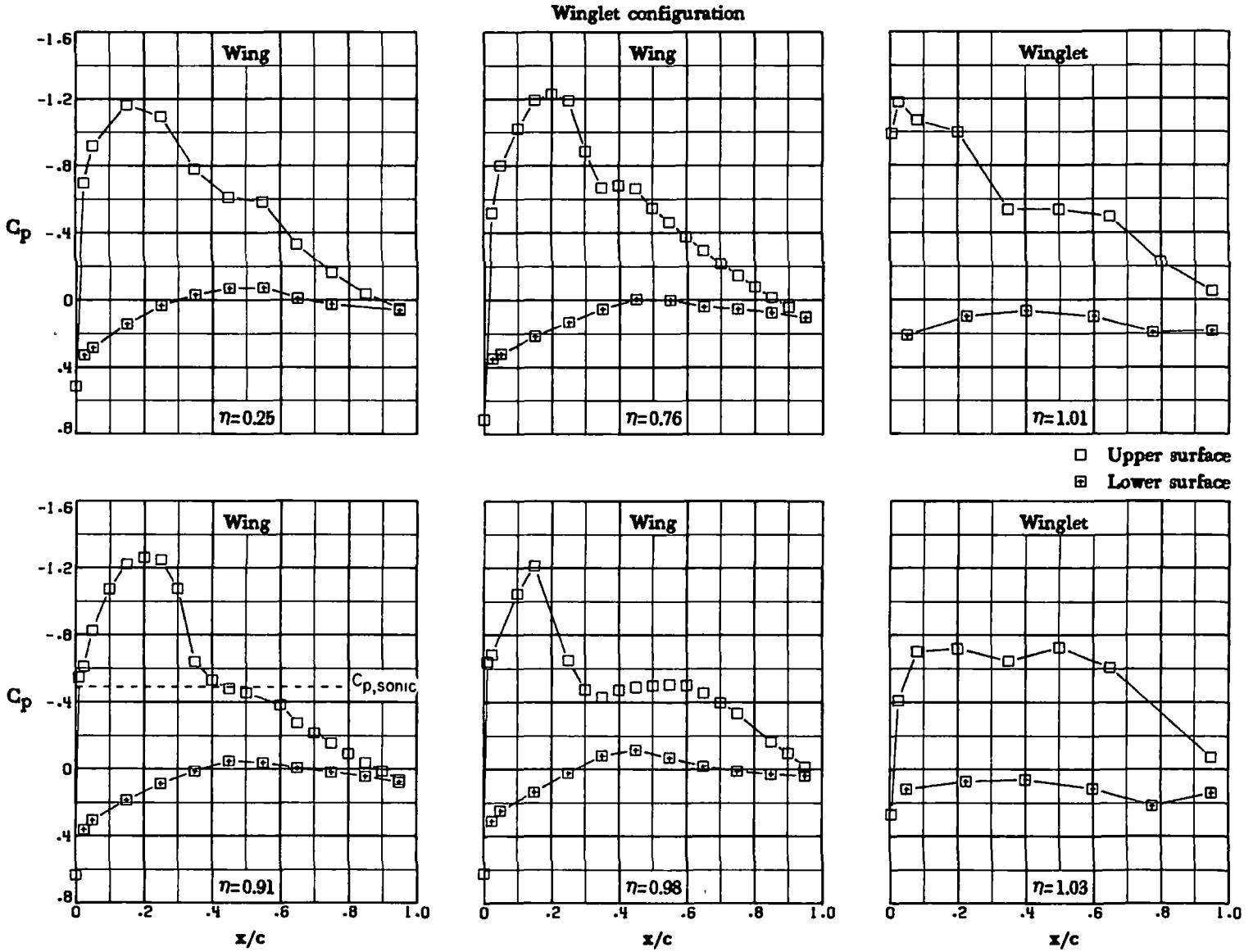

(1) $M_\infty = 0.78$; $\alpha = 4.0^\circ$.

Figure 13.- Continued.

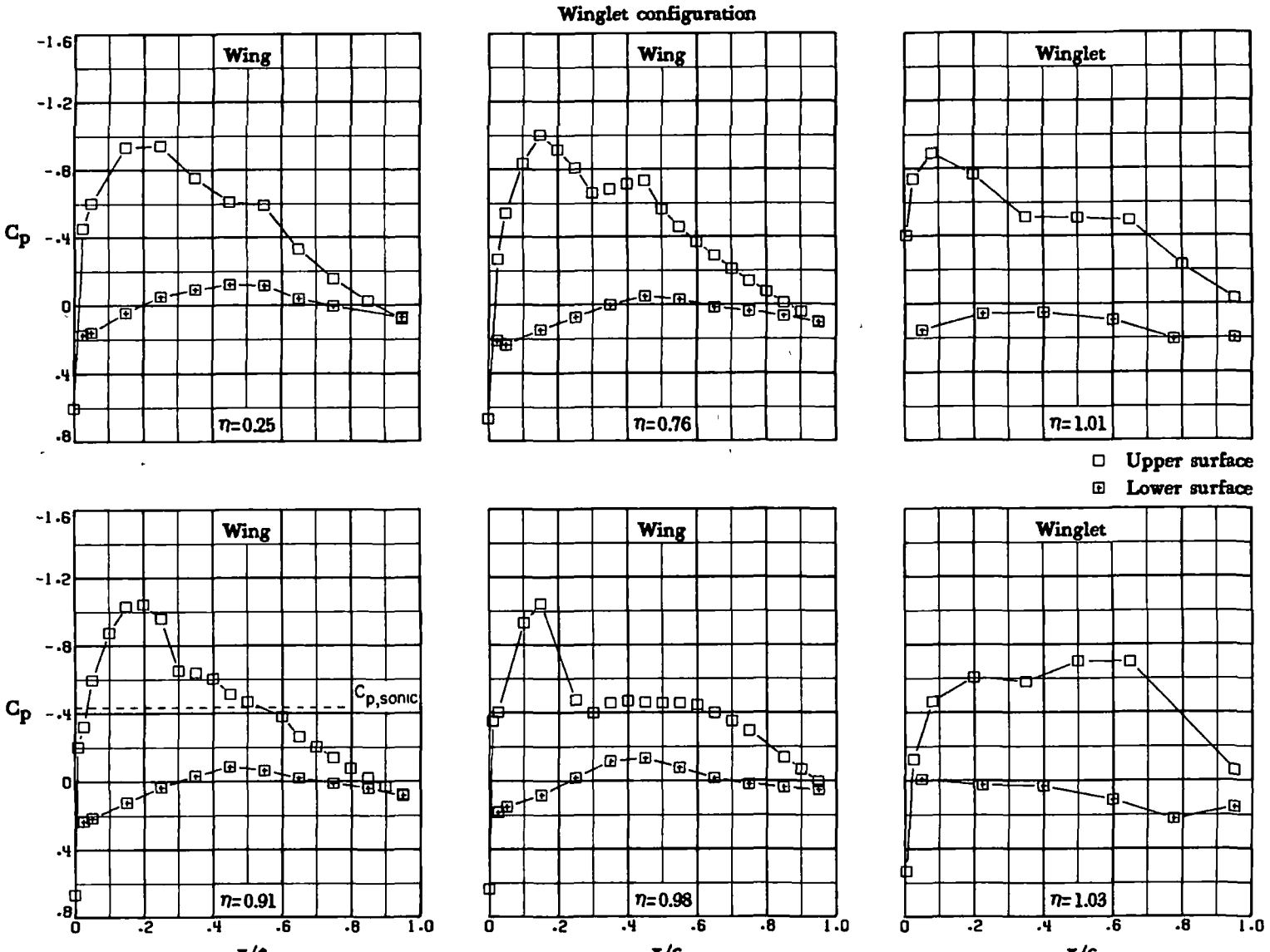

(m) M_∞ = 0.80; α = 2.5°.

Figure 13.- Continued.

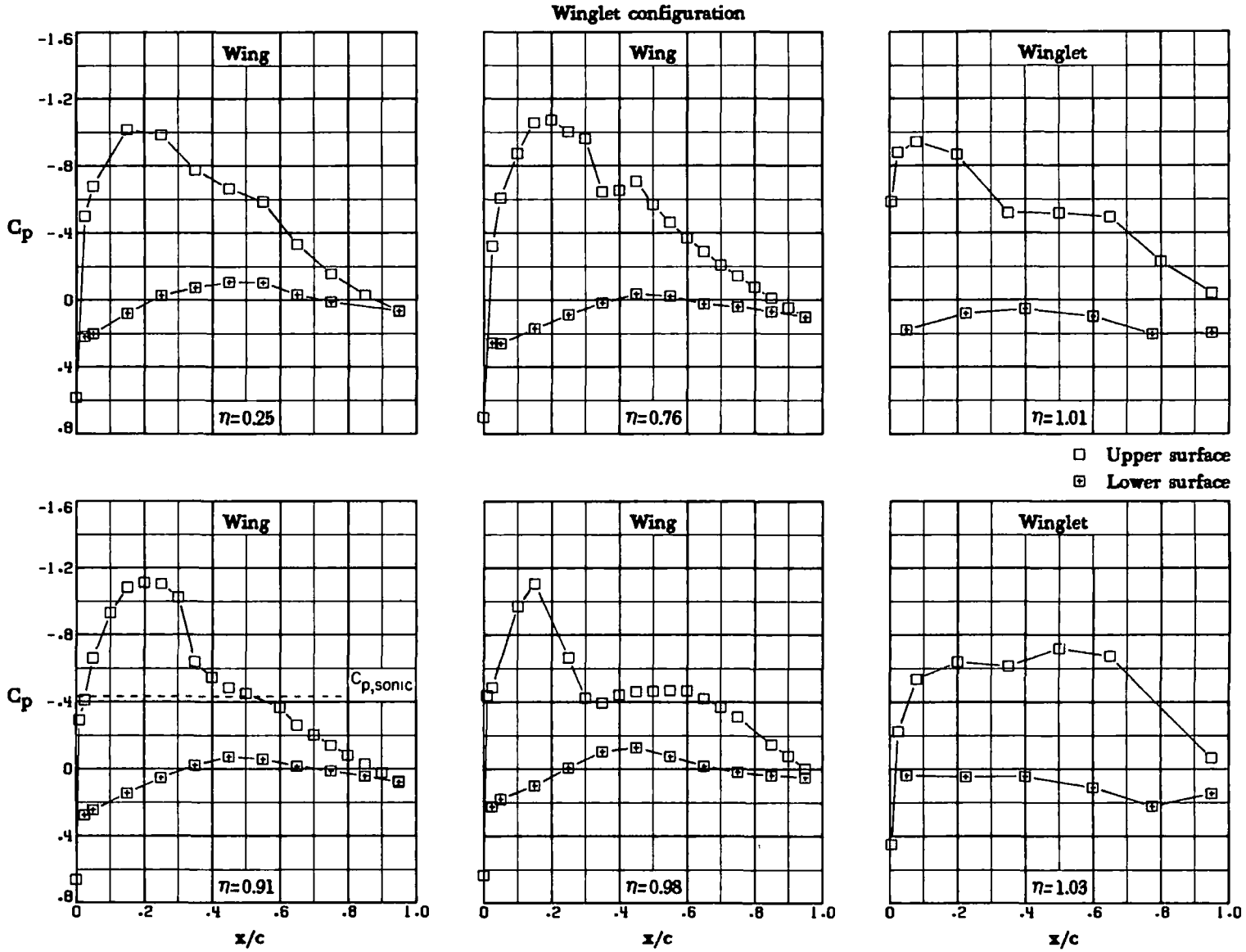

(n) $M_\infty = 0.80$; $\alpha = 3.0^\circ$.

Figure 13.- Continued.

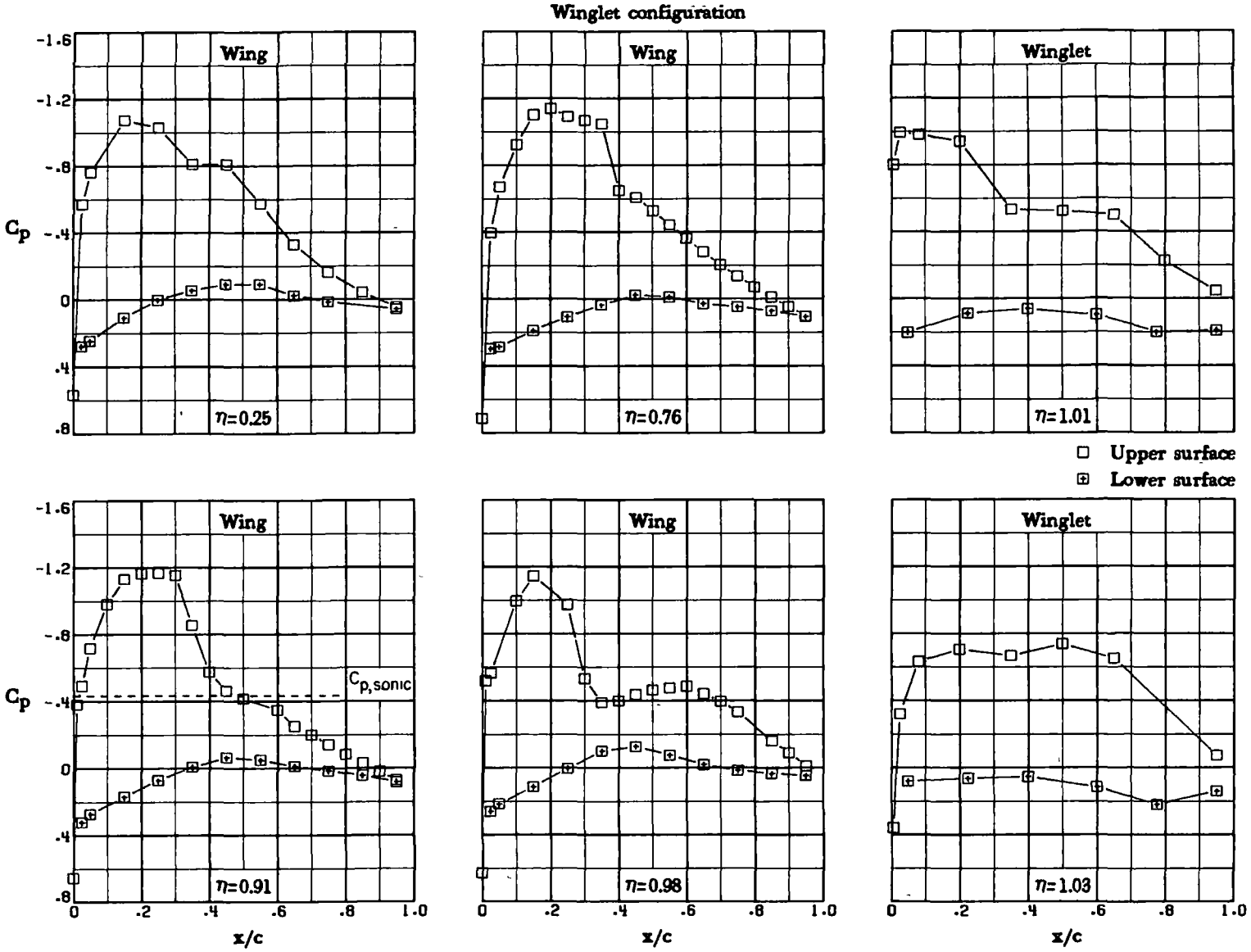

(o) $M_\infty = 0.80$; $\alpha = 3.5^\circ$.

Figure 13.- Continued.

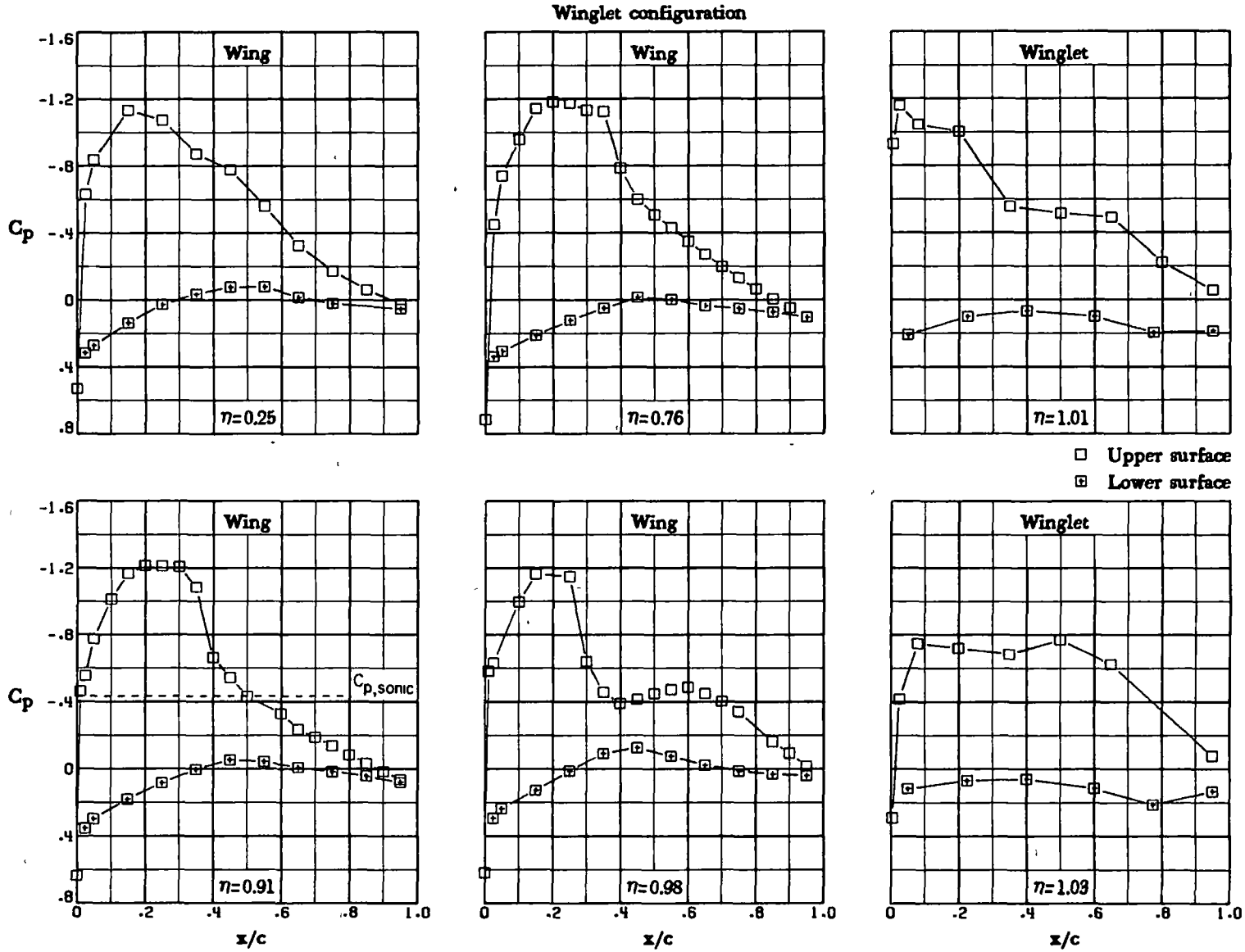

(p) $M_\infty = 0.80$; $\alpha = 4.0^\circ$.

Figure 13.- Concluded.

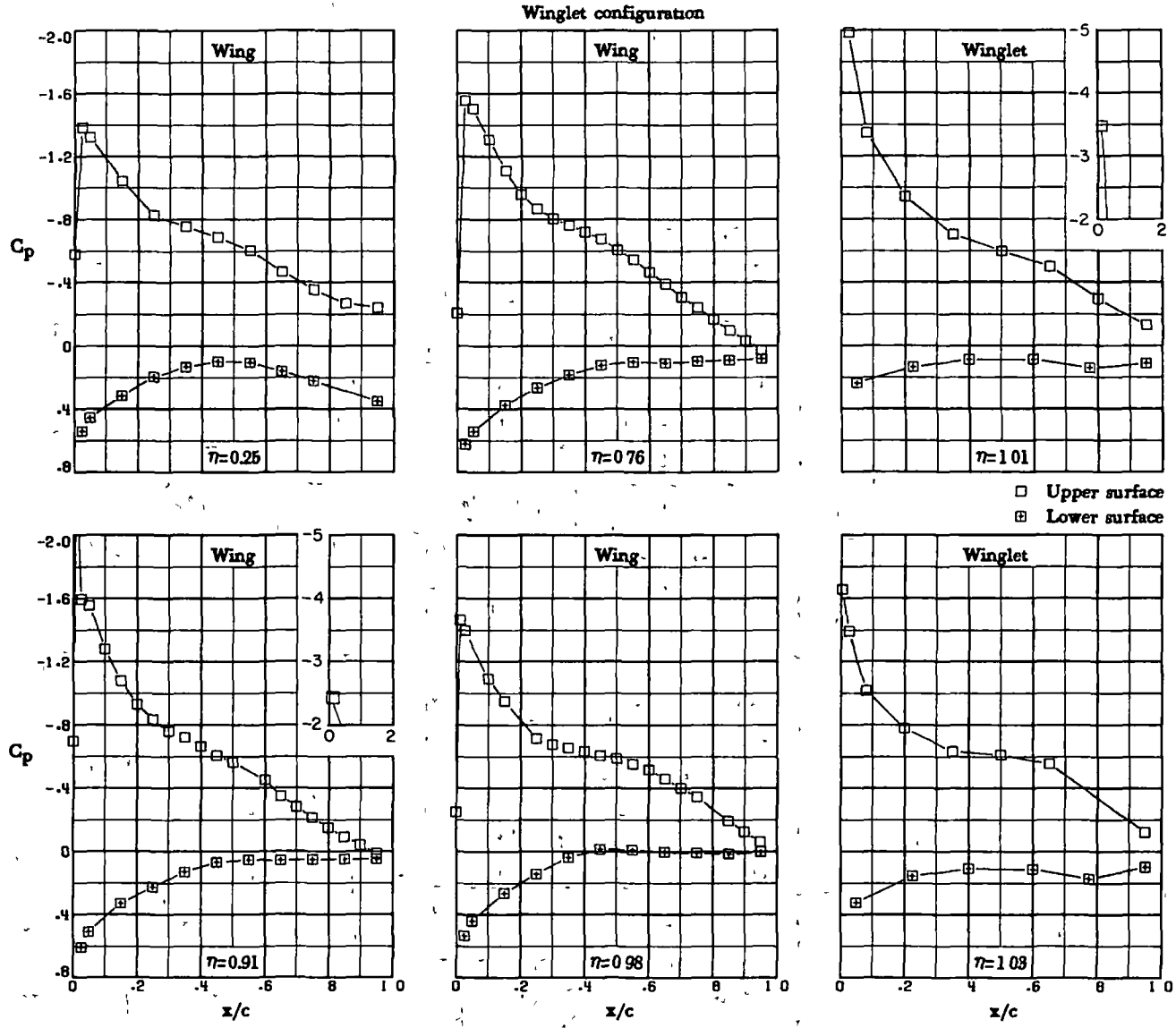

(a) $\alpha = 5^{\circ}$.

Figure 14.- Chordwise pressure distributions for winglet configuration with trailing-edge flaps. $M_{\infty} = 0.30$.

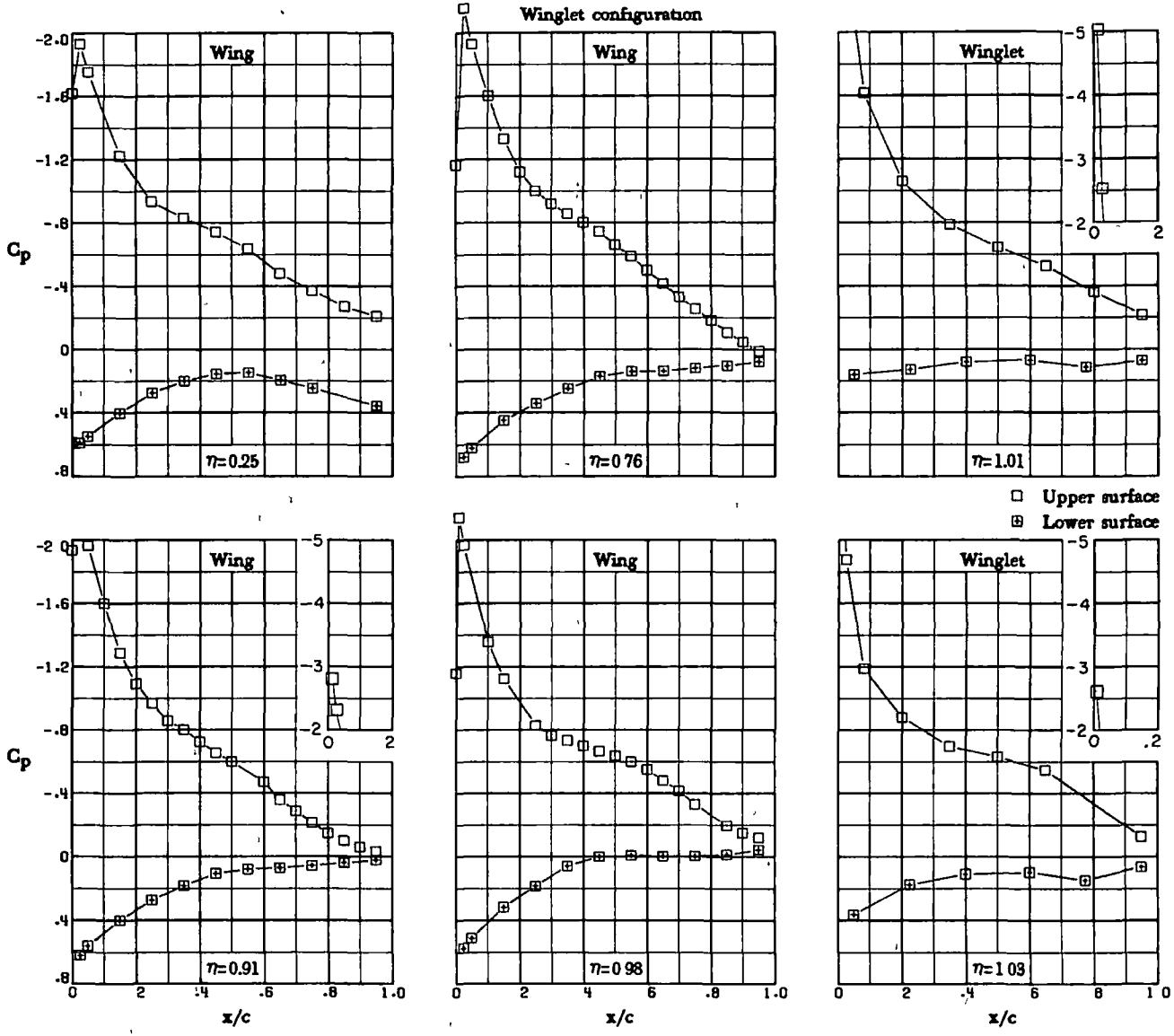

(b) $\alpha = 7^{\circ}$.

Figure 14.- Continued.

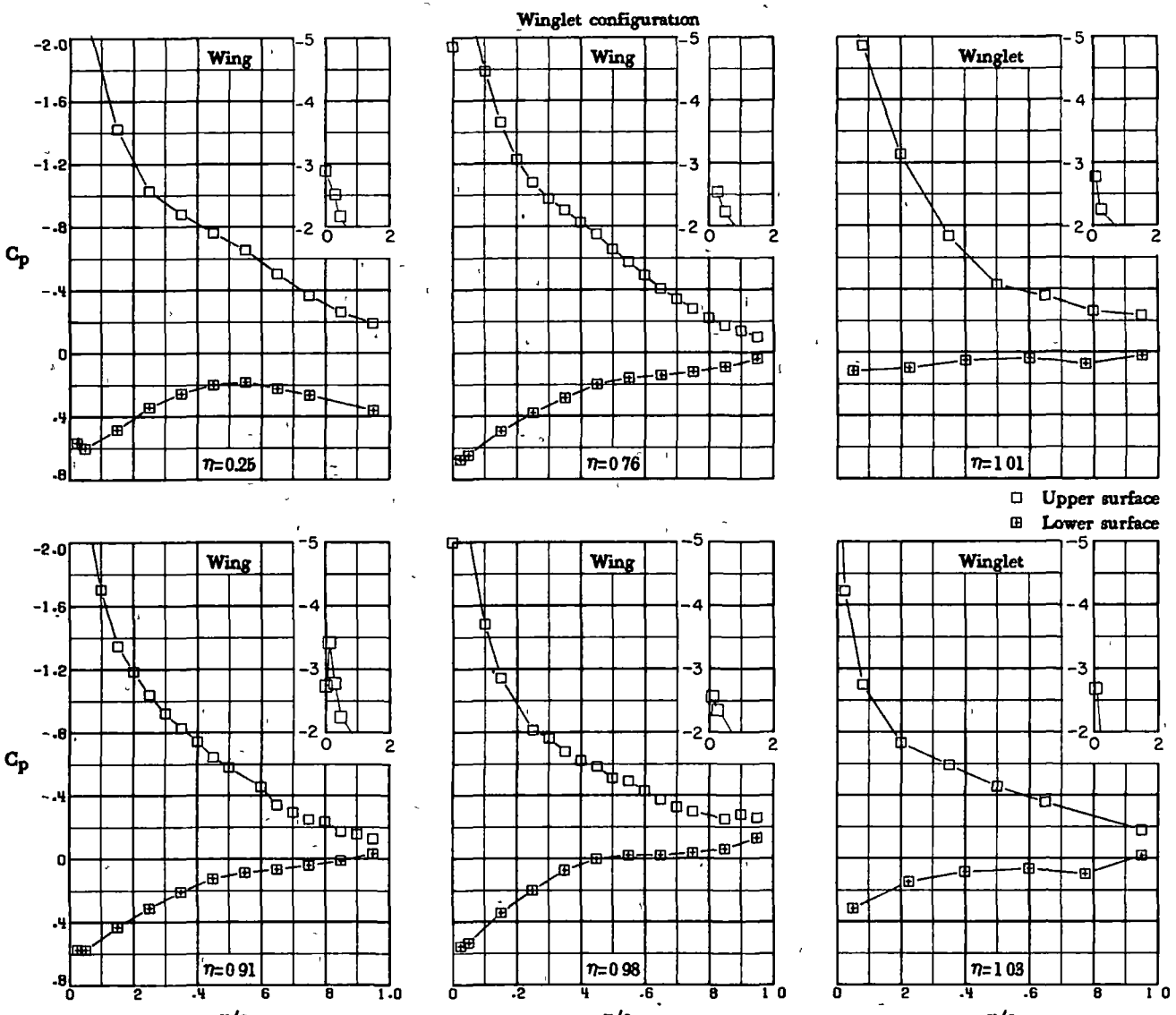

(c) $\alpha = 9^{\circ}$.

Figure 14.- Continued.

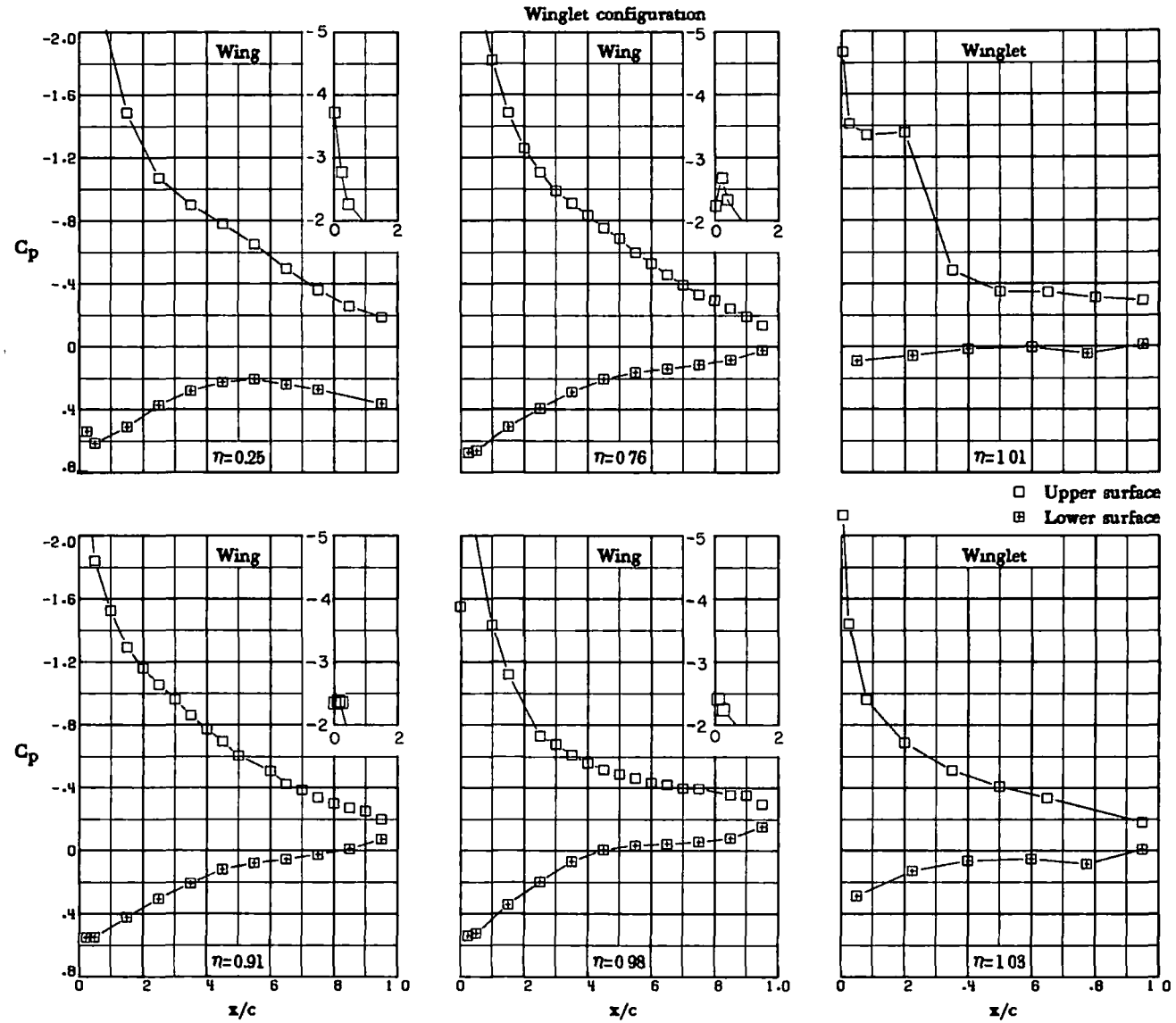

(d) $\alpha = 10^{\circ}$.

Figure 14.- Continued.

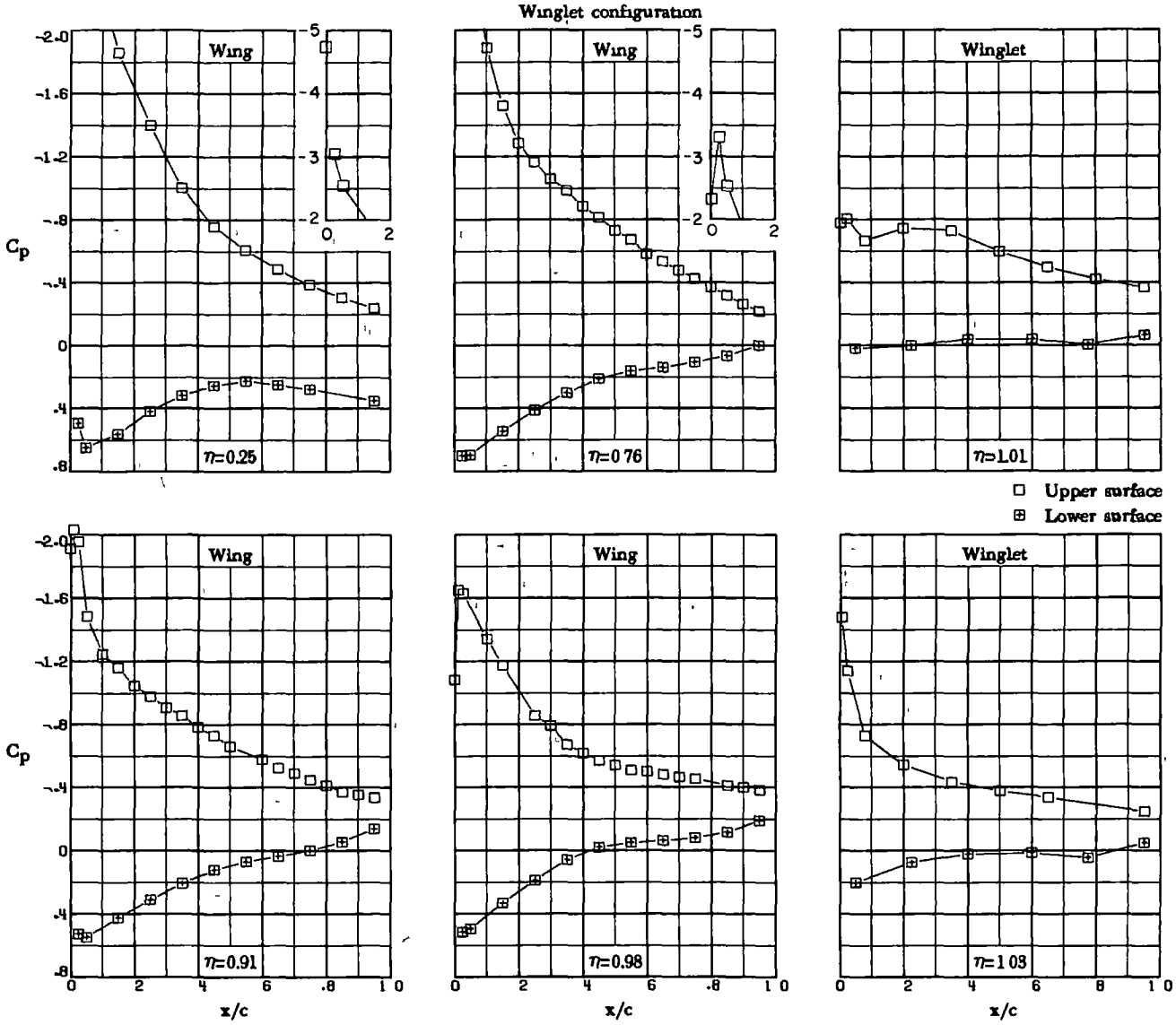

(e) $\alpha = 12^{\circ}$.

Figure 14.- Concluded.

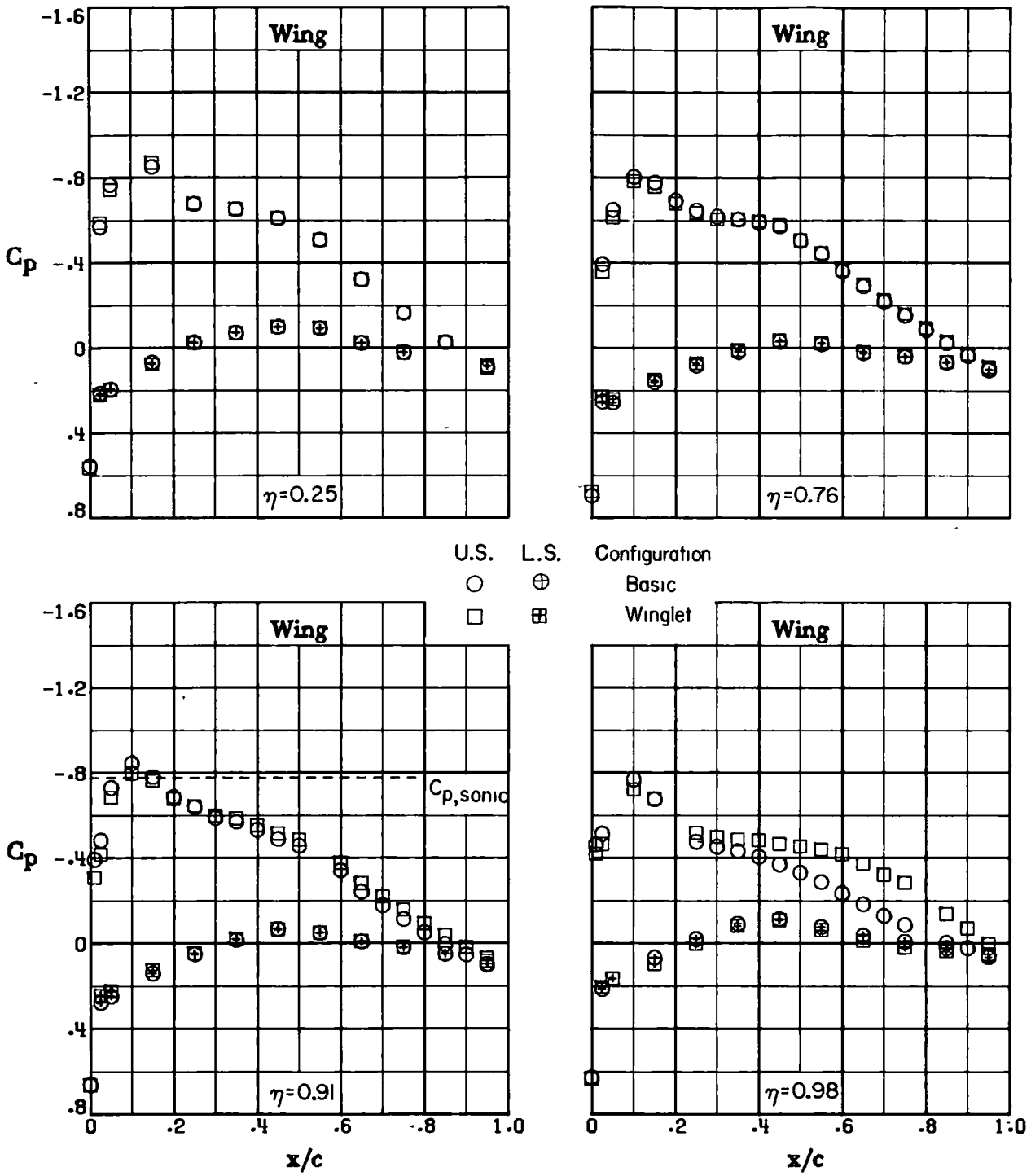

(a) $M_\infty = 0.70$; $\alpha = 2.5^\circ$.

Figure 15.- Comparison of chordwise pressure distributions for basic and winglet configurations.

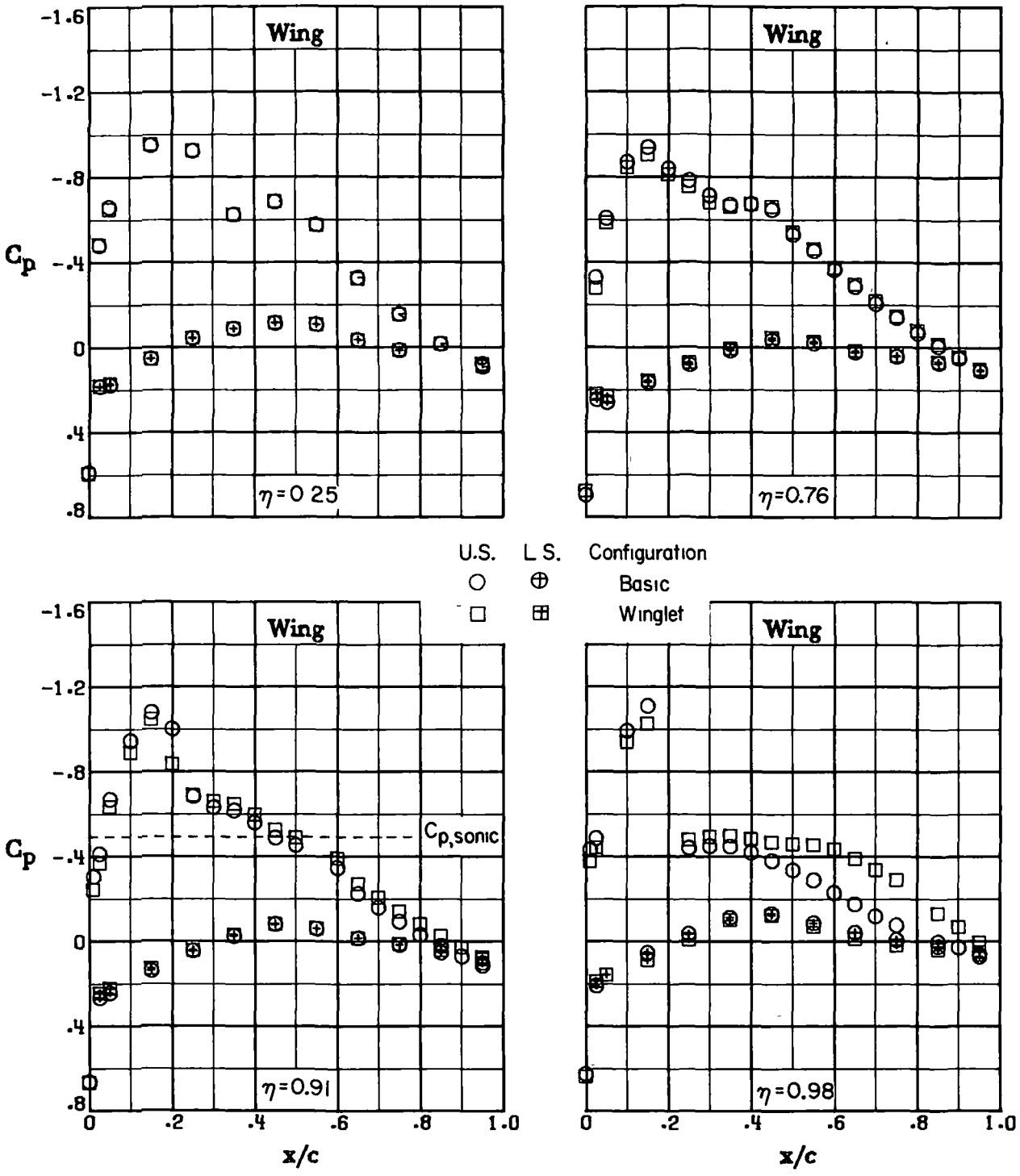

(b) $M_\infty = 0.78$; $\alpha = 2.5^\circ$.

Figure 15.- Concluded.

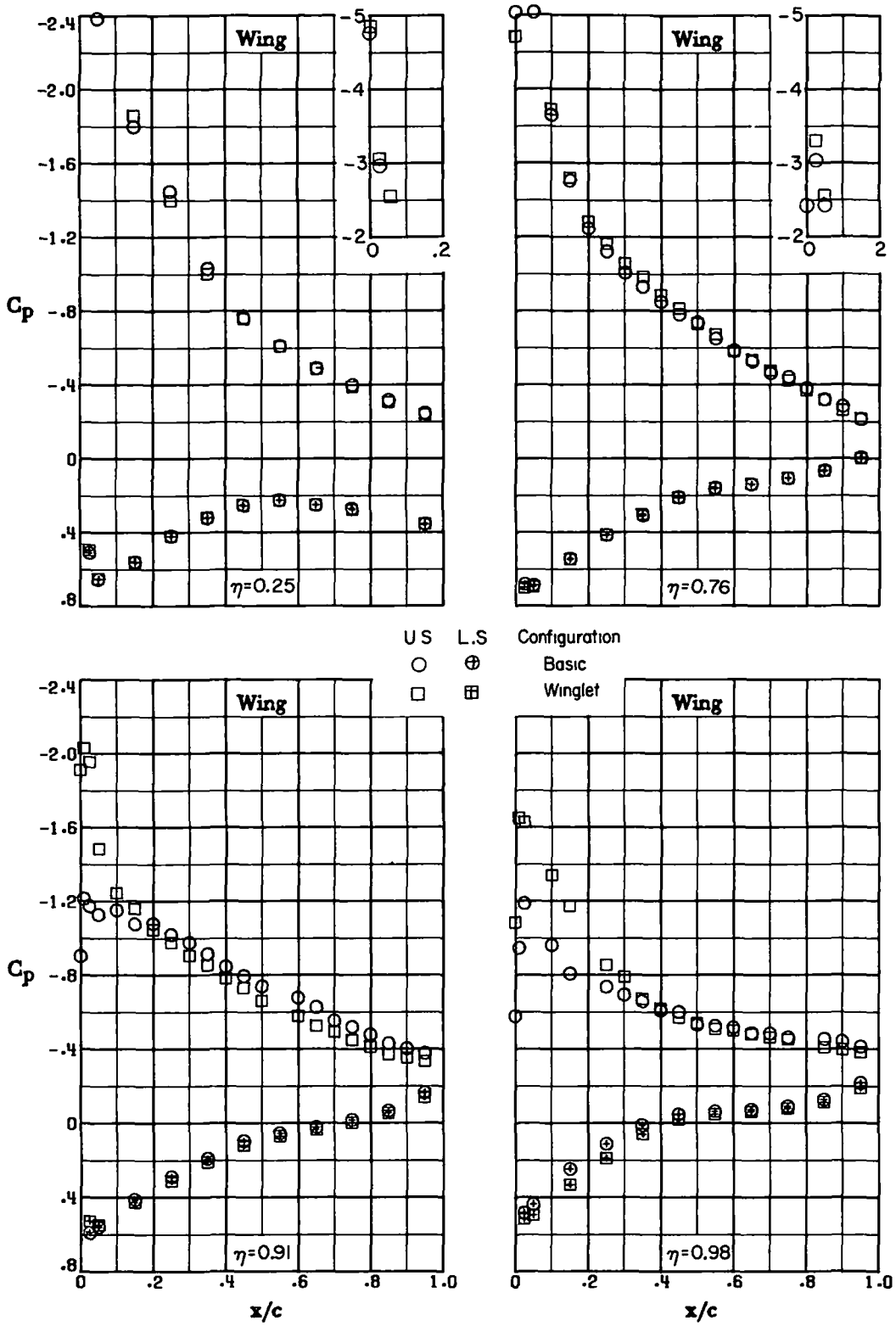

Figure 16.- Comparison of chordwise pressure distributions for basic and winglet configurations with trailing-edge flaps. M_∞ = 0.30; α = 12°.

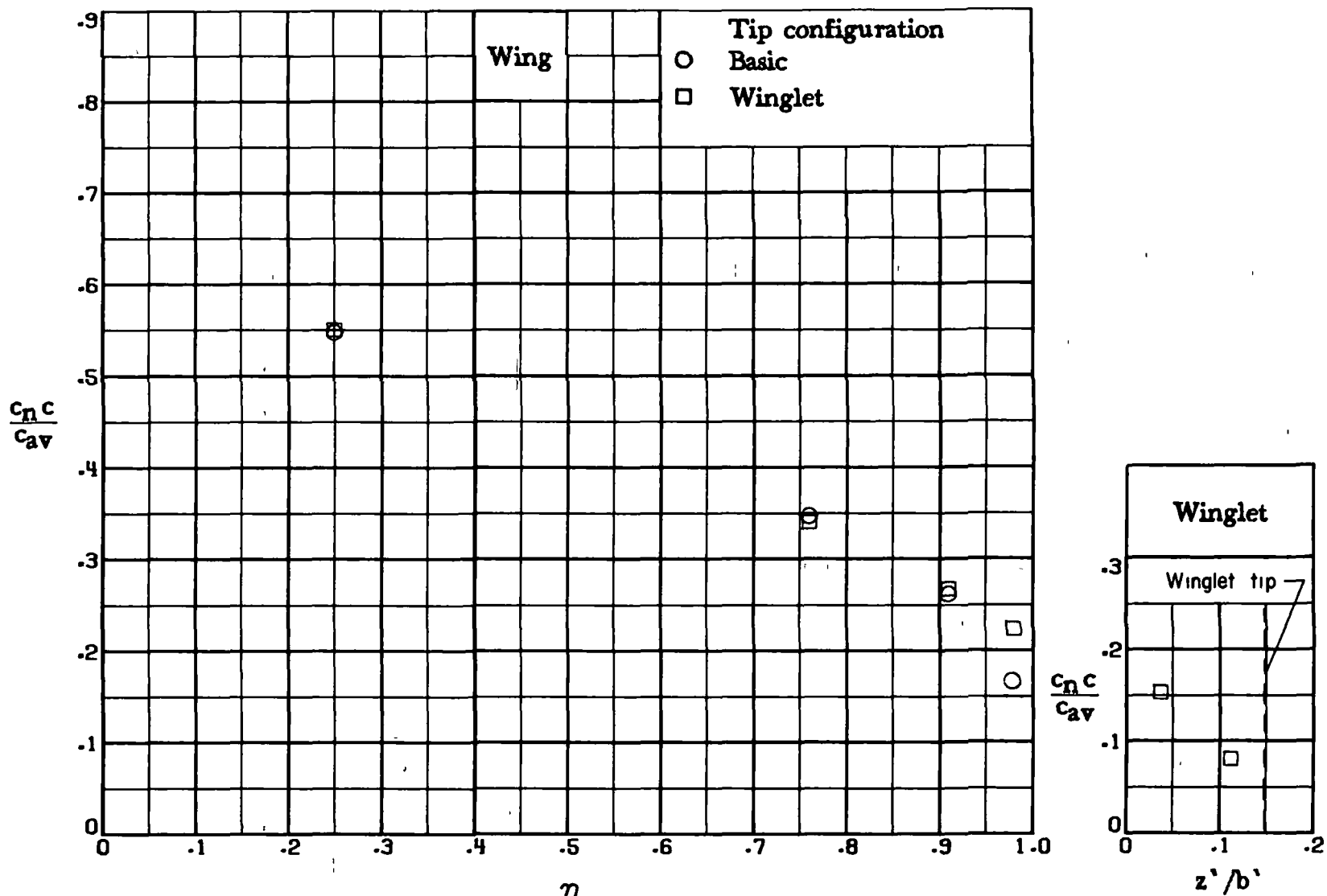

(a) $M_\infty = 0.70$; $\alpha = 2.5^\circ$.

Figure 17.- Spanwise load distributions for basic and winglet configurations.

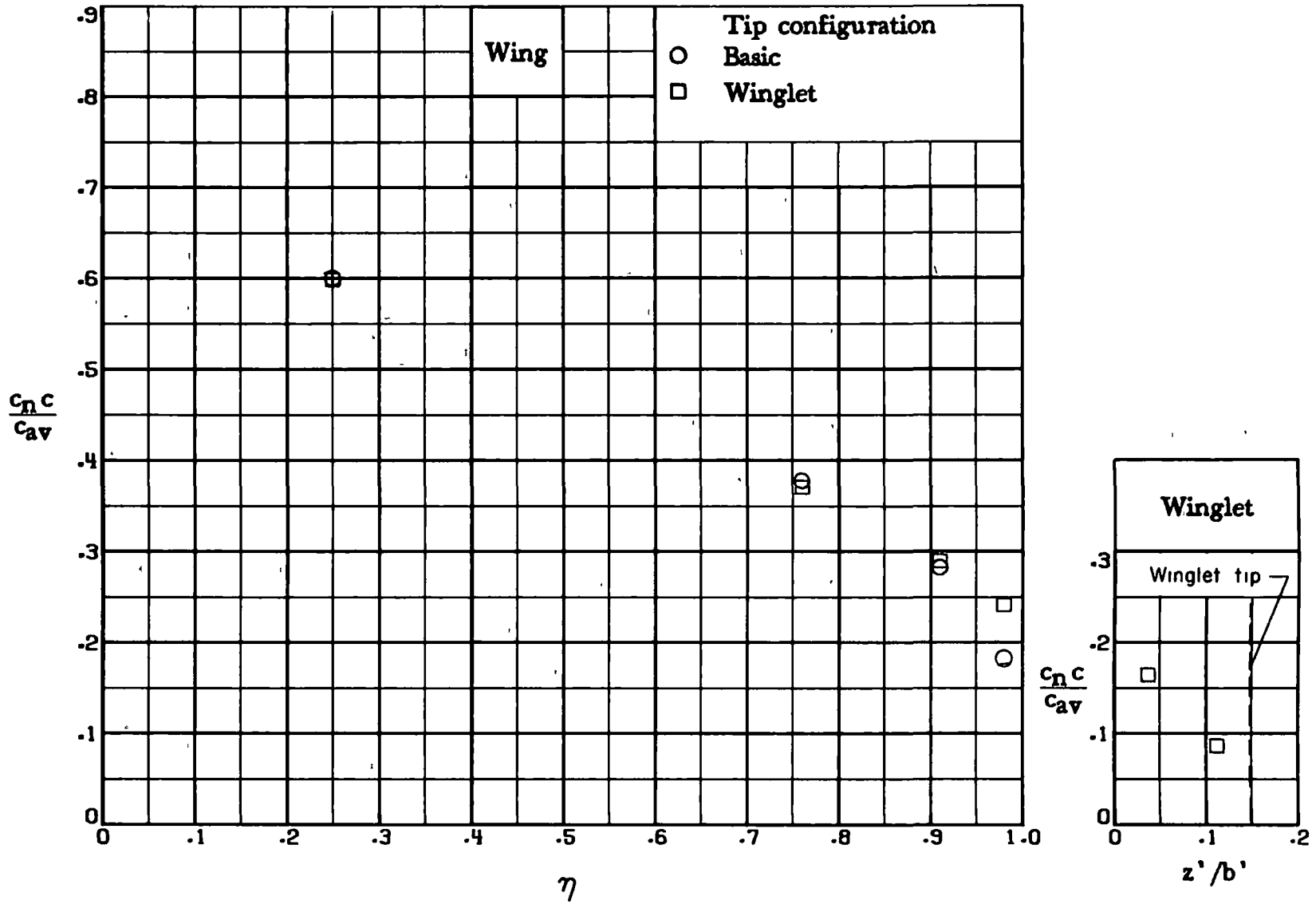

(b) $M_\infty = 0.70$; $\alpha = 3.0^\circ$.

Figure 17.- Continued.

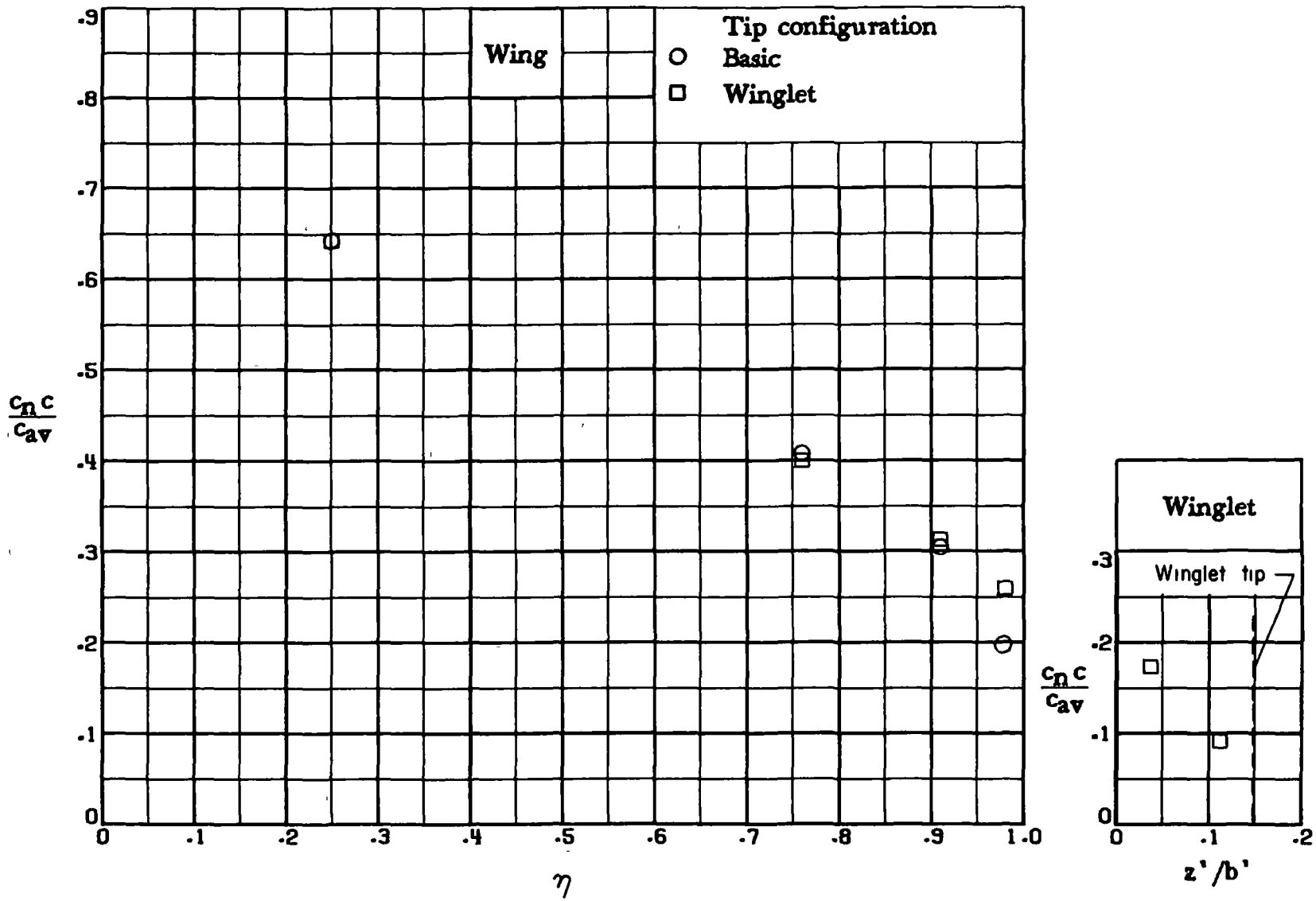

(c) $M_\infty = 0.70$; $\alpha = 3.5^\circ$.

Figure 17.- Continued.

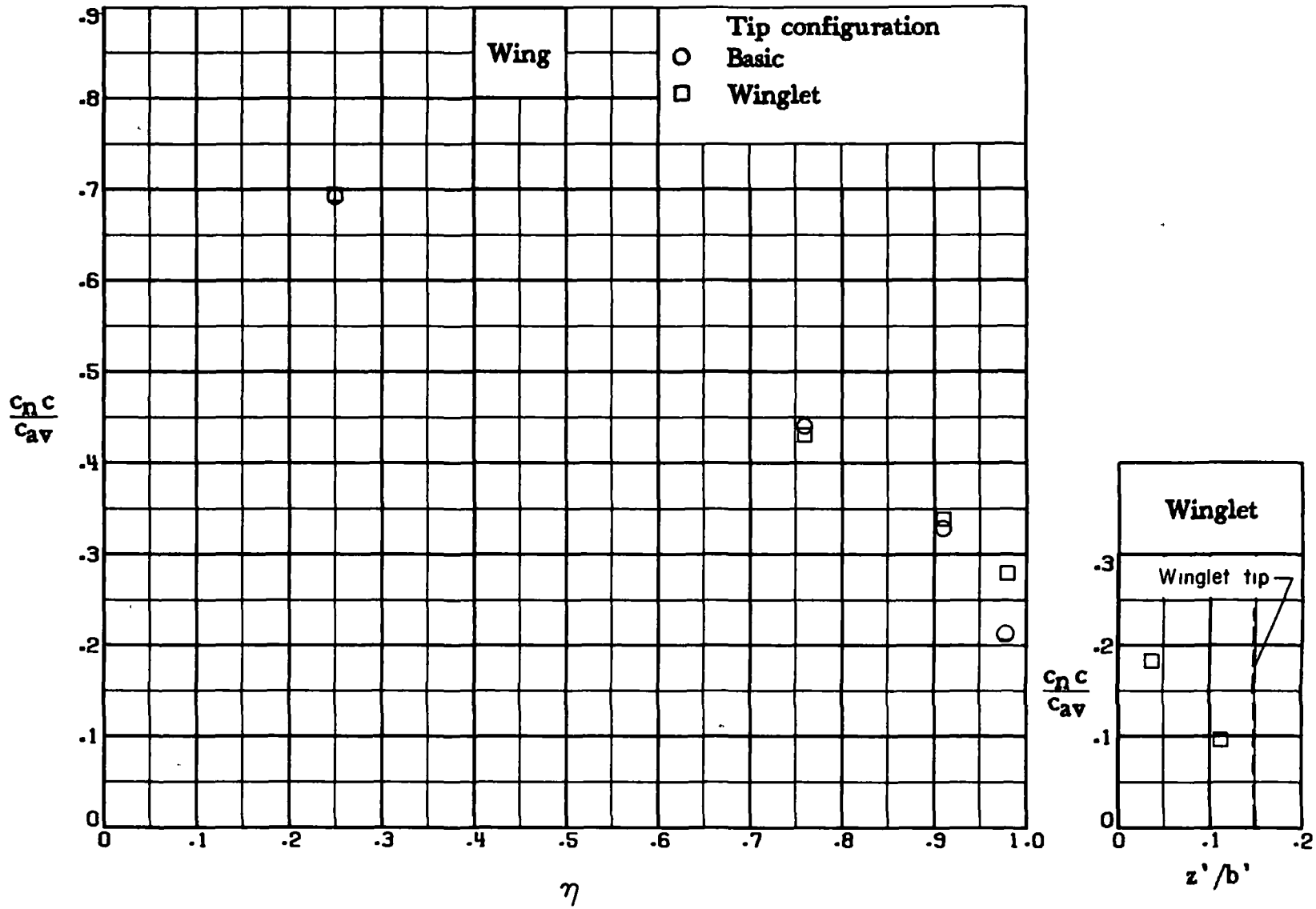

(d) $M_\infty = 0.70$; $\alpha = 4.0^\circ$.

Figure 17.- Continued.

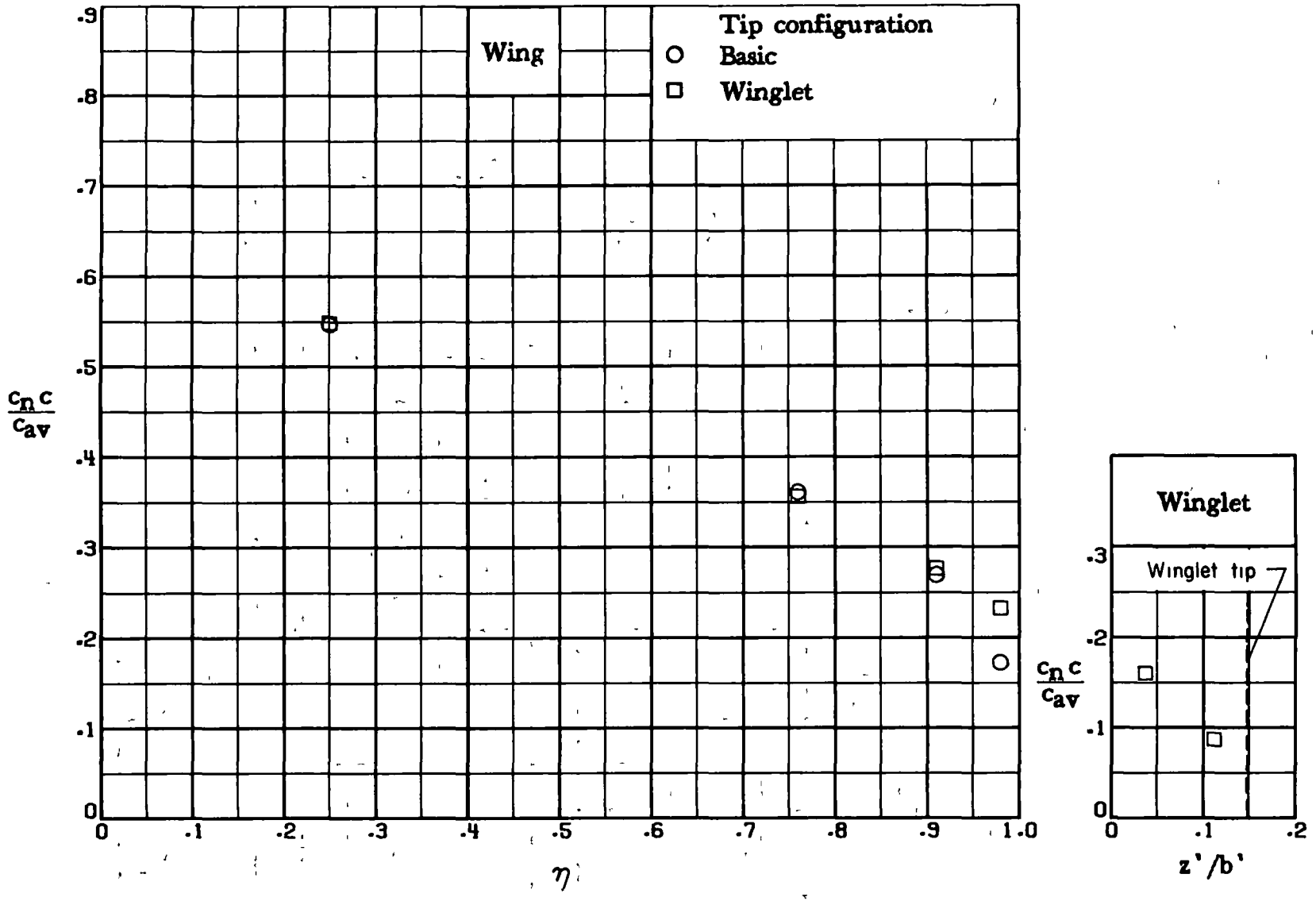

(e) $M_\infty = 0.75$; $\alpha = 2.5^\circ$.

Figure 17.- Continued.

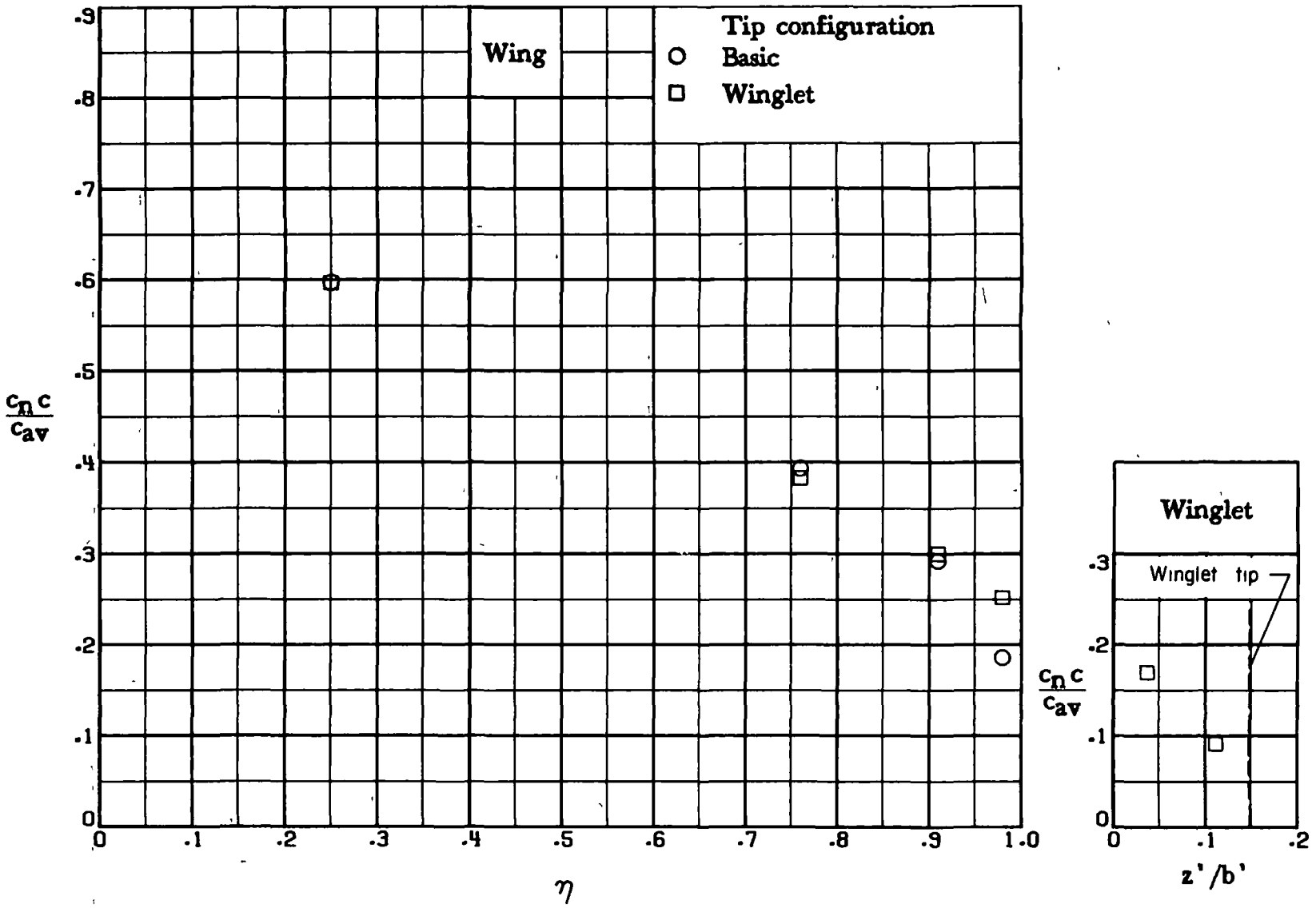

(f) $M_\infty = 0.75$; $\alpha = 3.0^\circ$.

Figure 17.- Continued.

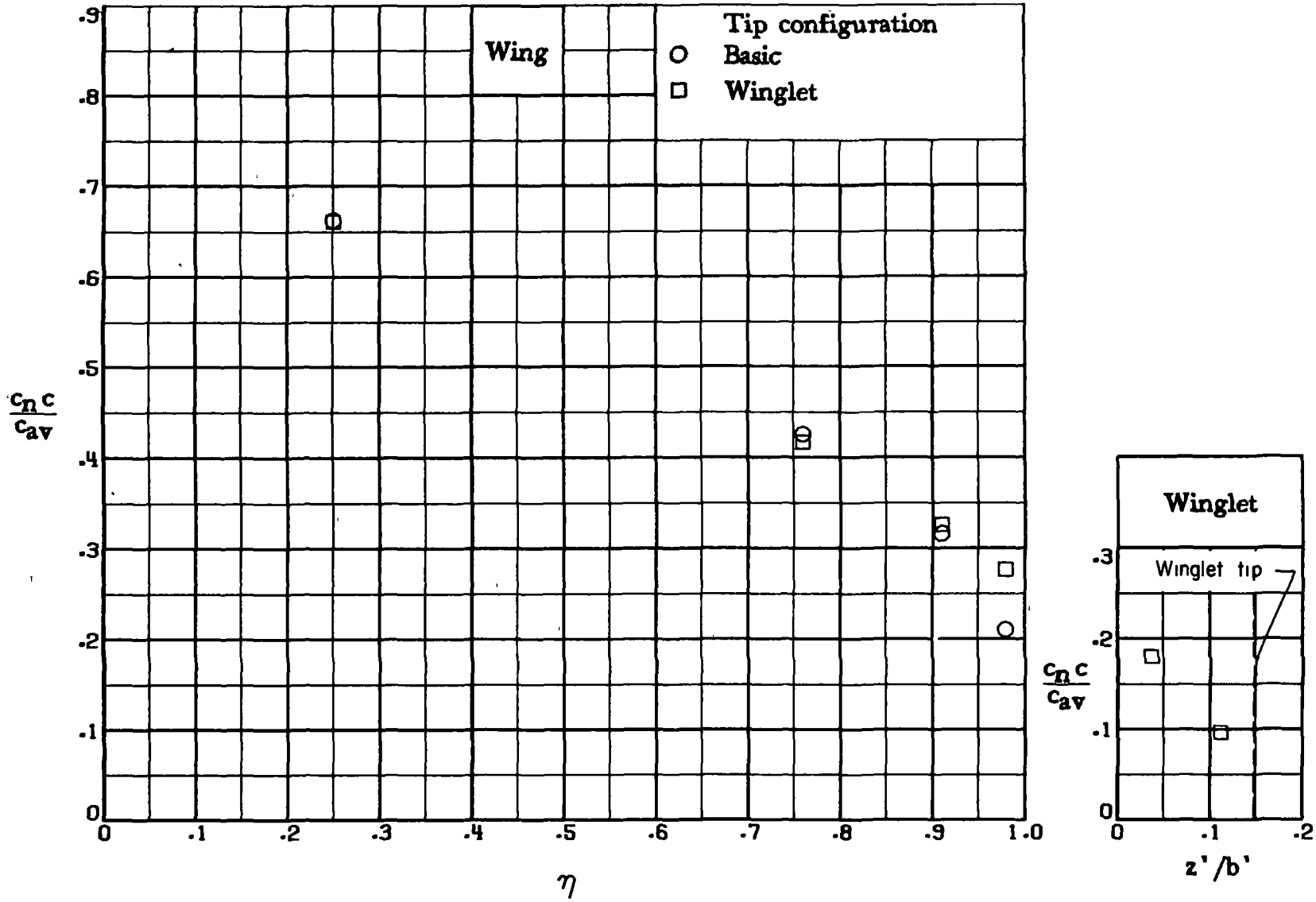

(g) $M_\infty = 0.75$; $\alpha = 3.5^\circ$.

Figure 17.- Continued.

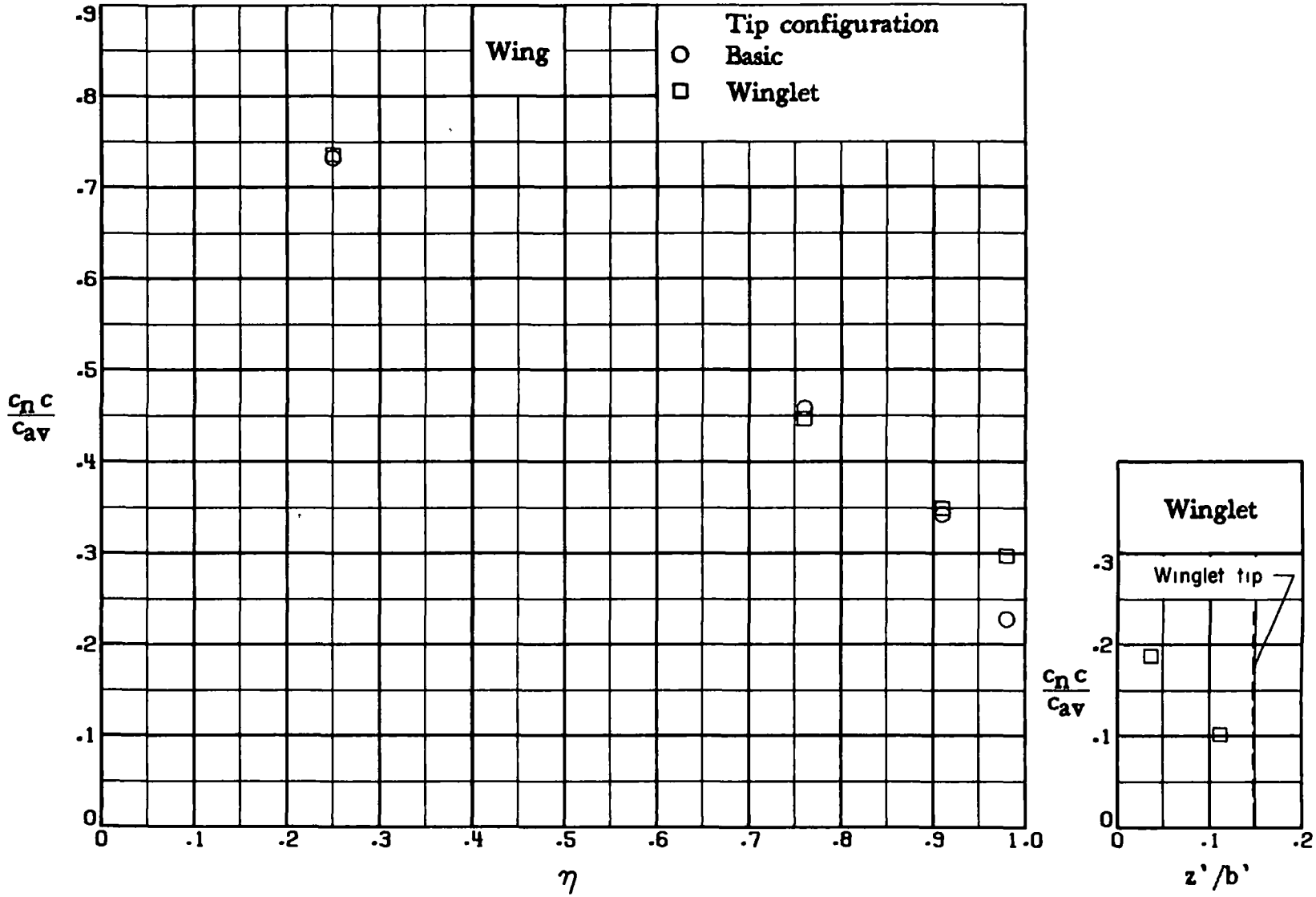

(h) $M_\infty = 0.75$; $\alpha = 4.0^\circ$.

Figure 17.- Continued.

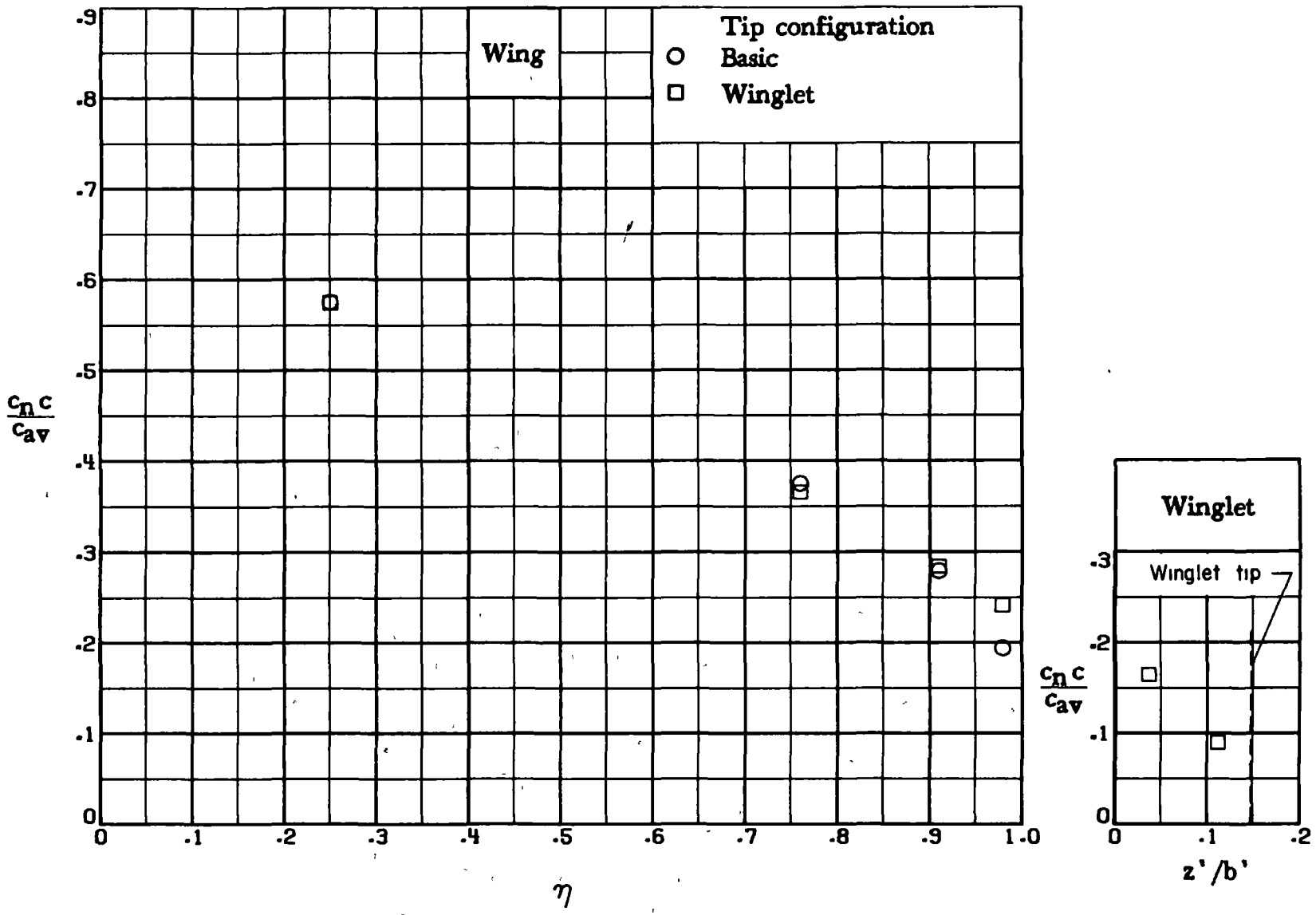

(i) $M_\infty = 0.78$; $\alpha = 2.5^\circ$.

Figure 17.- Continued.

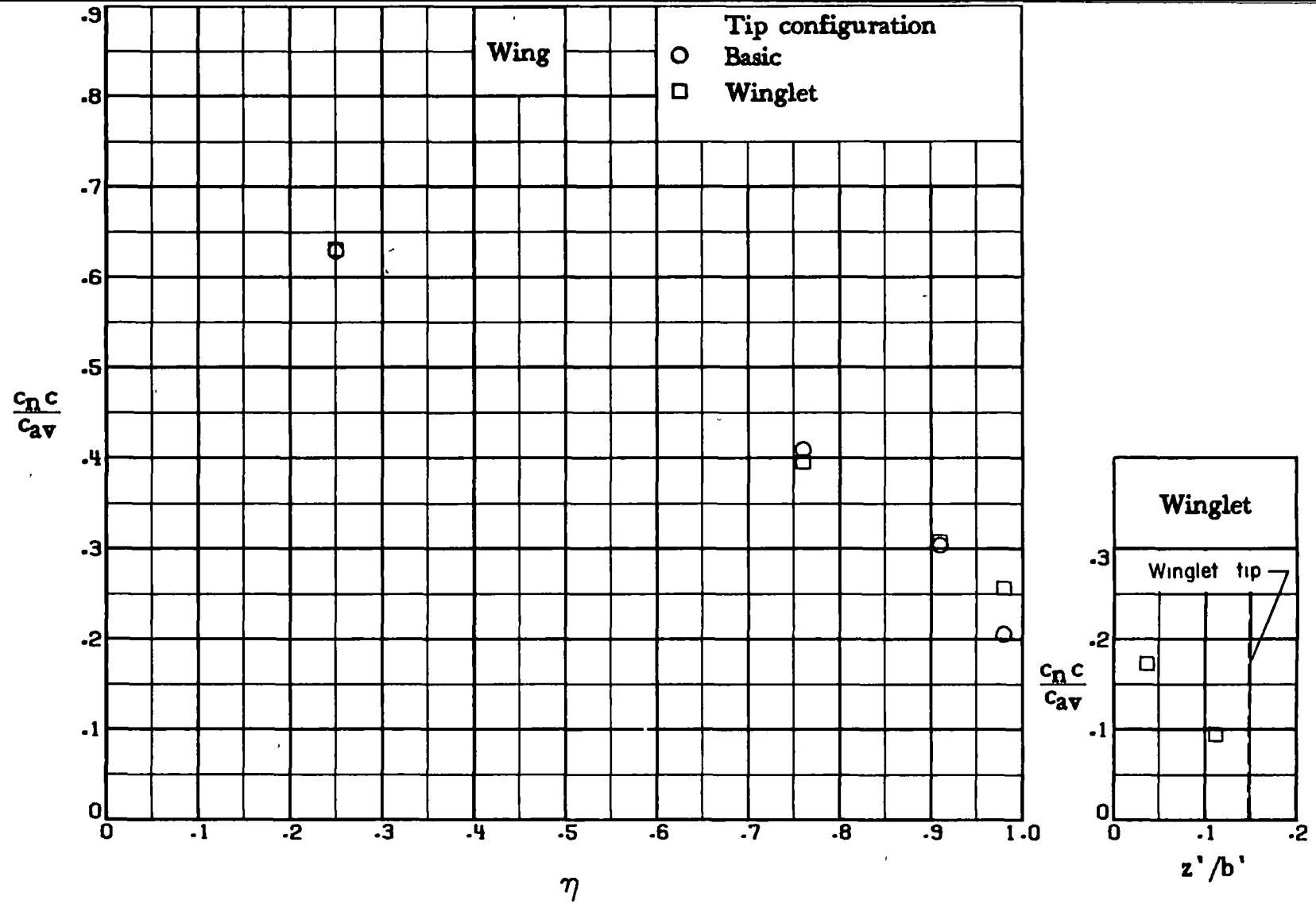

(j) $M_\infty = 0.78$; $\alpha = 3.0^\circ$.

Figure 17.- Continued.

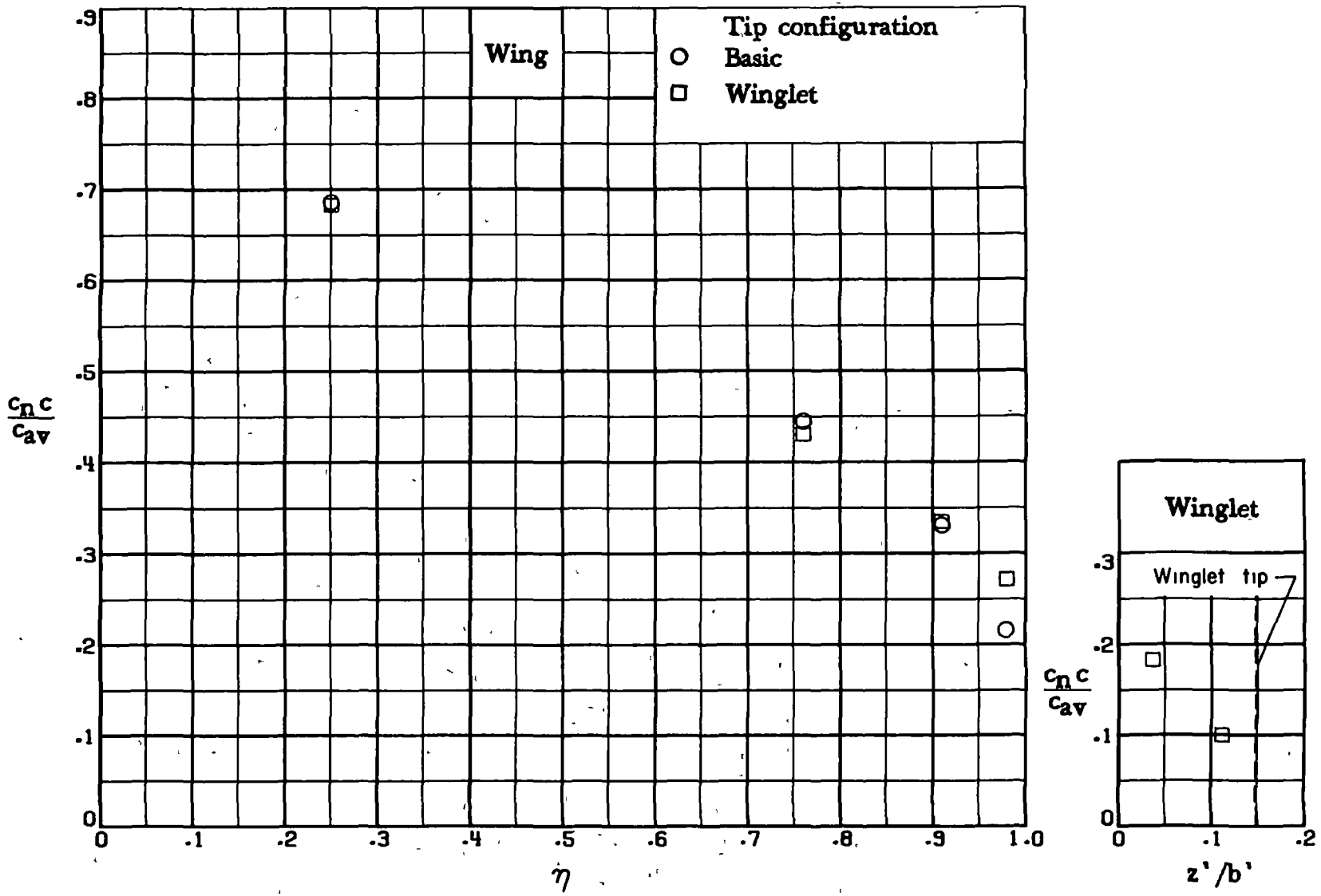

(k) $M_\infty = 0.78$; $\alpha = 3.5°$.

Figure 17.- Continued.

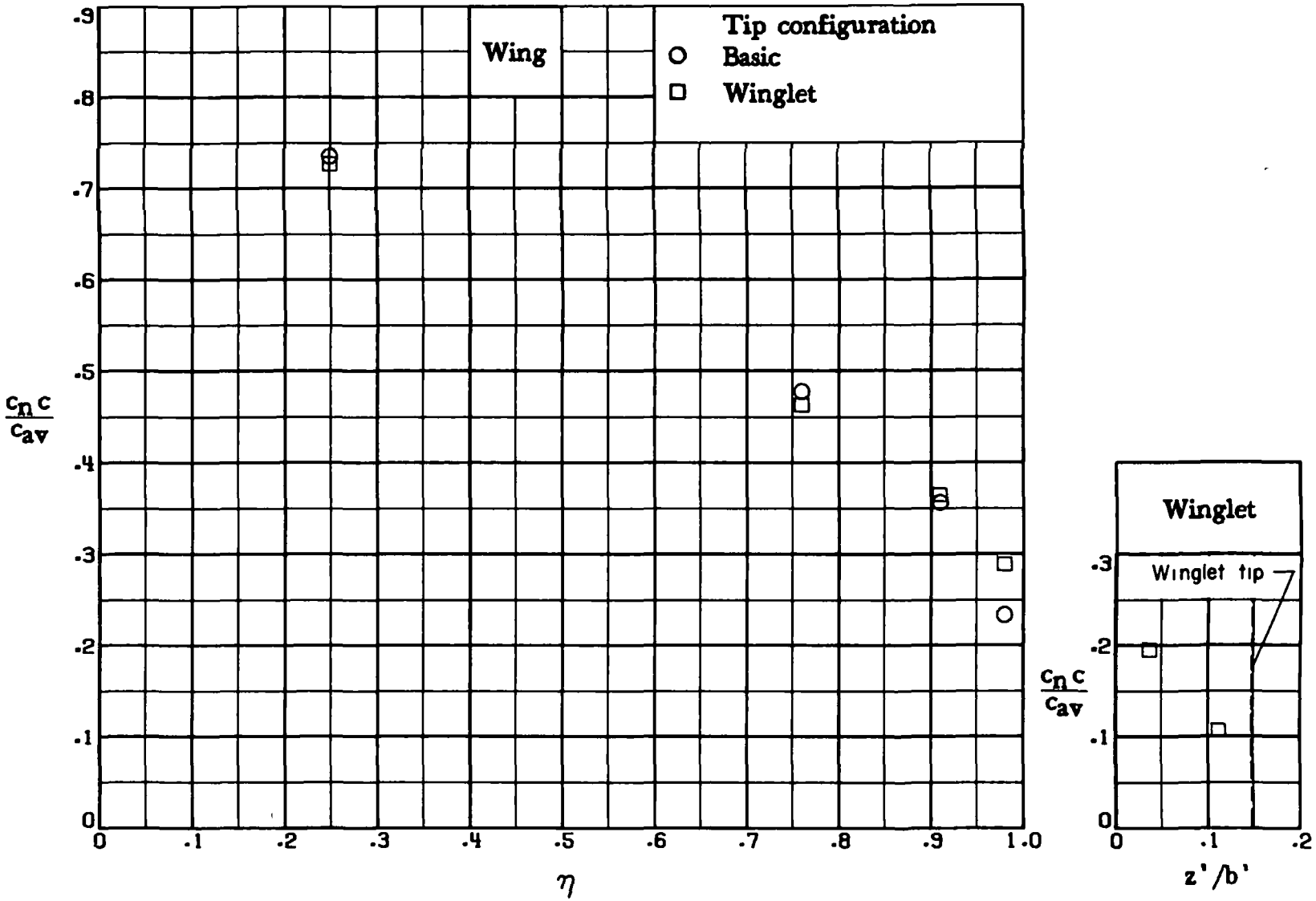

(1) $M_\infty = 0.78$; $\alpha = 4.0^o$.

Figure 17.- Continued.

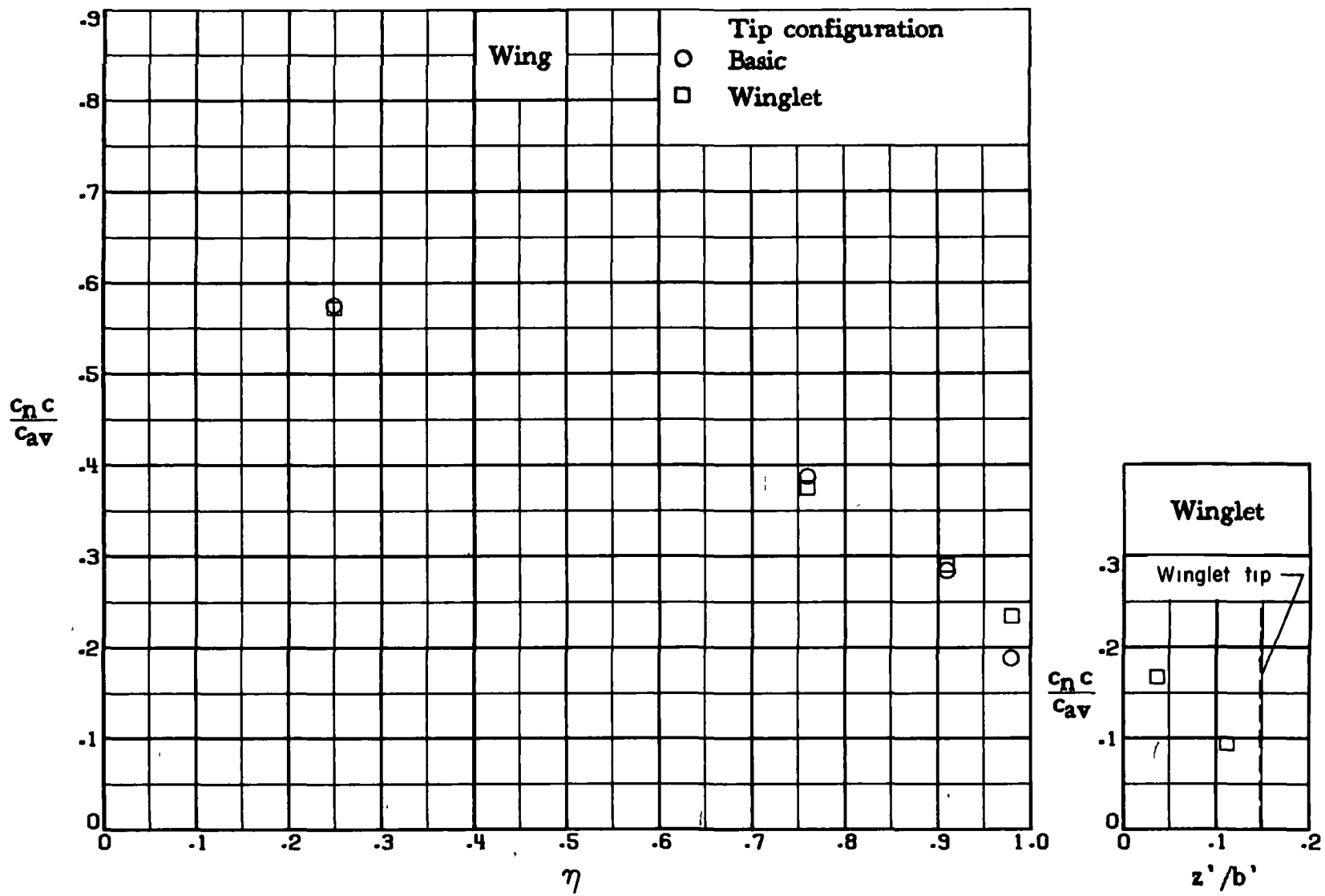

(m) $M_\infty = 0.80$; $\alpha = 2.5^\circ$.

Figure 17.- Continued.

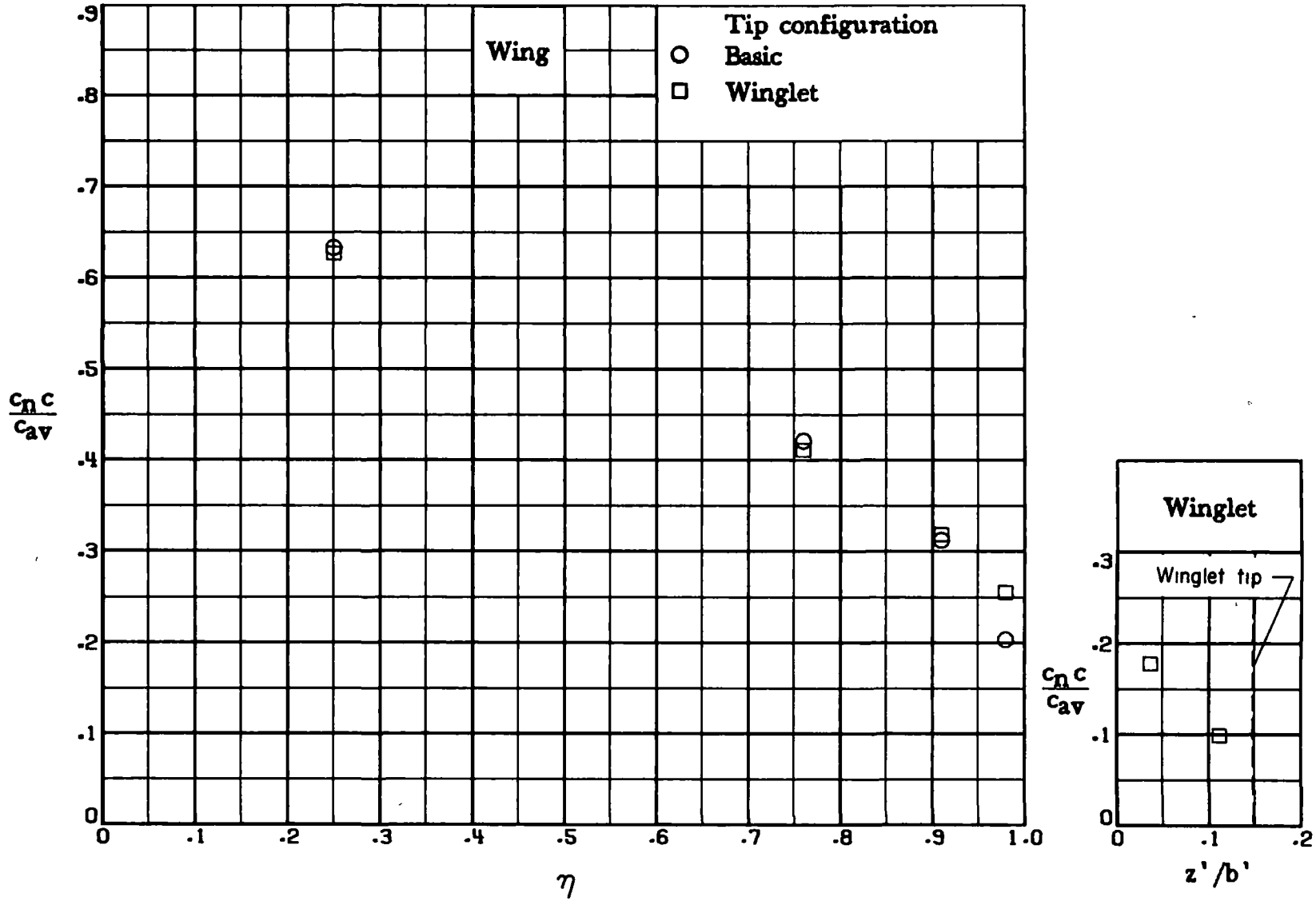

(n) $M_\infty = 0.80$; $\alpha = 3.0^\circ$,

Figure 17.- Continued.

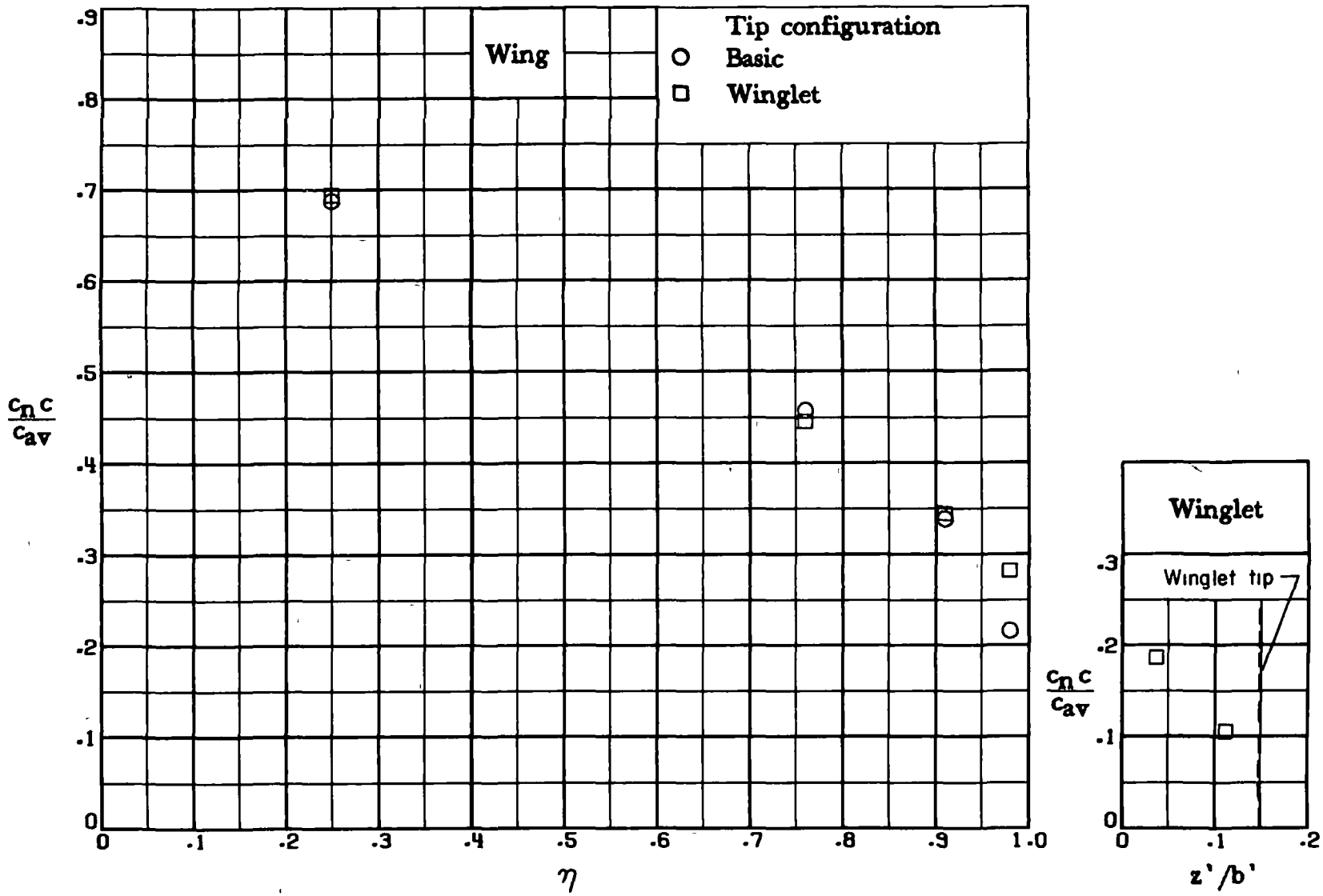

(o) $M_\infty = 0.80$; $\alpha = 3.5^\circ$.

Figure 17.- Continued.

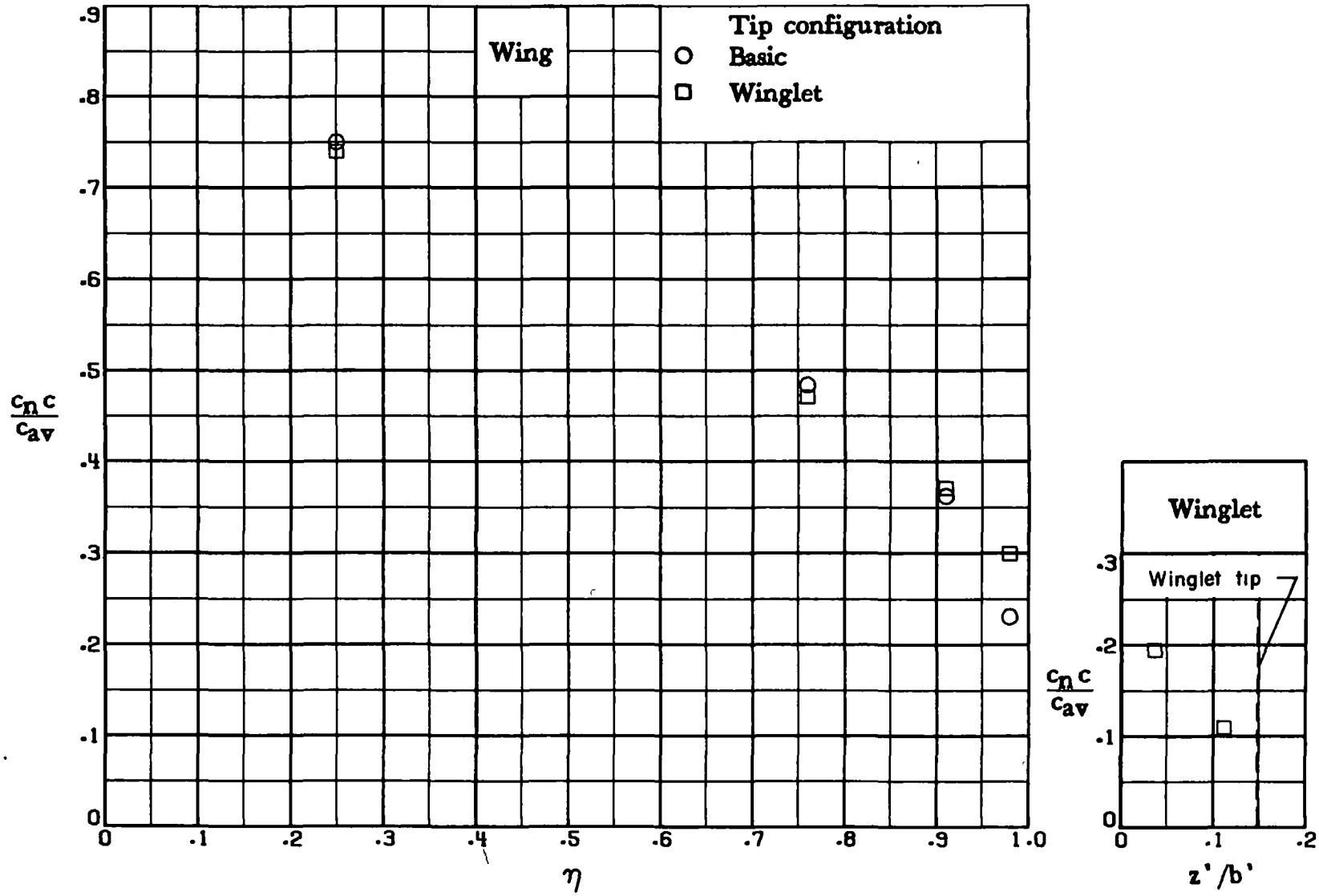

(p) $M_\infty = 0.80$; $\alpha = 4.0^\circ$.

Figure 17.- Concluded.

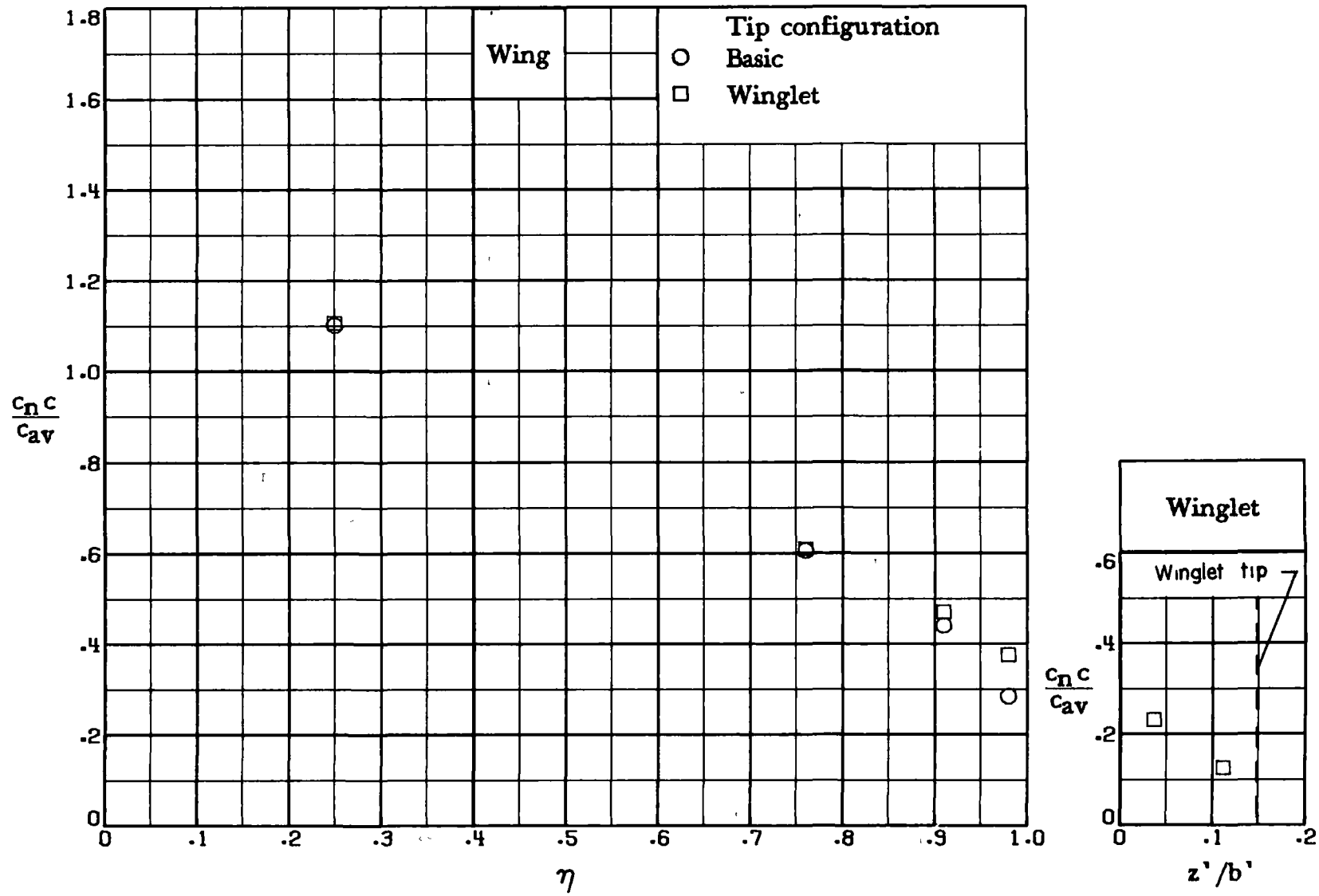

(a) $\alpha = 5^{\circ}$.

Figure 18.- Spanwise load distributions for basic and winglet configurations with trailing-edge flaps. $M_{\infty} = 0.30$.

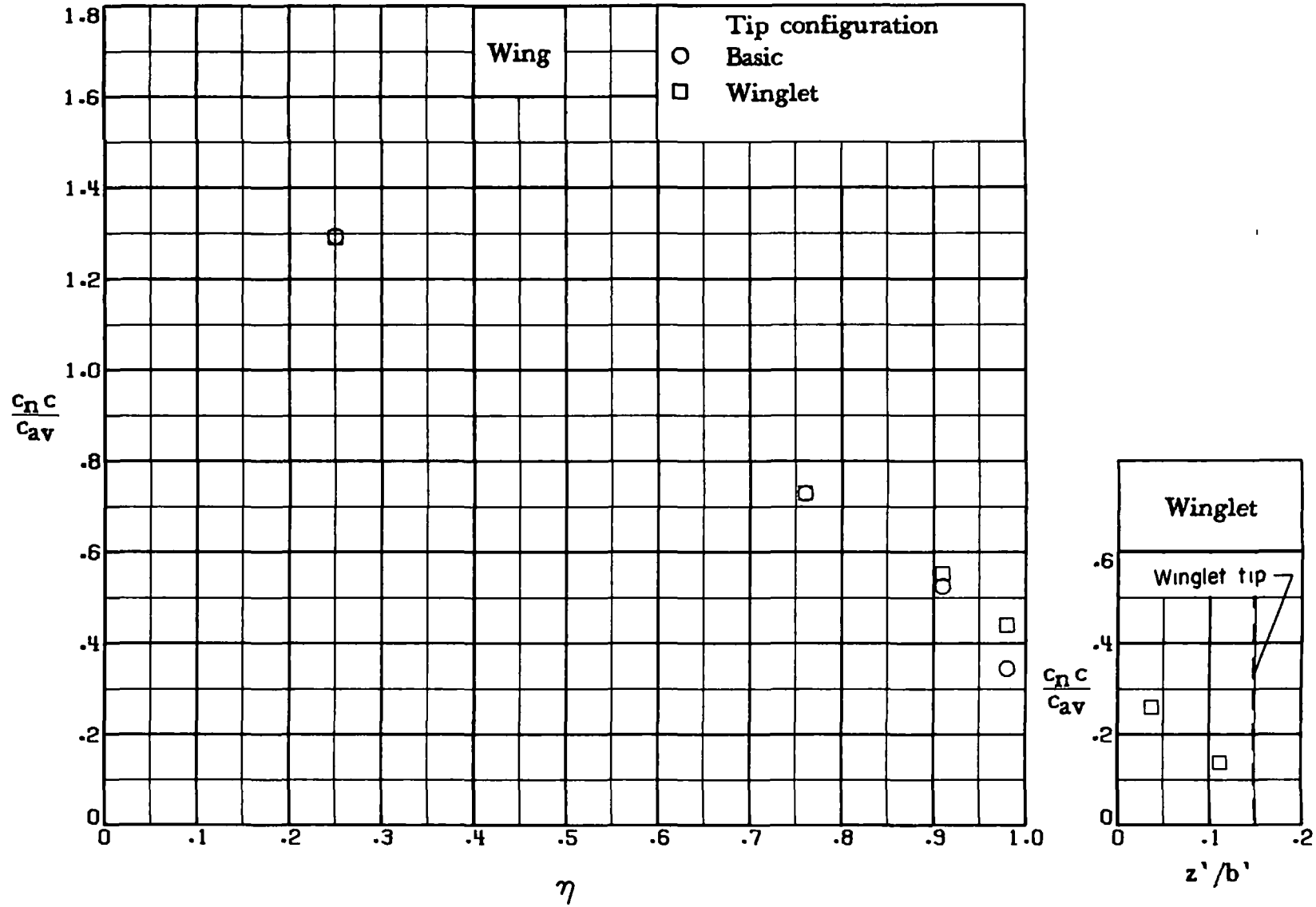

(b) $\alpha = 7^{\circ}$.

Figure 18.- Continued.

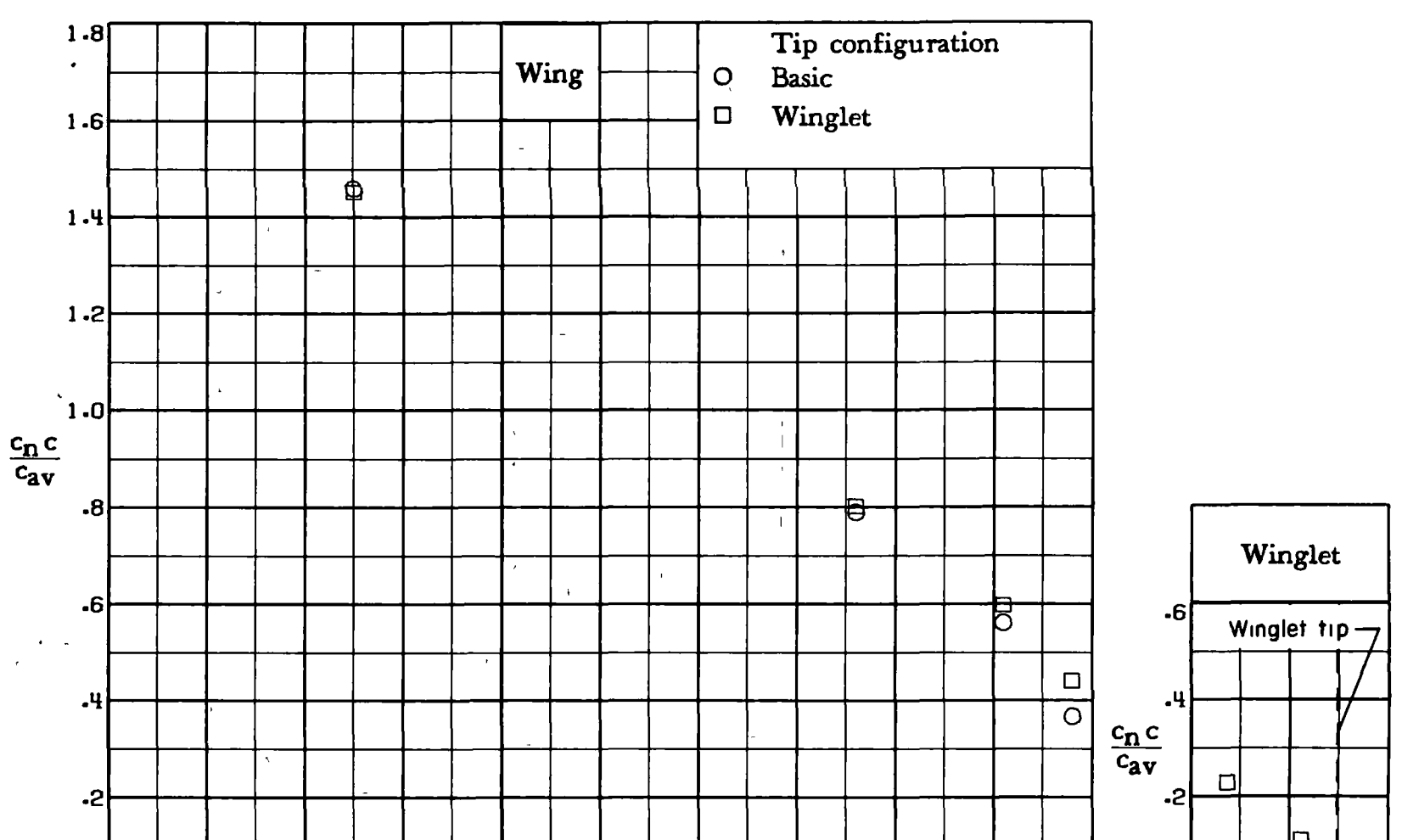

(c) $\alpha = 9^{\circ}$.

Figure 18.- Continued.

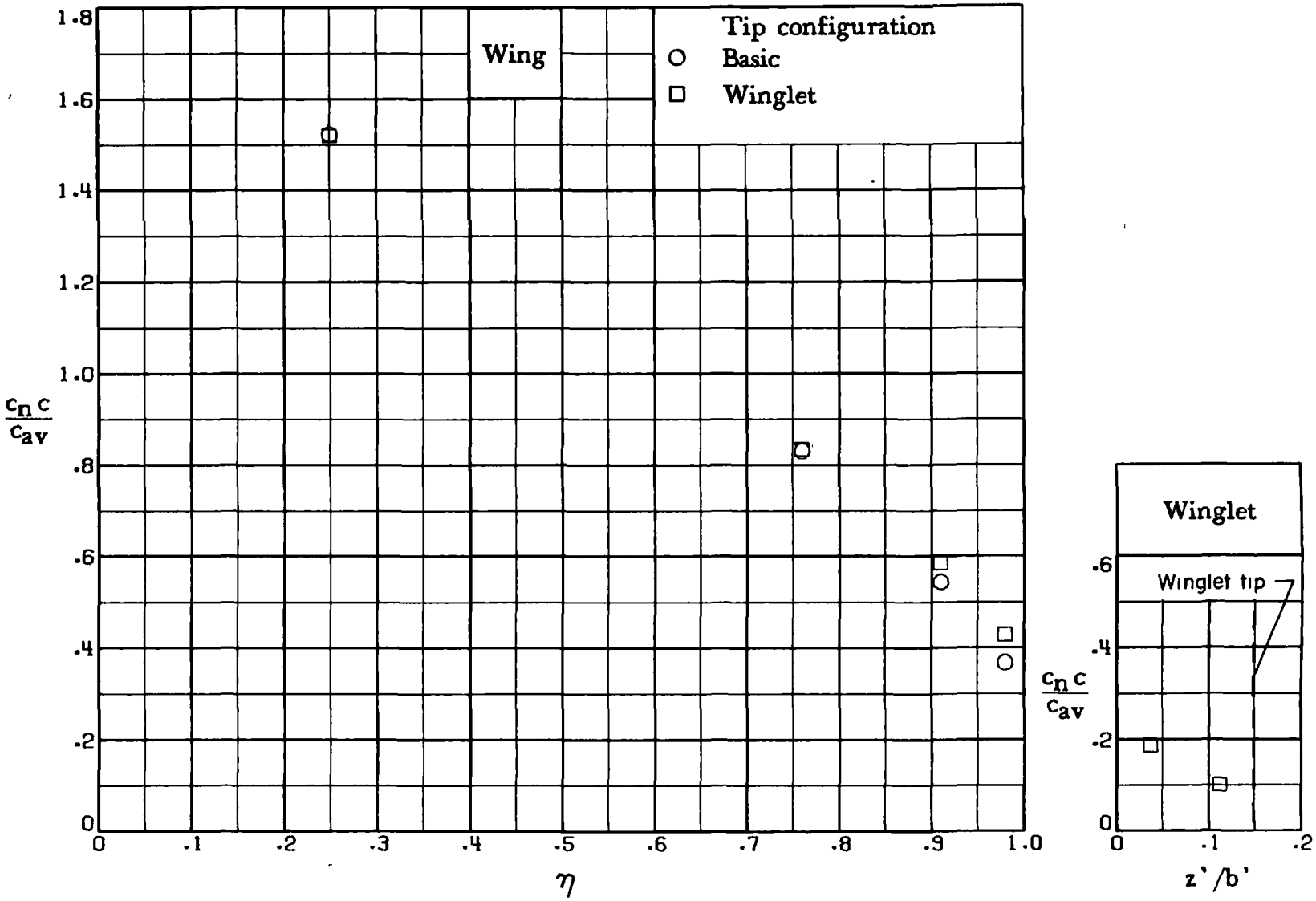

(d) $\alpha = 10^{\circ}$.

Figure 18.- Continued.

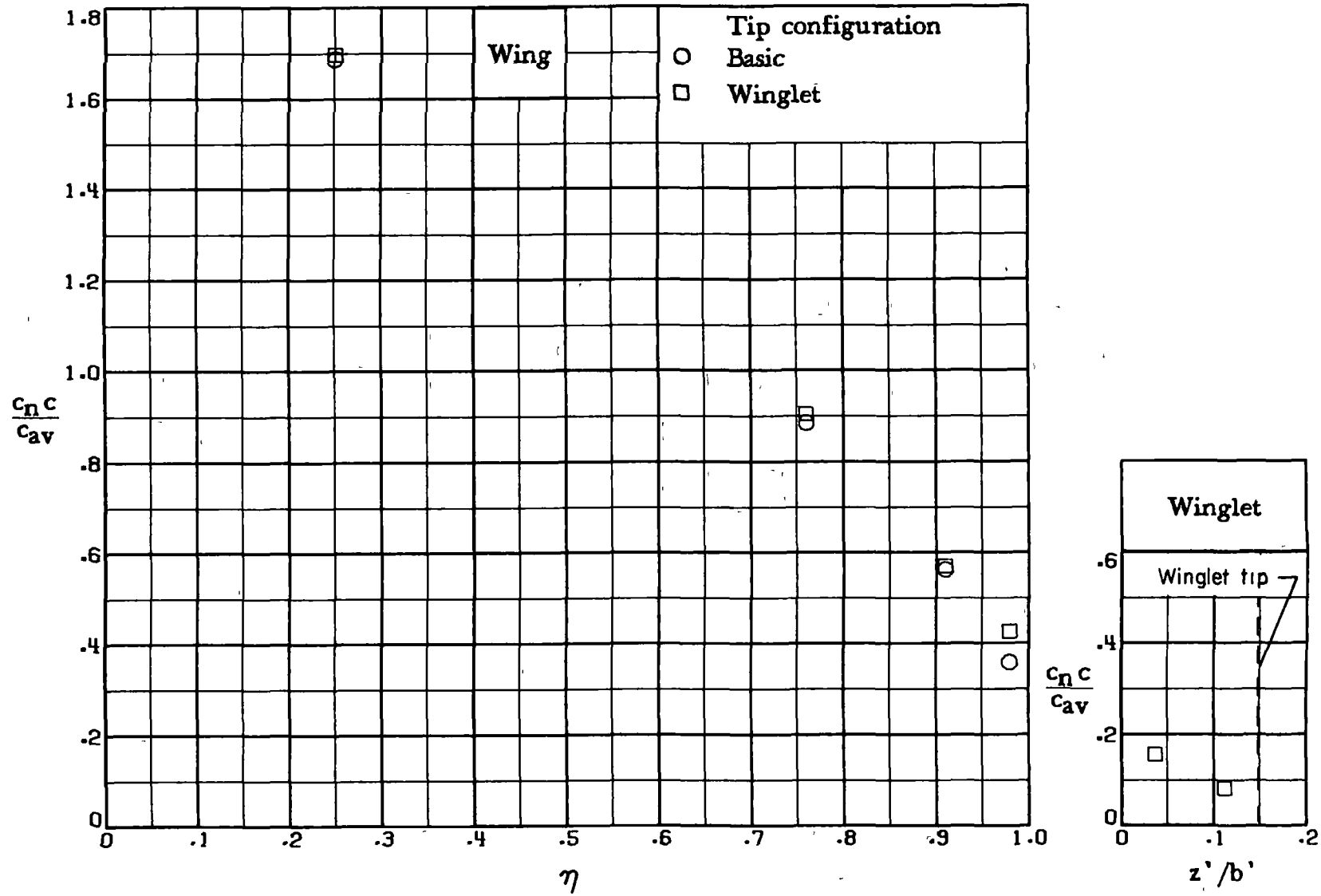

(e) $\alpha = 12^{\circ}$.

Figure 18.- Concluded.

1 Report No	2 Government Accession No	3 Recipient's Catalog No
NASA TM-78786		

4 Title and Subtitle	5 Report Date
EFFECT OF AN ALTERNATE WINGLET ON THE PRESSURE AND SPANWISE LOAD DISTRIBUTIONS OF A FIRST-GENERATION JET TRANSPORT WING	December 1978
	6 Performing Organization Code

7 Author(s)	8 Performing Organization Report No
Lawrence C. Montoya (Dryden Flight Research Center), Stuart G. Flechner and Peter F. Jacobs (Langley Research Center)	L-12519
	10 Work Unit No
	505-11-16-02

9 Performing Organization Name and Address	11 Contract or Grant No
NASA Langley Research Center Hampton, VA 23665	
	13 Type of Report and Period Covered
	Technical Memorandum

12 Sponsoring Agency Name and Address	14 Sponsoring Agency Code
National Aeronautics and Space Administration Washington, DC 20546	

15 Supplementary Notes

16 Abstract

Pressure and spanwise load distributions on a first-generation jet transport semispan model at subsonic speeds are presented. The wind-tunnel data were measured for the wing with and without an alternate winglet. The results show that the winglet affected the outboard wing pressure distributions and increased the spanwise loads near the tip.

17 Key Words (Suggested by Author(s))	18 Distribution Statement
Winglets Pressure distributions Spanwise load distributions Flaps	Unclassified - Unlimited Subject Category 02

19 Security Classif (of this report)	20 Security Classif (of this page)	21 No of Pages	22 Price*
Unclassified	Unclassified	92	$6.00

* For sale by the National Technical Information Service, Springfield, Virginia 22161

NASA-Langley, 1978

National Aeronautics and
Space Administration

Washington, D.C.
20546

Official Business
Penalty for Private Use, $300

THIRD-CLASS BULK RATE

Postage and Fees Paid
National Aeronautics and
Space Administration
NASA-451

U.S.MAIL

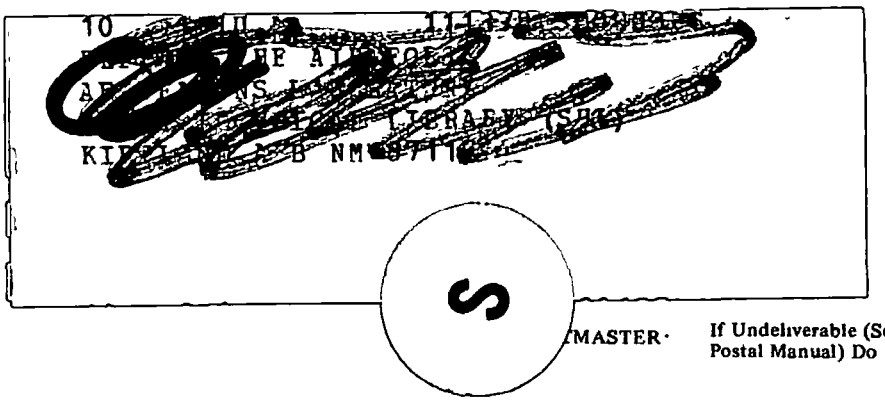

NASA

MASTER

If Undeliverable (Section 158
Postal Manual) Do Not Return